Space-time Description of Supersonic Jets with Thermal Non-uniformity

Kyle A. Daniel

Dissertation submitted to the Faculty of the
Virginia Polytechnic Institute and State University
in partial fulfillment of the requirements for the degree of

Doctor of Philosophy
in
Aerospace Engineering

K. Todd Lowe, Co-chair
Wing F. Ng, Co-chair
W. Nathan Alexander
Ricardo A. Burdisso
William J. Devenport

Nov 1st, 2019
Blacksburg, Virginia

Keywords: aeroacoustics, jet noise, near-field, schlieren, non-uniform, total temperature
Copyright 2019, Kyle A. Daniel

Space-time Description of Supersonic Jets with Thermal Non-uniformity

Kyle A. Daniel

(ABSTRACT)

The supersonic jet plumes that exhaust from the engines of tactical aircraft produce intense noise signatures that expose the Navy personnel working on the deck of aircraft carriers to dangerously high levels of noise that often results in hearing damage. Reducing the noise radiated by these supersonic plumes is of interest to the Department of Defense and is the primary motivation of this research. Fundamentally, jet noise reduction is achieved by manipulating the nozzle boundary condition to produce changes in the turbulence development and decrease the acoustic efficiency of coherent structures. The research presented here focuses on a novel jet noise reduction technique involving a centered thermal non-uniformity that alters the base flow by introducing a temperature-driven centerline velocity deficit into a perfectly expanded Mach 1.5 jet. The results indicate 2 ± 0.5 dB reductions in peak narrowband spectral sound pressure levels upstream of peak directivity directions for the non-uniform jet compared to a thermally uniform baseline, even for static thrust matched conditions. This reduction is hypothesized to be related to perturbations induced by the thermal non-uniformity that convect inside the irrotational core and reduce the correlation length scales of turbulence at locations far downstream. This hypothesis was evaluated by studying the coherent turbulence via its convective hydrodynamic footprint in the near-field. An indirect investigation of the near-field using a far-field-informed model of the wavenumber-frequency spectra indicate a reduction in the energy contained in the tail of the wavenumber spectra amplitude, suggesting a reduction in the size of large scale structures. A direct evaluation of the spatio-temporal behavior of the near-field was performed using temporally resolved schlieren images. Space-time correlations of the frequency-filtered near-field identified high frequency acoustic waves radiated by compactly coherent turbulent structures and low frequency Mach waves produced by large scale instabilities. In the thermally non-uniform case these features and their sources were found to be decorrelated at downstream regions. These results provide strong evidence that a centered thermal non-uniformity reduces the radiated noise compared to a uniform baseline by shortening the correlation length scales of coherent structures in regions far from the nozzle exhaust.

Space-time Description of Supersonic Jets with Thermal Non-uniformity

Kyle A. Daniel

(GENERAL AUDIENCE ABSTRACT)

A more complete understanding of the intense noise sources present in supersonic jet plumes is of value to both government and industry, and is a necessary step towards optimizing noise reduction techniques. Tactical aircraft that operate on the deck of aircraft carriers expose Navy personnel to dangerously high levels of noise that often results in permanent hearing damage. Supersonic jet noise reduction is also of relevance to the recent efforts to revitalize supersonic air transport over land. For supersonic air transport to become a reality, the noise produced by these future aircraft during takeoff and landing must meet the increasingly stringent community noise requirements. Fundamental jet noise research is needed to guide the design of future engine architectures for these aircraft to ensure their commercial success. The research presented herein examines a novel noise reduction technique that involves a centered thermal non-uniformity consisting of a heated jet plume with a spot of locally cooler, slower moving air concentrated along the centerline of a Mach 1.5 jet. This temperature driven velocity deficit is shown to reduce the radiated noise by up to 2.5 dB at peak frequencies and at angles just outside of the peak directivity direction. The cause of the noise reduction is hypothesized be related to a reduction in the size of the coherent structures that radiate a majority of the noise produced by turbulent jets. This hypothesis is evaluated by examining the 'footprint' of the coherent structures in the ambient field directly outside of the jet shear layer in an area called the near-field. An indirect investigation of the near-field using a far-field informed analytic model suggests a reduction in the size of large scale structures. A direct evaluation of the space time structure of the near-field was performed using temporally resolved schlieren images. Statistical processing of the density gradient provided by the schlieren images revealed acoustically intense structures known as Mach waves and high frequency acoustic waves. These features and their sources, large scale instabilities and compactly coherent turbulence, were found to be decorrelated by the introduction of the thermal non-uniformity. These results provide strong evidence that the centered thermal non-uniformity produces a noise benefit by reducing the size of the turbulent structures.

Acknowledgments

First I want to thank my advisors, Dr. K. Todd Lowe and Dr. Ng Wing, for their support and guidance throughout my PhD. You have both pushed me to achieve things I never thought possible and have helped me become researcher I am today. Further, I want to thank the remaining members of my committee Dr. William J. Devenport, Dr. W. Nathan Alexander, and Dr. Ricardo Burdisso for your feedback and support. Special thanks goes to my friend and colleague Dr. David Mayo Jr. Much of the work presented here is a product of our engaging conversations and his support and companionship have helped shape many of the accomplishments of this work. I also want to thank my fellow graduate students, who I have become great friends with during my time at Virginia Tech. We have all experienced a lot, and not all of it great, but the community we've built together has given me experiences that I am extremely grateful for. A few of the people I want to thank include, Ashley Saltzman, Dr. David Mayo Jr., Agastya Balantrapu, Aaron Defreitas, Christopher Hickling, Chi Young Moon, Matthew Boyda, Dr. Tamy Guimarães, and Tyler Vincent. Special thanks in this regard goes out to Christopher Hickling. Our evening conversations at the LUD, morning coffee routine, and timed working sessions have helped kept me sane throughout graduate school. I owe you one Glib Glob. I also want to thank my family for their unwavering support throughout the course of my PhD, with specific thanks going to my parents Kate and Frank Daniel. Lastly, I dedicate this dissertation to my grandparents, Bernice and Gary Kauffman, and Hannelore and Gerhard Daniel. You've taught me that goals worth pursuing are not always meant to be easy.

Contents

List of Figures

List of Tables

Chapter 1

Introduction

A more complete understanding of the physics linking the energetic turbulent sources in supersonic free jets to the significantly weaker radiated sound field is of value to the US Department of Defense and a necessary step towards optimizing noise reduction techniques. A deeper knowledge of the sources of jet noise, and therefore how to reduce them, is desirable first due to the high intensity noise produced by the supersonic plumes of tactical aircraft. Prior to takeoff and during landing these tactical aircraft expose personnel working on the deck of aircraft carriers to dangerously high noise levels that often results in permanent hearing damage [1]. Supersonic jet noise reduction is also of relevance to the recent efforts to revitalize supersonic air transport over land. For supersonic air transport to become a reality, the noise produced by these future aircraft must meet the increasingly stringent community noise requirements [2]. Fundamental jet noise research is needed to guide the design of future engine architectures for these aircraft to ensure their commercial success.

Fundamentally, a reduction in jet noise is achieved by manipulating the nozzle boundary condition to produce changes in the turbulence development and decreasing the acoustic efficiency of coherent structures. Common jet noise reduction techniques such as chevrons [3], fluidic injection [4], and offset multi-stream nozzles [5] alter the base flow in unique ways and change different aspects of the turbulence development. Studies of these various techniques, their unique base flows, and the characteristics of the altered acoustic fields they produce have helped identify characteristics of the acoustically efficient turbulence.

The measurement techniques used to study the turbulence development of free jets have come far over the last few decades with the advent of non-intrusive laser-based velocimetry measurements that include PIV, DGV, and LDA. However, while these measurements can provide either a spatially or temporally resolved measure of the flow field, the connection between the acoustically efficient turbulence and the radiated sound field is not fully understood. The difficultly in understanding the connection between the turbulent jet plume and the radiated acoustic field stems from the distinct behaviors of the energetic turbulent structures and the relatively weak acoustic field. The vastly different energetics of these fields makes isolating the acoustically efficient parts of the turbulence and how they relate to the far-field difficult [6].

Recent experimental studies [7, 8, 9, 10, 11] have overcome this problem by examining the features of these acoustically efficient structures via the pressure field directly outside of the jet shear layer. The near pressure field acts as a wavenumber filter that removes

the energetically intense, acoustically inefficient, turbulent fluctuations. The convective 'footprint' of large scale structures are typically measured experimentally using extensive microphone arrays located very close to the shear layer [8, 11].

The research in the present dissertation adds to our understanding of the relationship between the nozzle boundary condition and the turbulence development by studying the near and far acoustic fields of a novel noise reduction method involving a centered thermal non-uniformity. The temperature-driven centerline velocity deficit introduced by the centered thermal non-uniformity is hypothesized to induce perturbations along the jet centerline that convect downstream and alter the structure of coherent turbulence at locations far from the nozzle exhaust. This dissertation evaluates that hypothesis by studying the structure of the near-field indirectly via a far-field-informed model of the near-field wavenumber-frequency spectra and directly using space-time correlations of time-resolved schlieren measurements.

1.1 Structure and content

Chapter 1: This chapter will introduce the major topics of the dissertation as well as outline its structure and the major contributions it makes to the field of jet noise.

Chapter 2: Here a literature survey of topics relevant to this dissertation will be presented. The information contained in this chapter outlines the gaps in the current state of knowledge that the research presented herein addresses.

Chapter 3: This chapter presents a published peer reviewed journal article in the AIAA Journal entitled, "Use of Thermal Non-Uniformity to Reduce Supersonic Jet Noise". The study first characterizes the acoustic benefit of jets with centered thermal non-uniformities as compared to a thermally uniform baseline. The changes in the wavenumber-frequency spectrum of the near-field pressure related to this acoustic benefit is evaluated indirectly using a far-field-informed analytic model.

Chapter 4: This chapter presents a manuscript that will be submitted for publication in the Journal of Fluid Mechanics entitled "The Density Near-field of a Non-Uniformly Heated Jet." This study examines the space-time structure of the density near-field and the changes induced in it by the thermal non-uniformity using space-time correlations of time-resolved schlieren.

1.2 Attributions

The content of this dissertation was aided by several mentors and colleagues whose individual contributions are described below.

Dr. David E. Mayo Jr. is a PhD who, during his time as a doctoral candidate, worked

closely with me on this project. He is a co-author on all of the journal papers and most of the conference proceedings presented here. We equally developed the methodology used to generate the thermal non-uniformity studied in this dissertation. The experimental investigation of the far-field acoustics and the near-field density gradient were was made with his support. Further he supported the conceptualization of the hypotheses and conclusions discussed in this study.

Dr. K. Todd Lowe is the primary advisor and committee chair for the research presented here. He acted in equal parts with Dr. Ng to acquire the funding for this project and provided supervision of this research. Further Dr. Lowe supported the conceptualization of the hypotheses and conclusions discussed in this study and reviewed and edited the writing of the journal papers and conference proceedings presented here.

Dr. Wing F. Ng is a co-advisor and committee co-chair for the research presented here. He acted in equal parts with Dr. Lowe to acquire the funding for this project and provided supervision of this research. Further Dr. Ng supported the conceptualization of the overarching research goals and of this study and reviewed and edited the writing of the journal papers and conference proceedings presented here.

1.3 Achievements

The major accomplishments of this dissertation are detailed below:

- The identification of a centered thermal non-uniformity as a potentially promising noise reduction technique. Results demonstrate that despite a modest impact on the mean velocity field, centered thermal non-uniformities reduce the radiated noise by up to 2.5 dB in the peak narrowband spectra. This suggests potential for exploiting this phenomenon by using more substantial non-uniformities that could be achieved in full-scale engines running at afterburning conditions.

- The identification of high-frequency acoustic waves radiated by integral length turbulent structures and Mach waves in the near density field using space-time correlations of time-resolved schlieren measurements. The introduction of the thermal non-uniformity was found to decorrelate these structures at locations far from the nozzle exhaust. These results demonstrate the use of time-resolved schlieren imaging as a relatively simple, but effective tool to analyze the spatio-temporal behavior of the near-field.

- The development, design, and implementation of the hardware modifications necessary to introduce a secondary unheated stream into the plenum of the heated jet and generate the thermal non-uniformities studied in this dissertation. The design and validation of a ground-based microphone array capable of accurately measuring the far-field narrowband spectra of the jets studied in this dissertation. The ground array

enhances the facility capabilities by allowing accurate far-field acoustic measurements to be performed.

1.3.1 Claims

Key contributions of this work to the field of jet noise and the major claims it makes are as follows:

- The introduction of a centered thermal non-uniformity reduces the radiated noise in supersonic jets by up to 2.5 dB in the peak narrowband spectra. These reductions are greater than what is expected from a uniform profile jet with an equivalent mass flowrate and are driven by subtle change in the turbulence development.
- The centered thermal non-uniformity has the effect of reducing the correlation length scales of coherent structures in regions far from the nozzle exhaust. This decorrelates Mach waves radiated from regions near the potential core collapse and produces the observed acoustic benefit.
- The energetic interaction of compactly coherent structures in the shear layer produce high frequency acoustic waves that propagate with directivities close to the sideline direction.

1.3.2 List of Publications

Peer-reviewed Journal Publications:

- **Daniel, K.A.**, Mayo, D. E., Jr., Lowe, K. T., and Ng, W. F., "Use of Thermal Non-Uniformity to Reduce Supersonic Jet Noise," AIAA Journal, 2019. doi:10.2514/1.J058531
- Mayo Jr., D.E., **Daniel, K.A.**, Lowe, K. T., and Ng, W. F., "The Mean Flow and Turbulence Characteristics of a Heated Supersonic Jet with an Offset Total Temperature Non-Uniformity," AIAA Journal, 2019. doi:10.2514/1.J058163
- **Daniel, K.A.**, Mayo Jr., D.E., Lowe, K. T., and Ng, W. F., 2019, "The Density Near-field of a Non-Uniformly Heated Jet," Journal of Fluid Mechanics, (not yet published)
- Mayo Jr., D.E, **Daniel, K.A.**, Lowe, K.T., and Ng, W.F., "Statistical Flow Structures in Heated Supersonic Jets with Offset Temperature Non-Uniformities", AIAA Journal, (not yet published)

Conference Proceedings:

- **Daniel, K.A.**, Mayo, D. E., Jr., Lowe, K. T., and Ng, W. F., "Space-time Description of the Denisty Near-field in a Non-Uniformily Heated Jet," 25th AIAA/CEAS Aeroacoustics Conference, AIAA Paper 2019-2472, 2019. doi: 10.2514/6.2019-2474

- Mayo Jr., D.E, **Daniel, K.A.**, Lowe, K. T., and Ng, W. F., "Statistical Flow Structures in Heated Supersonic Jets with Offset Temperature Non-Uniformities," 25th AIAA/CEAS Aeroacoustics Conference, AIAA Paper 2019-2708, 2019. doi: 10.2514/6.2019-2708

- **Daniel, K.A.**, Mayo, D. E., Jr., Lowe, K. T., and Ng, W. F., "Experimental Investigation of the Pressure Field of a Heated Supersonic Jet with a Centered Total Temperature Non-Uniformity," 55th AIAA Aerospace Sciences Meeting, AIAA Paper 2019-1300, 2019. doi:10.2514/6.2019-1300

- Quinn, A. M., Daniel, **Daniel, K.A.**, K. T., and Ng, W., "Outdoor Acoustic Measurements of the Virginia Tech Heated Supersonic Jet Rig Using Ground Microphones," 55th AIAA Aerospace Sciences Meeting, AIAA Paper 2019-1581, 2019. doi:10.2514/6.2019-1581

- **Daniel, K.A.**, Mayo, D. E., Jr., Lowe, K. T., and Ng, W. F., "Experimental Investigation of the Impacts of Total Temperature Non-Uniformities on the Flow and Acoustic Fields of a Heated Supersonic Jet, 176th Meeting of Acoustical Society of America, Nov, 2018. (Abstract Only)

- **Daniel, K.A.**, Mayo, D. E., Jr., Lowe, K. T., and Ng, W. F., "Experimental Investigation of the Very Near Pressure Field of a Heated Supersonic Jet with a Total Temperature Non-Uniformity," 24th AIAA/CEAS Aeroacoustics Conference, AIAA Paper 2018-3145, 2018. doi:10.2514/6.2018-3145

- Mayo Jr., D.E, **Daniel, K.A.**, Lowe, K.T., and Ng, W.F., "The Flow and Turbulence Characteristics of a Heated Supersonic Jet with an Offset Total Temperature Non-Uniformity", 24th AIAA/CEAS Aeroacoustics Conference, AIAA AVIATION Forum, (AIAA 2018-3144)

- Mayo Jr., D.E, **Daniel, K.A.**, Lowe, K. T., and Ng, W. F., "Experimental Investigation of a Heated Supersonic Jet with Total Temperature Non-Uniformity," 23rd AIAA/CEAS Aeroacoustics Conference, AIAA Paper 2017-3521, 2017. doi:10.2514/6.2017-3521.

Bibliography

[1] Aubert, A. and McKinley, R., "Measurements of jet noise aboard us navy aircraft carriers," *AIAA Centennial of Naval Aviation Forum" 100 Years of Achievement and Progress"*, 2011, p. 6947.

[2] Huff, D. L., Henderson, B. S., Berton, J. J., and Seidel, J. A., "Perceived noise analysis for offset jets applied to commercial supersonic aircraft," *54th AIAA aerospace sciences meeting*, 2016, p. 1635.

[3] Rask, O., Kastner, J., and Gutmark, E., "Understanding how chevrons modify noise in supersonic jet with flight effects," *AIAA journal*, Vol. 49, No. 8, 2011, pp. 1569–1576.

[4] Powers, R. W., Kuo, C.-W., and McLaughlin, D. K., "Experimental comparison of supersonic jets exhausting from military style nozzles with interior corrugations and fluidic inserts," *19th AIAA/CEAS aeroacoustics conference*, 2013, p. 2186.

[5] Stuber, M., Lowe, K. T., and Ng, W. F., "Synthesis of convection velocity and turbulence measurements in three-stream jets," *Experiments in Fluids*, Vol. 60, No. 5, 2019, pp. 83.

[6] Jordan, P. and Colonius, T., "Wave packets and turbulent jet noise," *Annual review of fluid mechanics*, Vol. 45, 2013, pp. 173–195.

[7] Arndt, R. E., Long, D., and Glauser, M. N., "The proper orthogonal decomposition of pressure fluctuations surrounding a turbulent jet," *Journal of Fluid Mechanics*, Vol. 340, 1997, pp. 1–33.

[8] Tinney, C. and Jordan, P., "The near pressure field of co-axial subsonic jets," *Journal of Fluid Mechanics*, Vol. 611, 2008, pp. 175–204.

[9] Mollo-Christensen, E., "Jet noise and shear flow instability seen from an experimenter's viewpoint," 1967.

[10] Kuo, C.-W., Buisson, Q., McLaughlin, D. K., and Morris, P. J., "Experimental investigation of near-field pressure fluctuations generated by supersonic jets," *19th AIAA/CEAS aeroacoustics conference*, 2013, p. 2033.

[11] Suzuki, T. and Colonius, T., "Instability waves in a subsonic round jet detected using a near-field phased microphone array," *Journal of Fluid Mechanics*, Vol. 565, 2006, pp. 197–226.

[12] Piot, E., Casalis, G., Muller, F., and Bailly, C., "Investigation of the PSE approach for subsonic and supersonic hot jets. Detailed comparisons with LES and linearized Euler

equations results," *International Journal of Aeroacoustics*, Vol. 5, No. 4, 2006, pp. 361–393.

Chapter 2

Review of Literature

2.1 Components of Supersonic Jet Noise

The noise radiated by supersonic jets is generated by three distinct mechanisms: screech, broad-band shock associated noise, and turbulent mixing noise [1]. While the focus of this dissertation is on turbulent mixing noise, a brief overview of the production mechanisms and radiation characteristics of each noise type is discussed.

Broad-band shock-associated noise is produced by the non-linear interaction between coherent turbulent structures and quasi-periodic shock cell structures. This produces noise over a broad-band range of frequencies that radiates primarily in the upstream direction [2]. Screech noise is produced by an acoustic feedback loop that starts with instability waves produced by excitations to the thin shear layer near the nozzle lip. As the instability wave propagates downstream it grows in amplitude and interacts at some point with the quasi-periodic shock cells. This interaction completes the feedback loop by producing an acoustic disturbance that travels upstream to excite the thin shear layer near the nozzle. This process produces tonal noise that radiates primarily in the upstream direction [3]. The intensity of screech noise decreases with temperature and therefore does not contribute greatly to the radiated noise of tactical air vehicles which typically operate with large total temperature ratios [1].

Turbulent mixing noise is produced by large scale coherent structures that are correlated over distances much larger than the integral turbulence length scale and are characterized by features similar to amplitude modulated instability waves [1]. The high level of coherence of these structures makes them extremely efficient at radiating noise that dominates angles close to the downstream jet axis [4]. Note this is typically where navy personnel working on the decks of aircraft carriers are located. Large scale turbulent mixing noise is the primary focus of the current dissertation and will be elucidated further below.

2.2 The Acoustic Far-field

We begin by describing the general characteristics of sound produced by turbulent mixing noise as measured from what is known as the far-field. The far-field as defined as an area

far away from the turbulent flow where the pressure field is well approximated by the linear acoustic wave equation. In the far-field, the pressure intensity decays radially as r_0^{-2} while in the polar direction, θ_0, the sound field is highly directive, with the peak noise occurring at angles close to the downstream axis [1]. In supersonic jets the peak noise direction is dependent on the velocity of the most energetic coherent structures, u_c. These structures produce intense Mach wave radiation when their convective Mach number is supersonic i.e., $\theta_0 = \cos^{-1} 1/M_c$. Note here the convective Mach number is defined using the ambient speed of sound, $M_c = u_c/c_\infty$ [1]. For cold and moderately heated supersonic jets this leads to peak directivities in the range of $130^\circ < \theta_0 < 160^\circ$. At these angles the peak of the pressure autospectrum typically occurs at Strouhal numbers in the range 0.1<St<0.2, and decays exponentially at offpeak frequencies. Here the Strouhal number is a non-dimensional frequency defined as $St = fD/U_j$. The pressure autospectrum similarly decays exponentially at polar observer angles upstream of the peak, leading to the highly directive nature of the turbulent mixing noise [5, 6]. The over-all sound pressure level (OASPL), or the autospectrum integrated across all frequencies, is a strong function of the velocity of the jet as was first shown by Lighthill [7], where the OASPL scales with the jet velocity as U_j^8. For jets with velocities higher than 600 m/s the OASPL scales with U_j^3 [8].

The character of the far-field is captured by simple models, such as the similarity spectra of Tam et al. [9]. Using an extensive jet noise database the authors preformed an empirical fit of the data and developed similarity spectra representing what they hypothesized were two distinct noise sources; noise produced by large scale turbulence structures and fine scale turbulence. These similarity spectra where shown to adequately predict the shape of the autospectrum of both subsonic and supersonic axisymmetric jets. Unfortunately, because this model is empirical it provides no information about the characteristics of the turbulent noise sources and how they may be manipulated to reduce jet noise. To address this, we begin by summarizing the relationship between features of the turbulence and the radiated acoustic field, starting with the Lighthill equation which provides the exact relationship between the acoustic pressure field and the turbulence sources in the jet.

2.3 Lighthill's Acoustic Analogy

The birth of modern aeroacoustics can be credited directly to the seminal work of Lighthill [7], who for the first time described exactly the relationship between the energetics of a turbulent flow and the radiated acoustic field. This relationship, called Lighthill's equation, is a rearrangement of the governing equations of fluid motion into a "wave-like equation" that describes the sound radiated in a quiescent environment by a turbulent field contained within a limited volume.

$$\frac{\partial^2 \rho}{\partial t^2} - c_\infty^2 \nabla^2 \rho = \frac{\partial^2 T_{ij}}{\partial x_i \partial x_j} \tag{2.1}$$

In the relationship shown above the left-hand side is the familiar acoustic wave equation and describes the propagation of acoustic waves through a stationary, uniform acoustic medium outside of the turbulent field. The term on the right-hand side represents both the generation of sound and how it propagates through the turbulent field. Here T_{ij} is known as Lighthill's stress tensor and is defined as, $T_{ij} = \rho u_i u_j + (p - \rho c_\infty^2)\delta_{ij} - \sigma_{ij}$.

The source term treats the turbulent flow as a uniform acoustic medium that is subjected to an external stress which is equivalent to the difference between the stresses in the real turbulent flow field and the stresses in a uniform acoustic medium. Further, this external stress field will have the directivity and decay characteristics of a field of distributed quadrupole sources whose strength per unit volume is equal to the stress tensor T_{ij}.

The stress tensor T_{ij} also provides insight into the sources of turbulence noise and what terms may be ignored for specific cases. The source is comprised of the turbulence self-interaction term, $\rho u_i u_j$, the compressive stress tensor, p, the density variation, ρ, and the viscous stresses, σ_{ij}. In the case of a turbulent jet with no solid surfaces present, the self-interaction term is the dominate contributor to the stress tensor. For high Reynolds number flows the contribution by the viscous shear stress tensor is minimal and can be neglected. However for cases with large temperature gradients the density term becomes important and cannot be ignored.

Lighthill's formulation is extremely powerful as it explicitly shows the relationship between the acoustic field and the turbulence sources, and thus contains information regarding the acoustically important characteristics of the turbulence. However extracting this information from Lighthill's equation is not a straightforward task. To predict the sound field one must know the space-time correlation of the stress tensor T_{ij} at every point in flow which, especially for heated supersonic jets, is an extremely formidable task. Further, there are other limitations to the original formulation of Lighthill's acoustic analogy, most notably the breakdown that occurs at supersonic Mach numbers. To address these issues a number of studies have built upon the original work of Lighthill to include supersonic convection effects and models for the space-time correlation functions. A number of these studies are discussed below.

2.4 Extensions of the Acoustic Analogy

Of particular relevance to the noise produced by high speed jets is the extension of Lighthill's theory by Ffowcs Williams [8], who included the effect of turbulent convection velocities in the sonic and supersonic ranges. Lighthill [7] showed for low subsonic Mach numbers the convection of an equivalent volume of distributed quadrupole sources augments the quadrupole efficiency by a factor of $(1 - M_c \cos\theta_0)^{-6}$. At sonic speeds this factor becomes singular and represents a breakdown in Lighthill's formulation, indicating a different noise generation mechanism is present in supersonic flows.

This breakdown and the new noise mechanism it indicates can be explained using the idea of the equivalent quadrupole field and how it highlights the relative inefficiency with which turbulence converts kinetic energy into noise. Compared to other sound mechanisms, such as the vibration of a solid object that can be described as a dipole source, a quadrupole is less efficient due to how the waves produced by its substituent sources destructively interfere with each other.

The cancellation effect of the substituent sources of a quadrupole is related to how an observer hears the sound produced by each quadrupole element simultaneously. For this to occur quadrupole components closer the observer must emit later in time. The time lag between the emission of sound from each quadrupole element increases as a quadrupole convects towards an observer and results in a diminished cancellation effect. The increase in the acoustic efficiently of the quadrupole with its convection speed is accounted for by the factor $(1-M_c\cos\theta_0)^{-6}$ mentioned previously. However, when a quadrupole convects towards an observer sonically, the sound radiated by each substituent source cannot destructively interfere and an observer instead hears the noise radiated by the substituent monopoles [8]. At this condition a quadrupole radiates with maximum acoustic efficiency, the efficiency of its substituent monopoles, and produces intense sound waves known as Mach waves. At supersonic speeds a quadrupole continues to radiate at maximum efficiency, but only along directions where the projected velocity is sonic. This leads to the well-known directivity of Mach wave radiation where $\theta_0 = \cos^{-1} 1/M_c$.

Further extensions of Lighthill's acoustic analogy includes models of the space-time correlation of the stress tensor, which can be used to identify acoustically important characteristics of the turbulence. Papamoschou et al. [10] analyzed a general form of the space-time correlation of the Lighthill stress tensor and isolated terms representing the turbulence intensity and the axial and temporal correlation functions, which were shown to be related to the convection speed and coherence length of a turbulence source. By assuming an exponential form for the time correlation the authors demonstrated the acoustic efficiency of turbulence scales non-linearly with its convection speed, suggesting an efficient way to achieve noise reduction is through a reduction in the convection velocity. Further they showed that while turbulence intensity is important to noise production, large reductions in the turbulent kinetic energy (around 50%) are needed to provide any reasonable decrease in noise ($\sim$ 3dB). While the axial and radial correlation functions are known to be major contributors to the acoustic efficiency of turbulence Papamoschou [11] states the ability of jet noise reduction techniques to break up large coherent structures located far from the nozzle region is unclear, given the tendency of the shear layer to reorganize itself into large vorticial motions [12].

Equivalent source models, while useful in regards to their ability to identify some of the salient characteristics of turbulent mixing noise, still suffer in their ability to accurately predict the far-field radiated sound, particularly in the peak noise direction. Fortunately, much progress has been made on other fronts involving the identification and description of large scale turbulent structures. A summary of the characteristics of these features and the efforts to describe them using simple models is presented below.

2.5 Large scale Turbulent Structures

It was not until the early 1960's that it was first discovered that the turbulence present in the jet plume is not entirely stochastic, i.e., the turbulent field is not comprised of many small, statistically independent quadrupole volume sources [13, 14]. Rather, there exist large scale features that are characterized by correlation lengths much larger than the integral turbulence length scale. These large scale structures are extremely efficient at radiating noise and dominate the far-field at angles close to the downstream axis. Therefore, understanding the characteristics of these features is integral to developing a description of the acoustically relevant characteristics of the turbulence development and how they may be augmented by changes in the jet boundary condition. In the rest of this section we highlight characteristics of the large scale turbulent structures in the turbulent flow field and the pressure near-field, as well as summarize some of the major instability-based modeling efforts.

2.5.1 Signatures in the Turbulent Flow Field

A visual example of the extensive axial coherence of the large scale instabilities was shown by Moore [15], who conditionally averaged schlieren imaging using Fourier decomposed pressure signals from an azimuthal ring of microphones located near the shear layer. Sets of schlieren images were conditionally averaged using a trigger event defined using of peaks of the zeroth and first Fourier modes of the microphone signal. The resulting conditionally averaged schlieren images captured the axisymmetric and helical shape of the zeroth mode and first Fourier modes and demonstrate the high level of organization and axial coherence that characterizes these large scale structures.

The extensive axial coherence of these structures was measured quantitatively by Fuchs [14] who, using pressure measurements of the turbulent plume, showed these features were correlated over distances much larger than the integral length scale in the axial, radial, and azimuthal directions. Further, these structures also convect, and are characterized by a relatively constant convection velocity in the developmental region of the jet [16, 17, 18]. In high subsonic and supersonic jets the convection speed has typically been shown to be $\sim 0.7u_c/U_j$ [19].

While the large scale turbulence displays extensive coherence, they comprise a relatively low amount of energy compared to the much more energetic, random turbulence. Because of this, extracting the features of the coherent structures in the velocity field is not straightforward and relies on decomposition methods such as proper orthogonal decomposition to isolate the coherent structure of the flow field [4]. This difficultly is often mitigated by measuring the signature of these structures from the pressure field directly outside of the shear layer in an area called the near-field.

2.5.2 Signatures in the Acoustic Near-field

The characteristics of the large scale turbulent structures can also be captured by measuring their convective 'footprint' in the pressure field directly outside of the shear layer.This area, called the near-pressure field, is advantageous as it filters out the highly energetic, acoustically inefficient fluctuations of the more disorganized turbulence. Further, because pressure is a scalar field there is a significant reduction in the complexity of the experimental measurements and its statistical processing. These characteristics lead Keast and Maidanik [20] to describe the near-field as providing, "a unique means for studying the turbulence within."

For present purposes, the near-field is defined as the area outside of the rotational shear layer where the pressure fluctuations are small enough to be considered linear but not all fluctuations are acoustic. These non-acoustic pressure fluctuations are called hydrodynamic noise, or pseudo sound, and are characterized by an intensity that decays as r^{-6}. The boundary between the near-field and far-field is not a rigidly defined place in space, but rather it is frequency dependent. Arndt et al. [21] identified the edge of the near-field as consistent with an abrupt change in the shape of the pressure spectrum that occurred in the range $1 < ky_s < 2$, where k is the wavenumber magnitude and y_s is the distance to the shear layer center. This change in spectral shape represents the quickly decaying, energetic hydrodynamic field giving way to a purely acoustic field. Because the hydrodynamic fluctuation decays so quickly it captures relatively local information representing the convective signature of the large scale turbulence directly beneath in the shear layer. This implies that to fully capture the "footprint" of the underlying large scale structures, measurements must be made very close to the shear layer.

The signature of the large scale structures in the near pressure field are typically measured using extensive microphone arrays and extracted from the pressure signal using decomposition methods such as spectral proper orthogonal decomposition (SPOD) or Fourier decomposition [21, 22, 23]. These methods decompose the pressure field into orthogonal modes, or eigen vectors. In the case of SPOD this is a set of eigen vectors that optimally captures the signal variance within a frequency bin. A majority of the energy in the near-field is contained in the first few modes, with the zeroth mode typically dominating. This is shown to be true for both stream-wise SPOD modes and azimuthal Fourier modes in jets operating at a range of Mach numbers and temperatures, including unheated subsonic jets [21], heated high-subsonic jets [23] and heated supersonic jets [24]. Further, the eigenvectors of these decomposition analyses resemble instability waves, with amplitudes that grow, saturate, and decay with their axial evolution. High frequency waveforms saturate at locations close to the nozzle exhaust while the amplitude of lower frequency components saturated at locations further downstream.

We emphasize that many experimental studies measure only the axial and azimuthal wavenumbers in the near pressure field, with very few studies examining the radial wavenumber component. The reasons for this are likely two-fold; doing so would increase the number of sensors and the complexity of the measurement and that most studies assume the ax-

ial wavenumber component captures most of the relevant characteristics of the large scale structures.

The current dissertation aims to address this by measuring the both the axial and radial wavenumber components of the near-field by using the radial density gradient obtained from time resolved schlieren. Note that while schlieren provides path integrated quantities, because the axisymmetric mode contains a majority of the fluctuation energy, integration effects due to non-axisymmetric modes is likely to be small.

2.6 Instability-based Models

The large scale structures present in turbulent jets, when extracted from the velocity or pressure fields using decomposition methods such as SPOD, display characteristics similar to amplitude modulated instability waves. In response to this much work has been done to model the evolution of these large scale structures using instability-based analyses that describe the evolution of perturbations to the base flow using modal solutions.

In the literature there exist various approaches which are differentiated by the ansatz used. An ansatz, meaning approach in German, comprises the framework of the instability analysis used. This includes the type of stability analysis (linear or non-linear), the assumptions built into it (parallel flow, weakly parallel flow, etc.), and the type of base flow used as an input.

From a basic viewpoint these different instability analyses model the large scale structures as convecting instabilities. In the case of a traveling wave with constant amplitude, theory predicts it will only produce hydrodynamic pressure fluctuations when convecting with subsonic phase speeds. However, if the homogenous wave convects supersonically it will radiate intense Mach waves and can be thought of as analogous to fluid moving supersonically over a wavy wall [1]. An advecting pressure disturbance with a subsonic convection velocity will radiate noise if it has an amplitude that varies with axial distance [25]. In this case the convecting disturbance is comprised of a spectrum of wavenumbers and will have wave components with supersonic phase speeds. It is in this way a 'wave packet' with a subsonic group velocity can radiate noise. The amount of energy radiated by a wave packet depends on its envelope, with specific forms producing a superdirective acoustic field [25], which occurs when the radiated sound decays exponentially with polar angle, as is observed in the far-field of free jets.

One of the most well-known instability models is the linear instability wave solution of Tam and Chen [26] and its extensions [27, 28, 29]. In developing the ansatz for this stability analysis a few insightful assumptions are made regarding the physical behavior of the flow. First because the spreading rate of the mean flow in high speed jets is a weak function of axial distance, Tam and Chen [26] assumed the local changes in the turbulence statistics are negligible. This assumption allows the large scale fluctuations to be represented by a superposition of normal wave modes, n, and leads to the following expression:

$$p(r,\theta,x,t) = \sum_{-\infty}^{\infty} \int a_n(\omega) \frac{\hat{p}_n(r,x,\omega)}{|\hat{p}_n(r_{0.5},x,\omega)|} e^{\theta_n + n\phi - \omega t + \pi/2} d\omega \tag{2.2}$$

Here $\hat{p}_n(r,x,\omega)$ is the instability wave eigenfunction, $r_{0.5}$ is the radial location where the local mean velocity is half the mean velocity at the centerline, $\hat{p}_n(r_{0.5},x,\omega)$ is a normalization factor, $a_n(\omega)$ is the stochastic amplitude and $\theta_n = \int_0^\infty k_n(x,\omega)dx$. The stochastic amplitude function is modeled by making the assumption that the flow at the nozzle exhaust has no intrinsic length or time scale, owing to how the shear layer at this location is extremely thin. This implies all quantities with a length and time scale can be non-dimensionalized by the axial location, x, and the time term x/U_j. Tam and Chen [26] demonstrated the self-similarity the turbulence statistics by showing the axial turbulence spectra measured at various axial locations collapsed when plotted versus the Strouhal number, $St = fx/U_j$. This fact is an integral part of the linear instability wave model as it allows the wave amplitude to be modeled as if it were generated by random excitations at the nozzle lip.

The formulation above, however, has the major limitation that the amplitude of the instability wave remains constant, which is a consequence of the parallel flow assumption implicit in its formulation. As a consequence the model only predicts Mach wave radiation and cannot be applied to jets with subsonic convection speeds. This issue was resolved by Tam and Morris [28], who extended the original linear instability wave solution to account for spatially-growing instability waves using the method of multiple-scales expansion. The method of multiple-scales expansion, while typically referred to as a locally parallel solution, does account for the divergence of the mean flow and the spatial growth of disturbances. However, this method is not completely adequate as is it can only describe the evolution of disturbances inside the shear layer and cannot be applied to the acoustic field [30]. A uniformly valid linear instability wave solution was introduced by Tam and Burton [27]. Here the authors used the method of matched asymptotic expansions to match an inner solution, which describes the instability waves in the flow field, to an outer solution constructed with the Fourier transform that describes the propagation of sound in an acoustic field. Note in this formulation the authors only considered the evolution of a single instability wave. A complete linear instability wave solution capable of predicting the far-field was finally introduced by Tam and Chen [29], who built on the work of Tam and Burton [27] to consider a spectrum of instability waves. The authors compared the predicted sound field with the experimental far-field narrowband spectra measurements of Seiner et al. [6] and found the model agreed favorably at peak directives and high frequencies for a Mach 2 jet at varying temperatures.

While the linear instability models of Tam and co-authors are capable of modeling some of the salient features of the large scale instabilities, they do have disadvantages that can be improved upon. First linear instability models are incapable of predicting the overall amplitude of the instability wave. In the model of Tam and Chen [29] a constant related to the stochastic amplitude $a_n(\omega)$ was selected to provide a best fit between the measured

far-field spectra and the linear instability solution results. Further, while the method of multiple-scales expansion does account for a weakly diverging flow, it still assumes the jet flow is locally parallel and will break down for certain conditions. For jets with high Mach numbers the locally parallel assumption may be adequate, but will begin to fail for lower Mach number flows with higher shear layer spreading rates. Further the locally parallel solution breaks down at locations downstream of the potential core collapse and for low frequencies where the instability wavelength is comparable to the length of the potential core [22].

Recent instability-based models have overcome many of the issues of linear instability analysis by using the parabolized stability equations (PSE). Fundamentally, PSE decomposes each mode into two features; an amplitude function that varies slowly with axial distance and a wave function described by wavenumbers that similarly vary slowly. The resulting decomposition is then introduced in the linearized Navier-Stokes equations and parabolized by neglecting specific terms [12]. The resulting set of equations can more accurately describe the evolution of disturbances in a spreading jet and avoids many of the difficult numerical integration associated with linear instability analysis [30, 31].

Examples of PSE used to predict the far-field narrowband spectra include Sinha et al.[32], who extended the work of Gudmundsson and Colonius [33] and utilized the parabolized stability equations (PSE) informed by the mean flow field of an LES database. The authors demonstrated the PSE model prediction agreed well with the most energetic coherent component of the POD decomposed LES pressure and velocity fields. Further the authors compared the far-field acoustics predicted by the LES and the PSE model by projecting the pressure field of each using a Kirchoff surface. The PSE model matched the LES prediction quite well for peak directivity angles over almost all frequencies, but showed discrepancies for angles upstream of the peak.

Instability analyses are powerful in their ability to link the base flow to the evolution to large scale instabilities and provide insight into how the mean flow distribution can modify the acoustically important characteristics of the large scale structures. Next we present an overview of the various ways jet noise reduction techniques change the boundary condition at the nozzle exhaust to impact these acoustically important quantities and achieve noise reduction.

2.7 Jet Noise Reduction Techniques

The principal goal of jet noise research is to identify the acoustically important characteristics of the plume turbulence in an effort to understand how these characteristics may be modified to reduce their acoustic efficiency while minimizing thrust loss and changes to the engine architecture. Fundamentally, jet noise reduction techniques function by altering the turbulent plume development through modifications to the nozzle boundary condition.

These various nozzle boundary condition changes modify different aspects of the turbulence and thus have varying degrees of success in reducing the radiated noise. A number of jet noise reduction techniques are summarized to follow.

Chevrons are a jagged sawtooth pattern cut into the edge of the nozzle lip that encourages rapid mixing of the shear layer directly downstream of the nozzle. This modification to the nozzle geometry breaks up the formation of large scale structures in the upstream regions of the jet and results in far-field reductions at low frequencies [23]. The increased turbulent mixing also has the effect of increasing high frequency noise in what is typically termed 'high frequency lift' [34]. For supersonic over-expanded jets this effect is particularly noticeable as there is a large increase in the broad-band shock associated noise (BBSAN) which effectively cancels out the noise reduction benefit. This drastic increase in BBSAN is primarily due to the increase in the intensity of the turbulence that interacts with shock structures present in the jet [35].

Another noise reduction method is fluidic injection, which involves the injection of fluid into the expansion section of the nozzle or directly into the jet plume at the nozzle exhaust plane. This increases the streamwise vorticity of jets, promotes rapid mixing near the nozzle exhaust, and has shown to reduce all forms of jet noise with reductions up to 5dB OASPL [36, 37, 38, 39].

Recent studies of multi-stream jets have examined the acoustic noise benefits of offsetting the centered plume to create non-axisymmetric designs. This results in the shear layer between the center and outermost plume having a locally 'thinner' and 'thicker' side and has shown to produce global changes in the turbulence development of the outermost shear layer. Most notable of these characteristics is a reduction of the convection velocity of turbulent structures downstream of the potential core collapse [40]. These changes in the turbulence structure are associated with reductions of up to 8 dB in the narrowband sound pressure level at azimuthal locations aligned with the "thick" side of the jet [41]. While the offset is also accompanied by an increase in the sound pressure level at azimuthal angles aligned with the "thin" side of the jet [42], it implies the azimuthal directivity could be shaped in such a way to reduce noise at specific directives e.g., where navy personnel stand.

A jet noise reduction technique that is similar to the topic of the current dissertation are inverted velocity profile (IVP) jets. These are multi-stream jets where the inner core jet operates at a slower velocity then the higher speed bypass flow. Tanna [43] studied the noise benefits of these jets extensively as compared to a fully mixed equivalent (FMEQ). Here a FMEQ jet is defined as a uniform profile jet with the same area, mass flowrate, and thrust as the IVP jet being compared. IVP jets have shown to reduce the radiated noise at low frequencies while also slightly increasing noise at higher frequencies, resulting in reductions of up to 4 dB OASPL [43]. IVP jets also display similarities to axisymmetric thermal non-uniformities in how the centerline flow operates with a reduced velocity. However we emphasize the way these velocity deficits are driven are fundamentally different. Thermally non-uniform jets are single stream plumes with an area of reduced velocity driven by a

tailored total temperature distribution at the nozzle exhaust while IVP jets are multi-stream jet where the centermost jet operates at a slower velocity.

We note that all the described jet reduction techniques, with the exception of IVP jets, alter the nozzle boundary conditions along the outer circumference of the nozzle. We emphasize this point because the ability of these techniques affect large scale structures at locations far downstream from the nozzle exhaust is not clear [11]. Due to the natural tendency of the shear layer to organize itself into large vortical motions [12], altering the shear layer immediately downstream of the nozzle exhaust plane may not be the most efficient method to reduce turbulence mixing noise. The acoustic efficiency of large scale structures increases with their correlation length scales, which are known to grow with axial distance. Thus given a certain amount of energy with which the flow can be perturbed, it may be best to reduce the acoustic efficiency of large scale structures at downstream locations. This idea is the driving concept behind the centered thermal non-uniformity, which introduces perturbations along the centerline of the jet axis with the hypothesis that they will interact and disrupt the development of large scale structures at locations far downstream of the nozzle exhaust.

2.8 Concluding Remarks

The literature review above addresses the key concepts needed to set the groundwork for the analyses presented in chapters 3 and 4 and identifies the gaps in the current state of knowledge. Most importantly is the concept of large scale structures. These features are characterized by correlation lengths much larger than the integral turbulent length scale and can be modeled as linear instability waves with amplitudes that grow, saturate, and decay with axial distance. Another important characteristic of these structures is their convection velocity, which dictates the type of noise generated. At supersonic convection speeds these structures produce intense Mach wave radiation while at subsonic speeds they will radiate acoustic waves that dominate angles close to the downstream axis.

The signature of large scale structures can be measured indirectly from the near-field outside of the shear layer. The near pressure field filters out the more energetic, random, turbulent fluctuations and contains rapidly decaying hydrodynamic information that represents the convective footprint of the coherent structure in the shear layer directly beneath. Note that studies that examine the near-field pressure typically use extensive microphone arrays that are typically spaced in the axial and circumferential directions [22, 23]. These arrays are not spatially resolved and therefore cannot provide a visual representation of the spatial evolution of small wavelength features. This is especially true in the radial direction where the radial wavenumber component of structures is rarely measured.

The features of these large scale structures most relevant to their acoustic efficiency is their convection speed and correlation length scale. Most of the current jet noise techniques impact these characteristics by inducing perturbations directly into the shear layer at the nozzle

exhaust plane. As mentioned by Papamoschou [11], perturbations introduced to the shear layer directly near the nozzle may have a limited effect on the size of the spatial correlations in regions far downstream. Very few studies, if any at all, have examined the effect on the turbulence development when perturbations are introduced along the jet centerline.

The gaps in the literature expressed above are addressed by the studies presented in chapters 3 and 4, which examine the far-field and near-field characteristics of a heated supersonic jet with a centered thermal non-uniformity. The temperature-driven centerline velocity deficit introduced by the centered thermal non-uniformity is hypothesized to induce perturbations along the jet centerline that convect downstream and alter the structure of coherent turbulence at locations far from the nozzle exhaust. This dissertation evaluates that hypothesis by studying the structure of the near-field indirectly via a far-field-informed model of the near-field wavenumber-frequency spectra and directly using space-time correlations of time-resolved schlieren measurements.

Bibliography

[1] Tam, C. K., "Supersonic jet noise," *Annual review of fluid mechanics*, Vol. 27, No. 1, 1995, pp. 17–43.

[2] Tanna, H., "An experimental study of jet noise part II: Shock associated noise," *Journal of Sound and Vibration*, Vol. 50, No. 3, 1977, pp. 429–444.

[3] Raman, G., "Supersonic jet screech: half-century from Powell to the present," *Journal of Sound and Vibration*, Vol. 225, No. 3, 1999, pp. 543–571.

[4] Jordan, P. and Colonius, T., "Wave packets and turbulent jet noise," *Annual review of fluid mechanics*, Vol. 45, 2013, pp. 173–195.

[5] Tanna, H., "An experimental study of jet noise Part I: Turbulent mixing noise," *Journal of sound and Vibration*, Vol. 50, No. 3, 1977, pp. 405–428.

[6] Seiner, J. M., Ponton, M. K., Jansen, B. J., and Lagen, N. T., "The effects of temperature on supersonic jet noise emission," *14th DGLR/AIAA aeroacoustics conference*, Vol. 1, 1992, pp. 295–307.

[7] Lighthill, M. J., "On sound generated aerodynamically I. General theory," *Proceedings of the Royal Society of London. Series A. Mathematical and Physical Sciences*, Vol. 211, No. 1107, 1952, pp. 564–587.

[8] Ffowcs Williams, J., "The noise from turbulence convected at high speed," *Philosophical Transactions of the Royal Society of London. Series A, Mathematical and Physical Sciences*, Vol. 255, No. 1061, 1963, pp. 469–503.

[9] Tam, C., Golebiowski, M., and Seiner, J., "On the two components of turbulent mixing noise from supersonic jets," *Aeroacoustics conference*, 1996, p. 1716.

[10] Papamoschou, D., Xiong, J., and Liu, F., "Reduction of radiation efficiency in high-speed jets," *20th AIAA/CEAS aeroacoustics conference*, 2014, p. 2619.

[11] Papamoschou, D., "Modelling of noise reduction in complex multistream jets," *Journal of Fluid Mechanics*, Vol. 834, 2018, pp. 555–599.

[12] Fiedler, H., "Coherent structures in turbulent flows," *Progress in Aerospace Sciences*, Vol. 25, No. 3, 1988, pp. 231–269.

[13] Mollo-Christensen, E., "Jet noise and shear flow instability seen from an experimenter's viewpoint," 1967.

[14] Fuchs, H. V., "Space correlations of the fluctuating pressure in subsonic turbulent jets," *Journal of sound and vibration*, Vol. 23, No. 1, 1972, pp. 77–99.

[15] Moore, C., "The role of shear-layer instability waves in jet exhaust noise," *Journal of Fluid Mechanics*, Vol. 80, No. 2, 1977, pp. 321–367.

[16] Bradshaw, P., Ferriss, D. H., and Johnson, R., "Turbulence in the noise-producing region of a circular jet," *Journal of Fluid Mechanics*, Vol. 19, No. 4, 1964, pp. 591–624.

[17] Davies, P., Fisher, M., and Barratt, M., "The characteristics of the turbulence in the mixing region of a round jet," *Journal of Fluid Mechanics*, Vol. 15, No. 3, 1963, pp. 337–367.

[18] Lau, J., Fisher, M., and Fuchs, H., "The intrinsic structure of turbulent jets," *Journal of Sound and Vibration*, Vol. 22, No. 4, 1972, pp. 379–406.

[19] Liu, J., Corrigan, A. T., Kailasanath, K., and Gutmark, E. J., "Effects of temperature on noise generation in supersonic jets," *22nd AIAA/CEAS Aeroacoustics Conference*, 2016, p. 2937.

[20] Keast, D. and Maidanik, G., "Studies of the near-field noise properties of a small air jet Final report," 1966.

[21] Arndt, R. E., Long, D., and Glauser, M. N., "The proper orthogonal decomposition of pressure fluctuations surrounding a turbulent jet," *Journal of Fluid Mechanics*, Vol. 340, 1997, pp. 1–33.

[22] Suzuki, T. and Colonius, T., "Instability waves in a subsonic round jet detected using a near-field phased microphone array," *Journal of Fluid Mechanics*, Vol. 565, 2006, pp. 197–226.

[23] Tinney, C. and Jordan, P., "The near pressure field of co-axial subsonic jets," *Journal of Fluid Mechanics*, Vol. 611, 2008, pp. 175–204.

[24] Kuo, C.-W., Buisson, Q., McLaughlin, D. K., and Morris, P. J., "Experimental investigation of near-field pressure fluctuations generated by supersonic jets," *19th AIAA/CEAS aeroacoustics conference*, 2013, p. 2033.

[25] Crighton, D. and Huerre, P., "Shear-layer pressure fluctuations and superdirective acoustic sources," *Journal of Fluid Mechanics*, Vol. 220, 1990, pp. 355–368.

[26] Tam, C. K. and Chen, K., "A statistical model of turbulence in two-dimensional mixing layers," *Journal of Fluid Mechanics*, Vol. 92, No. 2, 1979, pp. 303–326.

[27] Tam, C. K. and Burton, D. E., "Sound generated by instability waves of supersonic flows. Part 2. Axisymmetric jets," *Journal of Fluid Mechanics*, Vol. 138, 1984, pp. 273–295.

[28] Tam, C. K. and Morris, P. J., "The radiation of sound by the instability waves of a compressible plane turbulent shear layer," *Journal of Fluid Mechanics*, Vol. 98, No. 2, 1980, pp. 349–381.

[29] Tam, C. K. and Chen, P., "Turbulent mixing noise from supersonic jets," *AIAA journal*, Vol. 32, No. 9, 1994, pp. 1774–1780.

[30] Malik, M. and Chang, C.-L., "Nonparallel and nonlinear stability of supersonic jet flow," *Computers & fluids*, Vol. 29, No. 3, 2000, pp. 327–365.

[31] Yen, C. and Messersmith, N., "Application of parabolized stability equations to the prediction of jet instabilities," *AIAA journal*, Vol. 36, No. 8, 1998, pp. 1541–1544.

[32] Sinha, A., Rodríguez, D., Brès, G. A., and Colonius, T., "Wavepacket models for supersonic jet noise," *Journal of Fluid Mechanics*, Vol. 742, 2014, pp. 71–95.

[33] Gudmundsson, K. and Colonius, T., "Instability wave models for the near-field fluctuations of turbulent jets," *Journal of Fluid Mechanics*, Vol. 689, 2011, pp. 97–128.

[34] Mengle, V., "Jet noise characteristics of chevrons in internally mixed nozzles," *11th AIAA/CEAS Aeroacoustics Conference*, 2005, p. 2934.

[35] Rask, O., Kastner, J., and Gutmark, E., "Understanding how chevrons modify noise in supersonic jet with flight effects," *AIAA journal*, Vol. 49, No. 8, 2011, pp. 1569–1576.

[36] Arakeri, V., Krothapalli, A., Siddavaram, V., Alkislar, M., and Lourenco, L., "On the use of microjets to suppress turbulence in a Mach 0.9 axisymmetric jet," *Journal of Fluid mechanics*, Vol. 490, 2003, pp. 75–98.

[37] Krothapalli, A., Arakeri, A., Greska, B., and Joseph, T., "High speed jet noise reduction using microjets," *8th AIAA/CEAS Aeroacoustics Conference & Exhibit*, 2002, p. 2450.

[38] Alkislar, M. B., Krothapalli, A., and Butler, G., "The effect of streamwise vortices on the aeroacoustics of a Mach 0.9 jet," *Journal of Fluid Mechanics*, Vol. 578, 2007, pp. 139–169.

[39] Powers, R. W., Kuo, C.-W., and McLaughlin, D. K., "Experimental comparison of supersonic jets exhausting from military style nozzles with interior corrugations and fluidic inserts," *19th AIAA/CEAS aeroacoustics conference*, 2013, p. 2186.

[40] Stuber, M., Lowe, K. T., and Ng, W. F., "Synthesis of convection velocity and turbulence measurements in three-stream jets," *Experiments in Fluids*, Vol. 60, No. 5, 2019, pp. 83.

[41] Henderson, B. S. and Leib, S. J., "Measurements and predictions of the noise from three-stream jets," *21st AIAA/CEAS aeroacoustics conference*, 2015, p. 3120.

[42] Henderson, B. S. and Huff, D. L., "The aeroacoustics of offset three-stream jets for future commercial supersonic aircraft," *22nd AIAA/CEAS Aeroacoustics Conference*, 2016, p. 2992.

[43] Tanna, H., "Coannular jets — Are they really quiet and why?" *Journal of Sound and Vibration*, Vol. 72, No. 1, 1980, pp. 97–118.

Chapter 3

Use of Thermal Non-Uniformity to Reduce Supersonic Jet Noise

Check for updates

Use of Thermal Nonuniformity to Reduce Supersonic Jet Noise

Kyle A. Daniel,* David E. Mayo, Jr.,† K. Todd Lowe,‡ and Wing F. Ng§
Virginia Polytechnic Institute and State University, Blacksburg, Virginia 24061

DOI: 10.2514/1.J058531

It is shown experimentally that thermal nonuniformity can reduce peak supersonic jet noise while keeping static thrust levels equivalent. A thermal nonuniformity is generated by introducing an unheated stream on the centerline of a plenum containing heated air. This axisymmetric arrangement was studied with the hypothesis that the convection and structure of plume turbulence could be changed by perturbations induced by the thermal nonuniformity. The results for ideally expanded and overexpanded jets indicate 2 ± 0.5 dB reductions in peak narrowband spectral sound pressure levels upstream of peak directivity directions for nonuniform jets compared with the baseline uniform jets, even for a modest temperature difference between the core jet and the unheated stream. The mechanisms for this reduction are examined based on wavenumber–frequency analyses using the far-field acoustic spectra, suggesting that peak spectral energies shift to higher wavenumbers when the thermal nonuniformity is introduced. Convection velocities of radiating structures calculated from the spectral peaks show a reduction of 10% for the design jet condition. These results indicate that temperature-driven velocity deficits may be useful for developing supersonic jet noise reduction strategies, while even greater reductions are thought feasible by increasing the ratio between the heated and unheated stream temperatures.

Downloaded by VIRGINIA TECH on September 27, 2019 | http://arc.aiaa.org | DOI: 10.2514/1.J058531

Nomenclature

A	=	nondimensional constant
a	=	radius of cylindrical surface, m
c_∞	=	ambient sound speed, m/s
D	=	primary jet exit diameter, m
f	=	frequency, Hz
f_c	=	characteristic frequency; U/D
f_s	=	sampling frequency, Hz
G_{11}	=	single-sided power spectral density of the far-field pressure, Pa^2/Hz
$H_0^{(1)}$	=	Hankel function of first kind
k	=	wavenumber, 1/m
M	=	Mach number
$\dot{m}$	=	mass flow rate, kg/m^3
NPR	=	nozzle pressure ratio; p_0/p_∞
N_{rec}	=	number of records
p	=	pressure, Pa
p_{ref}	=	reference pressure, Pa
R	=	microphone radius location, m
Re	=	Reynolds number; $\rho UD/\mu$
St	=	Strouhal number; fD/U
S_{11}	=	wavenumber–frequency spectrum on cylindrical surface, $(\text{Pa}^2 \cdot \text{m})/\text{Hz}$
$\mathcal{T}$	=	static jet thrust, N
T	=	temperature, K
TTR	=	total temperature ratio; T_0/T_∞
U	=	velocity, m/s
U_{eq}	=	equivalent velocity ratio, m/s
U_p/U_s	=	velocity ratio of outer to inner streams
u_c	=	convection velocity, m/s
u'	=	fluctuating velocity, m/s
x	=	jet axial coordinate relative to exhaust, m
y	=	jet vertical coordinate relative to centerline, m
z	=	jet horizontal coordinate relative to centerline, m
ΔC_{atm}	=	atmospheric correction
$\delta[]$	=	uncertainty interval operator
ρ	=	density, kg/m^3
Θ	=	Mach wave angle, deg
θ_0	=	polar angle, measured from jet upstream axis, deg
ω	=	radian frequency, rad/s

Subscripts

d	=	design condition
j	=	uniform jet exit condition
p	=	primary heated jet stream condition
$peak$	=	associated with peak wavenumber spectra amplitude
raw	=	uncorrected measurement
s	=	unheated secondary jet stream condition
x	=	axial component
0	=	total condition or angle referenced to the jet upstream axis
∞	=	ambient condition

Presented as Paper 2019-1300 at the AIAA SciTech Form, San Diego, CA, 7–11 January 2019; received 1 April 2019; revision received 22 August 2019; accepted for publication 27 August 2019; published online 25 September 2019. Copyright © 2019 by the authors. Published by the American Institute of Aeronautics and Astronautics, Inc., with permission. All requests for copying and permission to reprint should be submitted to CCC at www.copyright.com; employ the eISSN 1533-385X to initiate your request. See also AIAA Rights and Permissions www.aiaa.org/randp.

*Graduate Research Assistant, Department of Aerospace & Ocean Engineering. Student Member AIAA.

†Graduate Research Assistant, Department of Mechanical Engineering. Student Member AIAA.

‡Associate Professor, Department of Aerospace & Ocean Engineering. Associate Fellow AIAA.

§Alumini Distinguished Professor of Engineering, Department of Mechanical Engineering. Fellow AIAA.

I. Introduction

JET noise has become a topic of increasing concern over the last few decades, driven by increasingly stringent community noise requirements [1], hearing damage experienced by personnel on the deck of aircraft carriers [2], and renewed interest in overland supersonic transport [3]. Reducing the noise produced by tactical aircraft without compromising the stringent thrust, weight, and performance requirements set for these vehicles has proven to be a difficult task [4]. Despite these challenges many noise reduction methods have been developed that focus on altering turbulent mixing in the jet plume.

A variety of concepts have been shown in laboratories to offer some noise reduction benefit for supersonic jets, some of which are highlighted to follow. One such technique involves fluid injection into the diverging section of a supersonic nozzle. This induces the formation of streamwise vortices, increases turbulent mixing in the jet shear layer, and results in reductions of up to 5 dB in the overall sound pressure level (OASPL) in peak directivity directions for overexpanded jets [4]. These results have also been validated by large-eddy simulations [5]. Another noise reduction approach showing particular promise for high subsonic multistream jets is the use of eccentric co-annular nozzles. These configurations produce

Downloaded by VIRGINIA TECH on September 27, 2019 | http://arc.aiaa.org | DOI: 10.2514/1.J058531

non-axisymmetric plumes and have been shown to reduce jet noise when compared with axisymmetric jets at similar conditions. A plume from radially offset co-annular nozzles results in locally thinner and thicker regions of lower-velocity bypass flow around the hotter, faster moving core flow and leads to reductions up to 8 dB in peak noise directions along azimuthal angles aligned with the thicker regions [6,7]. Unfortunately, there is also an increase in narrowband spectral sound pressure levels at locations aligned with the thin side of the jet [8]. A third approach, inverted velocity profile (IVP) jets, makes use of a higher-speed outer-annulus stream and lower-speed inner stream, and has been shown to reduce noise when compared with a fully mixed equivalent jet (FMEQ) by up to 4 dB OASPL [9]. Here, an FMEQ jet is defined as a top hat profile jet with equal mass flow rate, area, and static thrust as compared with the IVP jet. The acoustic benefits of IVP jets have been found to primarily affect low-frequency ranges and have been attributed to significantly lower convection velocities and axial turbulence levels as compared with FMEQ jets.

Flow measurements of asymmetric multistream jets suggest a key mechanism for the acoustic benefit—a reduction in the convection speed of turbulent structures. Using time-resolved Doppler global velocimetry (TR-DGV) and particle image velocimetry (PIV) measurements, Stuber et al. [10] found that, compared with an axisymmetric case, offset jets had a shortened potential core and reduced eddy convection velocities at axial stations downstream of the potential core collapse. Further, the authors found that convection velocities near the core collapse region were much larger ($u_c = 0.8U_J$) than those in the shear layer ($u_c = 0.6U_J$) and hypothesized that these larger convection velocities represented structures produced by the interaction of high-momentum packets from the potential core with coherent turbulence in the shear layer. The authors concluded that the reduced potential core length observed in the offset jet case may alter the interaction between these irrotational core packets and shear layer turbulence, and could lead to the observed decrease in convection velocity. Past evidence supports the hypothesis that a decrease in the convection velocity of fast-moving structures near the core collapse region, and thus a lessening of their acoustic radiation efficiency [11], is a major contributor to the reduced radiated noise observed in offset multistream jets.

Also of relevance are Tam and Parish [12], who developed a model to predict the directivity and intensity of noise produced by the passage of unsteady "hot spots" through a military-style nozzle. The authors modeled these hot spots as a train of entropy wave pulses and predicted that they would radiate intense noise at angles to the downstream axis that are larger than the dominant Mach wave radiation angle.

The methods for jet noise reduction discussed above all involve nozzle modifications that change the mean flow distribution at the nozzle exit. Fundamentally, these amount to tailoring the distribution of temperature, density, and velocity at the nozzle exit and are thus related to the temperature nonuniformity approach presented in this paper. Heated jets with thermal nonuniformities have previously been studied by the current authors [13–17] for both centered and offset placements of a small unheated plume introduced in the nozzle plenum. The resulting axial evolution of the mean flow and turbulent structures in the thermally offset jet displayed striking similarity to multistream offset jets [17]. The centered nonuniformity was shown to create changes in the mean flow and turbulence structure evolution compared with the matched uniform temperature plume, particularly changing the flowfield near the potential core breakdown for the uniform plume [16], warranting the additional acoustics study reported herein. The current results show that a spatially compact, centered thermal nonuniformity reduces peak supersonic jet noise by 2 ± 0.5 dB compared with a thermally uniform jet. This reduction is observed even with equivalent static thrust levels between the uniform and nonuniform jets and despite a relatively modest temperature difference between the heated and unheated streams. Here equivalent static thrust is defined as when the static thrust values of the uniform and nonuniform jets are nearly equal when calculated with measured bulk flow properties. The presented results suggest that this reduction is related to a decorrelation of coherent turbulence, the evidence of which is shown through a shift of peak spectral energies to higher wavenumbers and the reduction in convection velocity of the highest-energy-containing structures.

This paper is organized as follows: Sec. II contains descriptions of the Virginia Tech heated supersonic jet rig and the experimental apparatus used to generate the centered thermal nonuniformity. The key results for far-field narrowband spectra and the wavenumber–frequency analysis using these data are discussed in Sec. III. The paper concludes with Sec. IV, summarizing the findings and their impact.

II. Experimental Methods

A. Jet Facility and Experimental Cases

The Virginia Tech heated supersonic jet rig (Fig. 1a) can support flows with TTR up to 3. The current study uses a contoured round nozzle ($M_d = 1.5$) with an exit diameter of 0.0381 m (1.5 in.), a design nozzle pressure ratio (NPR_d) of 3.67, and a Reynolds number of 8.5×10^5. The nozzle has a lip thickness of $0.013D$, a length of $2.23D$, and a contraction ratio of 2.1. The diverging section profile was designed using the method of characteristics to generate a nearly shock-free flow at design conditions. The profile of this nozzle was graciously provided by Ching-Wen Kuo and Dennis McLaughlin, stemming from their work at Penn State University [18]. Greater detail on the capabilities of the Virginia Tech facility can be found in the literature (e.g., [19]).

Total temperature nonuniformity (Fig. 1b) is created at the jet exit by introducing a secondary unheated air plume into the primary heated jet plenum centerline. Two streams of unheated air are directed into a custom manifold that is integrated into a flange. These streams impinge and accelerate through an interior secondary nozzle that terminates upstream of the throat at $2.23D$ axially upstream from the exhaust plane. The unheated air then advects through the supersonic nozzle and creates a concentrated spot with locally lower total temperature at the nozzle exhaust plane. In the subsequent sections, the centered thermal nonuniformity is referred to as the nonuniform centered (NUC) case.

All flow conditions, summarized in Table 1, are determined from total temperature and pressure measurements of the heated and unheated flows. These measurements were recorded using a National Instruments 9213 thermocouple module in an NI cDAQ-9184 chassis and a Scanivalve Corp. ZOC17IP/8Px-APC pressure transducer.

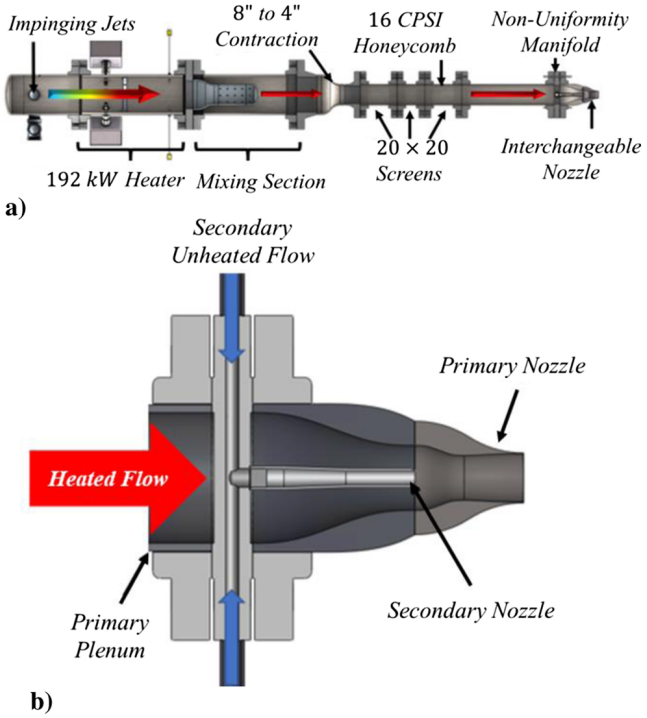

Fig. 1 Diagram of the a) heated supersonic jet rig and b) the centered thermal nonuniformity jet geometry.

Downloaded by VIRGINIA TECH on September 27, 2019 | http://arc.aiaa.org | DOI: 10.2514/1.J058531

Table 1 Experimental flow conditions

		Design		Overexpanded	
Uniform	TTR_j	2		2	
	NPR_j	3.67		2.59	
	$\dot{m}_j$, kg/s	0.56		0.39	
Heated plume	TTR_p	2		2	
	NPR_p	3.67		2.59	
	$\dot{m}_p$, kg/s	0.49	0.49	0.34	0.34
Unheated plume	TTR_s	1.0		1.0	
	NPR_s	3.7	4.6	2.7	4.4
	$\dot{m}_s$, kg/s	0.029	0.059	0.025	0.066
Ratios	$\dot{m}_s + \dot{m}_p/\dot{m}_j$	1.00	1.01	0.99	1.06
	$\mathcal{T}_s + \mathcal{T}_p/\mathcal{T}_j$	0.98	0.99	0.98	1.03

The mass flow rate of the unheated flow was monitored using static temperature and static pressure measurements across a Lambda-Square orifice meter. The total temperature field near the nozzle exhaust plane ($0.04x/D$) for the NUC and uniform cases was characterized using a vented total temperature probe. Data were acquired over a period of 5 s at 676 points spread over a $1.1D \times 1.1D$ grid in increments of $0.04D$.

The NPR of the heated uniform (NPR_j) and heated portion of the NUC (NPR_p) jets was selected to run at design and overexpanded conditions. Measurements at design conditions were performed to isolate the impact of thermal nonuniformity on the turbulent mixing noise from the noise produced by shock–turbulence interactions. Measurements were also conducted at overexpanded conditions to evaluate the impact on flows similar to those produced by carrier-based tactical aircraft at takeoff conditions.

The NPR of the secondary unheated plume in the NUC jet (NPR_s) was examined at two different values, a low blowing case just above NPR_p and a high blowing case far above NPR_p. The low blowing case was selected as it has minimum pressure and mass flow addition effects and is similar to a thermal nonuniformity that could be created in a full-scale engine by selectively heating only portions of the flow in the afterburner. The high blowing case adds additional mass to keep thrust levels between the NUC and uniform jets equivalent and follows similar reasoning to Tanna's comparison of IVP and FMEQ jets [9]. The matched static thrust comparison is also made to evaluate the acoustic benefit when taking into account the propulsion design constraints, while demonstrating that the difference in the radiated sound field is not simply a consequence of reduced thrust. In the following sections the above-described cases are referred to with the abbreviations listed in Table 2.

B. Far-Field Microphone Array

Far-field acoustics were measured using eight $1/4''$ 378C10 PCB microphones, located $100D$ from the jet exhaust plane at polar observer angles (θ_0), measured from the upstream axis—ranging 125° to 160° in increments of 5°.

Data were acquired using a model 482C series sensor signal conditioner and a 16-bit NI PIXe-6358 module over a ± 10 V bipolar range. The 378C10 PCB pressure microphone used has a flat frequency response from 5 Hz to 70 kHz at sound pressure levels up to 173 dB.

The heated jet rig was located on a concrete pad outside the test cell, with a ground microphone array measuring the far-field acoustics. The concrete pad acts as an almost perfect acoustic reflector and can be accounted for by halving the power spectral density. The ground microphone array was designed according to SAE standard AIR 1672B for outdoor far-field measurements, which is used by the aircraft industry to characterize the acoustic far-field of full-scale engines. Further details of the outdoor microphone technique used in this study can be found in the paper by Quinn et al. [20].

Table 2 Case nomenclature

Jet	Condition	NPR_s	Name
NUC	Design	3.7	D-NUC-L
		4.6	D-NUC-H
	Overexpanded	2.7	O-NUC-L
		4.4	O-NUC-H
Uniform	Design	— —	D-U
	Overexpanded	— —	O-U

C. Particle Image Velocimetry

The plume velocity field measurements were obtained using particle image velocimetry (PIV). Two LaVision Imager Pro X sCMOS cameras were mounted with 50 mm focal length Nikon lenses and 532 nm band-pass light filters to image particles illuminated by a 532 nm frequency-doubled Nd:YAG double-pulsed laser. The PIV images were collected using multiple overlapping planes of data that were recorded and postprocessed using LaVision DaVis 8.4 software. To minimize error in the velocity vector calculations, five image correlation passes with progressively smaller interrogation widows were performed on image sets consisting of 5000 and 2000 images for the uniform and NUC cases, respectively. This resulted in a vector spatial resolution of 1 mm × 1 mm ($0.026D \times 0.026D$). During data acquisition, thermal expansion of the jet plenum shifted the jet centerline location and introduced some misalignment into the spatial overlap between the PIV planes. This was accounted for in postprocessing by replacing the velocity at each pixel with a median value determined from samples surrounding the initial point. The velocity uncertainties related to the misalignment have been estimated previously. Information about the uncertainties, setup, and procedure used to record and process the PIV images is provided by Mayo et al. [17].

D. Far-Field Data Processing

Microphone data were sampled at 200 kHz for a 7 s period, resulting in 1.4×10^6 samples per microphone. Before digitization, the signals were amplified and conditioned (including a 100 kHz low-pass filter) using a PCB 428C signal conditioner. Single-sided spectral densities were estimated using the fast Fourier transform MATLAB function, with a Hanning window function and 50% record overlap. The resulting single-sided spectral densities were halved to account for the pressure doubling due to the concrete pad surrounding the facility and converted to uncorrected sound pressure levels (SPL_{raw}) using

$$SPL_{\text{raw}}(f) = 10\log_{10}(G_{11}/p_{\text{ref}}^2) \tag{1}$$

The raw spectra were adjusted by a humidity correction to account for atmospheric absorption [21] and a Strouhal number scaling according to

$$SPL(f) = SPL_{\text{raw}}(f) + \Delta C_{\text{atm}}(f) + 10 \times \log_{10} f_c \tag{2}$$

The 95% confidence interval in the single-sided power-spectral density is calculated according to [22]

$$\delta[G_{11}] = \frac{\sqrt{2}G_{11}}{\sqrt{N_{\text{rec}}}} \tag{3}$$

Estimates for the amplitudes of the wavenumber–frequency spectrum of radiating pressure fluctuations on a cylindrical surface surrounding the jet are determined from an analytical model derived by Morris [23] that makes use of the far-field narrowband spectra measurements. Here, the cylindrical surface is assumed to contain both radiating and nonradiating pressure fluctuations. The random nature of the pressure fluctuations on the surface is modeled following the method of Tam and Chen [24], in which turbulent structures are represented by a superposition of normal wave modes of the flow with amplitudes described by real random functions. In the Morris formulation, only the axisymmetric, zeroth-order azimuthal mode is considered. The amplitudes of the wavenumber spectra at constant frequency for a range of wavenumbers that correspond to varying polar observer angles were shown by Morris to be determined by

$$\frac{A^2|S_{11}((\omega\cos\theta_0)/c_\infty,\,\omega)\,|^2}{D^2} = \frac{\pi}{2}\left(\frac{R}{D}\right)^2 \times\left|H_0^{(1)}\left(\frac{\omega a\sin\theta_0}{c_\infty}\right)\right|^2 \frac{G_{11}(R,\theta_0,\omega)}{\rho_j^2 U_j^3 D} \tag{4}$$

Note that, because far-field acoustic data are used, only radiating wavenumber amplitudes are calculated, that is, $|k| \le \omega/c_\infty$. In the results presented in Sec. III.C, the values of $A|S_{11}((\omega\cos\theta_0)/c_\infty,\omega)|$ for each case are compared to evaluate the relative differences in the wavenumber distribution of the near-field wavenumber–frequency spectral amplitude at specific frequencies. A portion of the error in these comparisons is due to the averaging uncertainty in the narrowband spectra. The uncertainty in the amplitude of the wavenumber spectra is then estimated by calculating its derivative with respect to the single-sided power spectral density.

$$\delta[A|S_{11}((\omega\cos\theta_0)/c_\infty,\omega)|] = \frac{1}{2}\frac{A|S_{11}((\omega\cos\theta_0)/c_\infty,\omega)|}{G_{11}(R,\theta_0,\omega)} \times\delta[G_{11}(R,\theta_0,\omega)] \tag{5}$$

Wavenumbers along the spectral ridge of the wavenumber–frequency spectra provide the frequency-dependent convection velocity of structures when modeled using a wave packet analysis [23] by computing the phase speed,

$$\frac{u_c}{U_j} = \frac{\omega}{k_{\text{peak}}U_j} = \frac{2\pi St}{Dk_{\text{peak}}} \tag{6}$$

where the wavenumber associated with the peak spectral amplitude is used to determine the convection velocity of the highest-energy-containing structures.

III. Results and Discussion

The following section presents evidence that a thermal nonuniformity alters the wavenumber spectra and convection velocity of radiating structures, resulting in a reduction in the peak narrowband sound pressure levels of radiated noise. As mentioned previously the thermally nonuniform and thermally uniform jets will be referred to as the NUC and uniform cases, respectively. Each specific case will be referred to using the abbreviations in Table 2.

A. Plume Characteristics

Before examining the radiated noise results, it is insightful to consider the plume characteristics for both cases. Flowfield measurements have been obtained at the exit of the nozzle using a total temperature probe and in the axial/transverse planes using PIV.

The average total temperature exhaust profiles for both uniform and NUC jets are illustrated in Figs. 2a and 2b. The uniform (Fig. 2a) and the heated portion of the NUC jet (Fig. 2b) have a uniform temperature distribution with a 2.4% root-mean-square variation in TTR. In the NUC jet, a concentration of fluid with locally lower total temperature is observed. The unheated stream that produces this nonuniformity is initially injected at ambient temperature ($TTR = 1$). The increased local minimum TTR of 1.2 at the exhaust plane as shown in Fig. 2b is the result of mixing that occurs between the unheated plume and the surrounding heated flow.

To quantify the effect of the temperature nonuniformity on the velocity field, mean axial velocity contours from PIV measurements

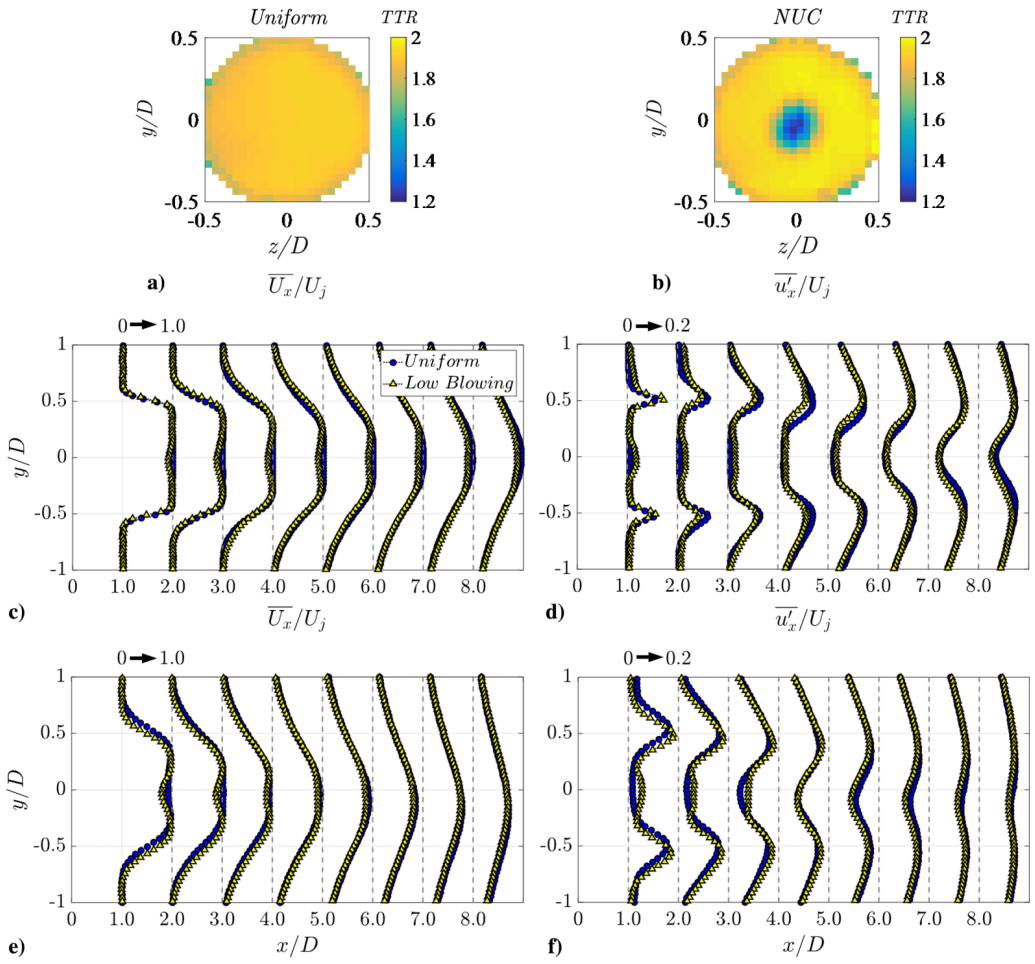

Fig. 2 Plume flowfield measurements. TTR contours at the nozzle exhaust plane for a) the uniform and b) NUC jets. Radial profiles of mean axial velocity of c) D-NUC-L, D-U cases and e) O-NUC-L, O-U cases. Mean axial turbulence levels of d) D-NUC-L, D-U cases and f) O-NUC-L, O-U cases.

Downloaded by VIRGINIA TECH on September 27, 2019 | http://arc.aiaa.org | DOI: 10.2514/1.J058531

Downloaded by VIRGINIA TECH on September 27, 2019 | http://arc.aiaa.org | DOI: 10.2514/1.J058531

of the D-NUC-L, D-U and O-NUC-L, O-U cases are compared (Figs. 2c and 2e). The thermal nonuniformity reduces the centerline velocity by approximately 10% in both the overexpanded and design jets. Although the magnitude of the velocity deficient decreases with axial distance, evidence of a perturbed base flow persists for axial locations up to $x/D = 5$ for the overexpanded jet and up to $x/D = 8$ for the design jet.

The velocity deficit induced by the thermal nonuniformity also produces a secondary shear layer along the jet centerline that alters the mean axial turbulence levels as shown for the D-NUC-L, D-U and O-NUC-L, O-U cases in Figs. 2d and 2f. The increase in turbulence intensity around the centerline is evidence of the perturbations induced by the thermal nonuniformity. This increase is greater in the overexpanded jet. At locations further downstream there is a decrease in the fluctuating velocity at radial locations that include the peak. Interestingly this reduction is much more apparent in the D-NUC-H case as compared with the O-NUC-H.

B. Far-Field Narrowband Spectra

The impact of the thermal nonuniformity on the acoustic field at angles ranging from 125° to 160° as measured from the upstream direction is depicted in the far-field narrowband spectra presented in Fig. 3. Spectra at all angles are plotted on the same chart with a 20 dB offset for clarity. The thickness of each line represents the 95% confidence interval, and so any difference in the sound pressure level between cases is statistically significant.

A comparison of the narrowband spectra from the NUC and uniform jets in Fig. 3 reveals measurable differences in the radiated noise. A small but statistically significant reduction of 2 ± 0.5 dB occurs at peak frequencies at 130° to 135° in the D-NUC-H and D-NUC-L cases (Fig. 3c). Similar magnitude reductions are observed in the O-NUC-H and O-NUC-L (Fig. 3d) cases at a slightly higher frequency range and at angles closer to the downstream axis, 135° to 140°. Further, there is very little difference between the spectra of the high- and low-blowing NUC cases, indicating that the pressure variation of the unheated stream has minimal impact on the radiated noise.

Polar plots of the OASPL (Figs. 4a and 4b) show similar results, with reductions of 2.5 dB for the D-NUC-H case at angles upstream of the peak noise range, 130° to 140°. The O-NUC-H has similar magnitude reductions, but over a larger range of polar angles that include the peak directivity direction, 130° to 145°. Although these reductions are small, so is the impact of the thermal nonuniformity on the mean velocity field. As shown in Figs. 2c and 2d the velocity deficit between the unheated and heated streams is about 5% over an area that is approximately 10% of the total exhaust area.

It is well known for turbulence-generated noise that small changes in velocity can have large impacts on the radiated sound field. We can demonstrate using a velocity scaling that the noise reduction benefit of the thermal nonuniformity is greater than simply a change in the mean velocity. Using the uniform jet velocity as a reference, the noise reduction expected from an FMEQ jet with a reduced velocity U_{eq} can be determined. Using a U^3 scaling typically used for jets with

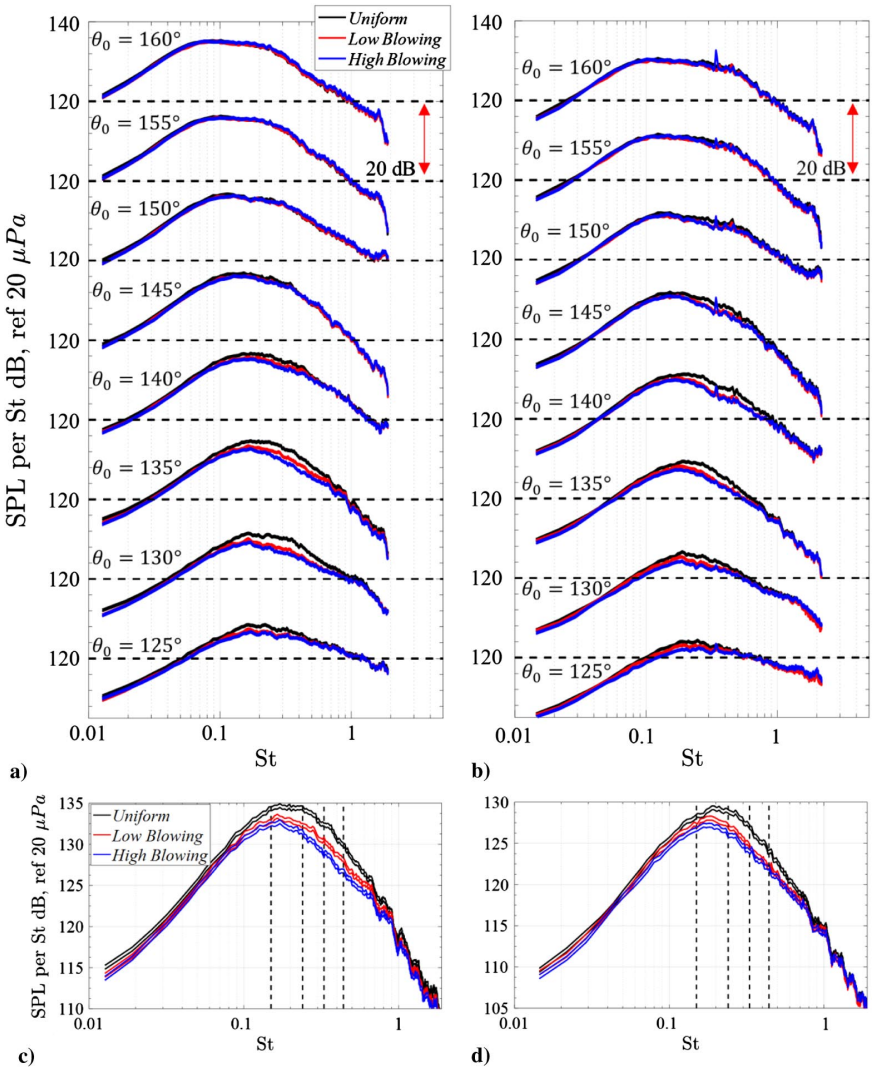

Fig. 3 Far-field narrowband spectra of a) design and b) overexpanded jets. Magnified view at $\theta_0 = 135°$ for c) design and d) overexpanded jets. Vertical dashed lines depict selected frequencies in Fig. 5.

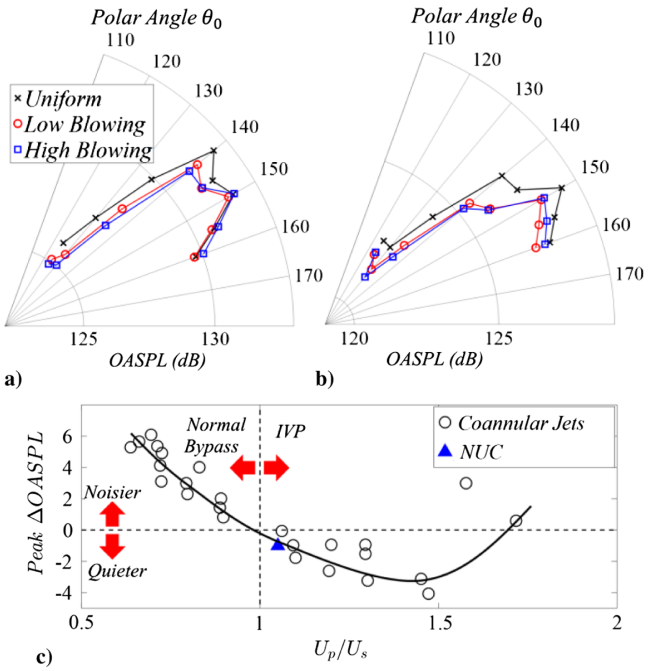

Fig. 4 OASPL of a) design and b) overexpanded jets. c) Reductions in peak OASPL from NUC and IVP jets. Co-annular jet data and the concept for this figure have been obtained from reference [9].

velocities greater than 600 m/s [11], that is, $10\log_{10}[(U_{eq}/U_j)^3]$, we find that the radiated noise will be reduced by 0.3 dB. To be conservative, it can also be shown that using a U^8 scaling [25] the difference in radiate noise is approximately 0.9 dB. In comparison the largest OASPL reduction observed is 2.5 dB. This scaling check provides further evidence that the noise reduction benefit of the thermal nonuniformity is greater than a reduction in the mean velocity and is most likely linked to subtle change in the turbulence.

The reduction in the peak OASPL for a modest velocity ratio of $U_p/U_s = 1.05$ is similar in magnitude to reductions observed in Tanna's study of IVP jets [9]. Figure 4c compares reductions in the peak OAPSL of IVP jets and the current NUC jet to demonstrate that the slight differences observed in the far-field are to be expected given the small impact on the mean velocity field.

The trend of increasing OASPL reduction with velocity ratio observed in the IVP data suggests that a reduction in the radiated noise may also scale with the temperature-driven velocity deficit in thermally nonuniform jets. Using large-eddy simulations of overexpanded jets with thermal nonuniformities, Brès et al. [26] found reductions of up to 5 dB in the peak narrowband spectra as compared with a uniformly heated jet. In their study the total temperature ratios of the heated and unheated streams of the thermal nonuniformity were approximately $TTR = 7$ and $TTR = 3$ respectively, or a velocity ratio of $U_p/U_s = 1.5$. This difference is much higher than the cases recorded in this paper.

Note that, while NUC and IVP jets shape the mean flow in similar ways, the method the NUC jet uses to generate a velocity deficit is fundamentally different. Two of the main differences are that 1) the velocity ratio in IVP jets is pressure driven and 2) the mean flow is shaped using multistream nozzles. This fact is significant when considering how a thermally nonuniform jet could potentially be implemented into a full-scale engine without any additional hardware or significant changes to the engine architecture. The narrowband spectra confirm that thermal nonuniformity reduces the radiated noise in peak directivity directions.

C. Near-Field Wavenumber Spectra

Further information regarding the mechanisms responsible for the far-field reductions can be extracted from the amplitude of the wavenumber spectra of radiating pressure fluctuations. This is accomplished using the relationship developed by Morris [23], which connects the far-field narrowband spectra with the wavenumber spectra of radiating pressure fluctuations on a cylindrical surface surrounding the jet. Here, amplitudes are calculated as a function of wavenumber using the autospectra from microphones in a polar arc array at a specific frequency. In the context of a wavenumber–frequency $(k - f)$ spectrum, this represents a constant frequency slice of the $k - f$ spectral maps as shown by Tinney and Jordan [27].

In the current analysis, a wavenumber at a given frequency represents a single polar angle where larger wavenumbers correspond to polar angles closer to the downstream jet axis. Figure 5 shows slices of the $k - f$ spectra for selected frequencies identified in the narrowband spectra in Figs. 3c and 3d by the vertical dashed lines. The sonic wavenumber, or the wavenumber above which pressure fluctuations become nonradiating at a given frequency, is also shown in Fig. 5 by vertical dashed lines.

The wavenumber spectra of cases D-NUC-L and D-NUC-H in Figs. 5a–5d reveal a decrease in the spectral amplitudes in the low-wavenumber tail that are associated with polar angles where the largest far-field reductions occur (130° to 145°). The wavenumber spectra of the O-NUC-L and O-NUC-H cases in Figs. 5e–5h show similar amplitude reductions at a larger range of wavenumbers that include the peak.

The acoustic energy contained in the tail of the wavenumber spectrum is related to the growth and decay of structures in the shear layer [27,28], that is, associated with the amplitude modulation of advecting turbulent pressure fluctuations [29]. The increase in energy at the highest wavenumbers shown in Figs. 5c and 5d for the D-NUC-H case suggests that the thermal nonuniformity may shift spectral energies to higher, nonradiating wavenumbers. However, this trend is not observed in the overexpanded case. This could be due to how fewer wavenumbers to the right of the peak are resolved and therefore any increase in energy at higher wavenumbers may occur at nonradiating wavenumbers not captured by the current analysis.

The wavenumber spectra also provide an insight into the phase velocity of the highest-energy-containing structures. These structures can be modeled as simple wave packets with constant convection velocities that are related to the peak wavenumbers by $k_{\text{peak}} = \omega/u_c$ [23]. In Figs. 5a–5d the peak wavenumbers of the D-NUC-H case appear to be slightly greater than the D-U case. The convection velocities tabulated with these peak wavenumbers for the above cases, shown in Table 3, agree with literature [23,30] and show an approximately 10% reduction in the convection velocity at the highest three reported frequencies in the D-NUC-H case. (The differences in the convection velocities of the O-U and O-NUC-H cases are very close to the measurement uncertainty and therefore are not reported in Table 3.)

Structures with supersonic phase speeds produce intense Mach wave radiation with directivity as a function of their convection velocity, $\Theta = \cos^{-1}(c_\infty/u_c)$. The Mach wave angle calculated using a convection velocity averaged across the reported frequencies for the D-U and D-NUC-H cases indicates that the D-NUC-H case ($\Theta = 150°$) has a slightly greater Mach wave angle compared with the D-U case ($\Theta = 140°$). Interestingly the reductions in the far-field spectra occur at angles in the range $125° < \theta_0 < 140°$. Pressure fluctuations with phase velocities greater than those reported in Table 3 will radiate Mach waves in this range. This may indicate that a portion of the observed reductions in the narrowband spectra of thermally nonuniform jets may be due to an interruption in the coherence or a reduction in the phase speed of turbulent structures that produce Mach wave radiation at these polar angles.

The evidence here and in other work by the authors [17] suggests that the reductions in the radiated sound field of thermally nonuniform jets are connected to changes in the turbulence convection and structure at multiple axial stations. Among other changes, the turbulence induced by the locally cooler, slower, centerline flow may interrupt the organized structure of large-scale turbulence over a range of axial distances, as is observed in noise reduction techniques such as chevrons [27] and fluidic injection [4,5]. Specifically, the results suggest that reductions may be present in the size and convection velocity of large-scale structures. This hypothesis is supported by the observed changes in the acoustic field,

Downloaded by VIRGINIA TECH on September 27, 2019 | http://arc.aiaa.org | DOI: 10.2514/1.J058531

Downloaded by VIRGINIA TECH on September 27, 2019 | http://arc.aiaa.org | DOI: 10.2514/1.J058531

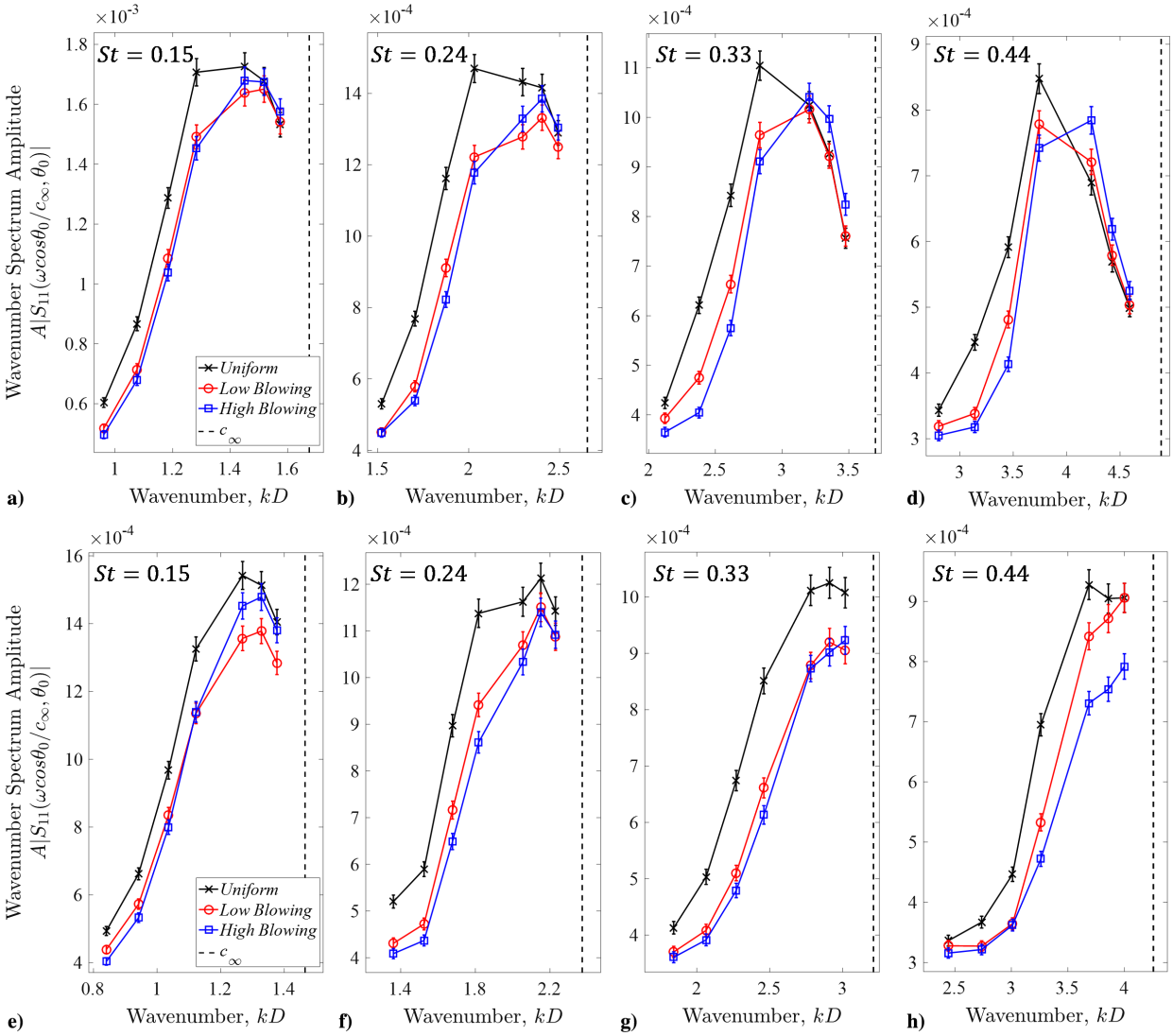

Fig. 5 Wavenumber spectra at select frequencies on cylindrical surface of radius $a = 1.5D$ for jets at a–d) design and e–h) overexpanded conditions.

namely, the shift of wavenumber–frequency energy to larger wavenumbers (i.e., to smaller spatial scales), the reduction in convection velocity of the highest-energy-containing radiating structures, and the decreases in the far-field narrowband spectra at polar angles directly outside of the Mach wave angle.

Lastly, the authors wish to emphasize that the $k - f$ analysis considers only the axisymmetric $m = 0$ mode, which may impact the interpretation of the results as Tam and Chen [31] and Seiner et al. [32] have suggested that the axisymmetric mode may not be the dominant one in heated supersonic jets, especially for large wavenumbers and frequencies. However, this point is the subject of some contention in the literature. Du and Morris [33] used near-field pressure fluctuations from a high-fidelity heated supersonic jet simulation. The authors showed that the projected acoustic solutions of wave packet sources filtered using POD capture the peak noise levels and radiation direction when only the zeroth azimuthal mode was considered. Further, experimental work by Kuo et al. [34] examined the azimuthal modal spectra of near-field pressure fluctuations of a heated supersonic jet ($TTR = 2.2$, $M = 1.5$) operating at conditions very similar to the present study. The authors found that the zeroth azimuthal mode was the dominate one for frequencies up to approximately $St = 0.4$. Therefore, although the highest frequency and wavenumber components of the $k - f$ spectra may need to be interpreted with some caution, the results still strongly imply that the thermal nonuniformity reduces the energy radiated by low-frequency, large-wavelength structures. It is in this regard that the authors believe that the current analysis offers valuable information by highlighting a potentially promising method to reduce jet noise as well as identifying possible avenues for further analysis.

Table 3 Convection velocities calculated from peak amplitudes of wavenumber spectra

	D-U	D-NUC-H
St	u_c/U_j	u_c/U_j
0.15	0.65	0.65
0.24	0.74	0.63
0.33	0.73	0.65
0.44	0.74	0.65

IV. Conclusions

The results from the current experimental study indicate that temperature nonuniformity can reduce supersonic jet noise. The current experimental analysis presents a step toward understanding the impact of thermally nonuniform exhaust profiles on the acoustic field surrounding high-speed, heated jets. Here, the far-field narrowband spectra of a heated Mach 1.5 jet with a uniform total temperature profile and a separate jet with a centered total temperature nonuniformity were analyzed to quantify the acoustic benefit and identify characteristics of impacted source mechanisms responsible for the change in the acoustic field.

The presence of a concentrated area of locally cooler, slower moving flow at the centerline of the jet reduced the radiated noise by 2 ± 0.5 dB upstream of peak noise directions for the design and overexpanded jet conditions examined. This small, but statistically significant, change had an associated reduction of 2.5 dB in OASPL at angles upstream of the peak noise direction.

The radiating portion of the wavenumber spectra of pressure fluctuations on a cylindrical surface surrounding the jet as determined from far-field measurements indicates a shift in the acoustic energy to larger, nonradiating wavenumbers. Further, in the design jet condition a reduction of approximately 10% in the convection velocity of structures associated with a wave packet model was found.

An important takeaway from these results is that despite a modest impact on the mean velocity field, shown to be a 5% reduction in the centerline mean axial velocity, the radiated noise was reduced by about 2 dB in peak noise directions. This suggests potential for exploiting this phenomenon by using more substantial nonuniformities that could be achieved in full-scale engines running at afterburning conditions.

Downloaded by VIRGINIA TECH on September 27, 2019 | http://arc.aiaa.org | DOI: 10.2514/1.J058531

Acknowledgments

This work was sponsored by Navy Grants N00014-16-1-2444 and N00014-14-1-2836, which are funded by the Office of Naval Research and managed by Steven Martens.

References

[1] Martens, S., Spyropoulos, J. T., and Nagel, Z., "The Effect of Chevrons on Crackle-Engine and Scale Model Results," *Proceedings of ASME Turbo Expo*, ASME Paper GT2011-46417, New York, 2011. doi:10.1115/GT2011-46417

[2] "Report on Jet Engine Noise Reduction," Naval Research Advisory Committee, Arlington, VA, 2009, https://www.nrac.navy.mil/docs/2009_FINAL_Jet_Noise_Report_4-26-09.pdf [retrieved 13 Aug. 2019].

[3] Huff, D. L., Henderson, B. S., Berton, J. J., and Seidel, J. A., "Perceived Noise Analysis for Offset Jets Applied to Commercial Supersonic Aircraft," *54th AIAA Aerospace Sciences Meeting*, AIAA Paper 2016-1635, 2016. doi:10.2514/6.2016-1635

[4] Powers, R. W., Kuo, C.-W., and McLaughlin, D. K., "Experimental Comparison of Supersonic Jets Exhausting from Military Style Nozzles with Interior Corrugations and Fluidic Inserts," *19th AIAA/CEAS Aeroacoustics Conference*, AIAA Paper 2013-2186, 2013. doi:10.2514/6.2013-2186

[5] Coderoni, M., Lyrintzis, A. S., and Blaisdell, G. A., "Large-Eddy Simulations Analysis of Supersonic Heated Jets with Fluid Injection for Noise Reduction," *AIAA Journal*, Vol. 57, No. 8, 2019, pp. 3442–3455. doi:10.2514/1.J057674

[6] Henderson, B. S., and Leib, S. J., "Measurements and Predictions of the Noise from Three-Stream Jets," *21st AIAA/CEAS Aeroacoustics Conference*, AIAA Paper 2015-3120, 2015. doi:10.2514/6.2015-3120

[7] Papamoschou, D., "Modelling of Noise Reduction in Complex Multistream Jets," *Journal of Fluid Mechanics*, Vol. 834, Jan. 2018, pp. 555–599. doi:10.1017/jfm.2017.730

[8] Henderson, B. S., and Huff, D., "The Aeroacoustics of Offset Three-Stream Jets for Future Commercial Supersonic Aircraft," *22nd AIAA/CEAS Aeroacoustics Conference*, AIAA Paper 2016-2992, 2016. doi:10.2514/6.2016-2992

[9] Tanna, H. K., "Coannular Jets—Are They Really Quiet and Why?" *Journal of Sound and Vibration*, Vol. 72, No. 1, 1980, pp. 97–118. doi:10.1016/0022-460X(80)90710-5

[10] Stuber, M., Lowe, K. T., and Ng, W. F., "Synthesis of Convection Velocity and Turbulence Measurements in Three-Stream Jets," *Experiments in Fluids*, Vol. 60, No. 5, April 2019, p. 83. doi:10.1007/s00348-019-2730-5

[11] Ffowcs Williams, J. E., "The Noise from Turbulence Convected at High Speed," *Proceedings of the Royal Society of London, Series A: Mathematical, Physical and Engineering Sciences*, Vol. 255, June 1962, pp. 469–503. doi:10.1098/rsta.1963.0010

[12] Tam, C. K. W., and Parish, S. A., "Noise of High-Performance Aircrafts at Afterburner," *20th AIAA/CEAS Aeroacoustics Conference*, AIAA Paper 2014-2754, 2014. doi:10.2514/6.2014-2754

[13] Mayo, D. E., Jr., Daniel, K. A., Lowe, K. T., and Ng, W. F., "Experimental Investigation of a Heated Supersonic Jet with Total Temperature Non-Uniformity," *23rd AIAA/CEAS Aeroacoustics Conference*, AIAA Paper 2017-3521, 2017. doi:10.2514/6.2017-3521

[14] Mayo, D. E., Jr., Daniel, K. A., Lowe, K. T., and Ng, W. F., "The Flow and Turbulence Characteristics of a Heated Supersonic Jet with an Offset Total Temperature Non-Uniformity," *24th AIAA/CEAS Aeroacoustics Conference*, AIAA Paper 2018-3144, 2018. doi:10.2514/6.2018-3144

[15] Daniel, K. A., Mayo, D. E., Jr., Lowe, K. T., and Ng, W. F., "Experimental Investigation of the Very near Pressure Field of a Heated Supersonic Jet with a Total Temperature Non-Uniformity," *24th AIAA/CEAS Aeroacoustics Conference*, AIAA Paper 2018-3145, 2018. doi:10.2514/6.2018-3145

[16] Daniel, K. A., Mayo, D. E., Jr., Lowe, K. T., and Ng, W. F., "Experimental Investigation of the Pressure Field of a Heated Supersonic Jet with a Centered Total Temperature Non-Uniformity," *55th AIAA Aerospace Sciences Meeting*, AIAA Paper 2019-1300, 2019. doi:10.2514/6.2019-1300

[17] Mayo, D. E., Jr., Daniel, K. A., Lowe, K. T., and Ng, W. F., "The Mean Flow and Turbulence Characteristics of a Heated Supersonic Jet with an Offset Total Temperature Non-Uniformity," *AIAA Journal*, Vol. 57, No. 8, 2019, pp. 3493–3500. doi:10.2514/1.J058163

[18] Kuo, C. W., McLaughlin, D. K., Morris, P. J., and Viswanathan, K., "Effects of Jet Temperature on Broadband Shock-Associated Noise," *AIAA Journal*, Vol. 53, No. 6, 2015, pp. 1515–1530. doi:10.2514/1.J053442

[19] Ecker, T., Lowe, K. T., and Ng, W. F., "Eddy Convection in Developing Heated Supersonic Jets," *AIAA Journal*, Vol. 53, No. 11, 2015, pp. 3305–3315. doi:10.2514/1.J053946

[20] Quinn, A. M., Daniel, K. A., Lowe, K. T., and Ng, W., "Outdoor Acoustic Measurements of the Virginia Tech Heated Supersonic Jet Rig Using Ground Microphones," *55th AIAA Aerospace Sciences Meeting*, AIAA Paper 2019-1581, 2019. doi:10.2514/6.2019-1581

[21] Douglas Shields, F., and Bass, H. E., "Atmospheric Absorption of High Frequency Noise and Application to Fractional-Octave Bands," NASA CR-2760, June 1977.

[22] Bendat, J. S., and Piersol, A. G., *Random Data Analysis and Measurement Procedures*, 4th ed., Wiley Series in Probability and Statistics, Wiley, Hoboken, NJ, 2019, pp. 249–285.

[23] Morris, P. J., "A Note on Noise Generation by Large Scale Turbulent Structures in Subsonic and Supersonic Jets," *International Journal of Aeroacoustics*, Vol. 8, No. 4, 2009, pp. 301–315. doi:10.1260/147547209787548921

[24] Tam, K. W., and Chen, K. C., "A Statistical Model of Turbulence in Two-Dimensional Mixing Layers," *Journal of Fluid Mechanics*, Vol. 92, No. 2, 1979, pp. 303–326. doi:10.1017/S002211207900063X

[25] Lighthill, M. J., "On Sound Generated Aerodynamically II. Turbulence as a Source of Sound," *Proceedings of the Royal Society of London, Series A: Mathematical, Physical and Engineering Sciences*, Vol. 222, No. 1148, March 1954, pp. 1–32. doi:10.1098/rspa.1954.0049

[26] Brès, G. A., Towne, A., and Lele, S. K., "Investigating the Effects of Temperature Non-Uniformity on Supersonic Jet Noise with Large-Eddy Simulation," *25th AIAA/CEAS Aeroacoustics Conference*, AIAA Paper 2019–2730, June 2019. doi:10.2514/6.2019-2730

[27] Tinney, C. E., and Jordan, P., "The Near Pressure Field of Co-Axial Subsonic Jets," *Journal of Fluid Mechanics*, Vol. 611, March 2008, pp. 175–204. doi:10.1017/S0022112008001833

[28] Crighton, D. G., and Huerre, P., "Shear-Layer Pressure Fluctuations and Superdirective Acoustic Sources," *Journal of Fluid Mechanics*, Vol. 220, June 1990, pp. 355–368. doi:10.1017/S0022112090003299

[29] Jordan, P., and Colonius, T., "Wave Packets and Turbulent Jet Noise," *Annual Review of Fluid Mechanics*, Vol. 45, No. 1, 2013, pp. 173–195. doi:10.1146/annurev-fluid-011212-140756

[30] Papamoschou, D., and Phong, V. C., "The Very Near Pressure Field of Single- and Multi-Stream Jets," *55th AIAA Aerospace Sciences Meeting*,

AIAA Paper 2017-0230, 2017.
doi:10.2514/6.2018-1739

[31] Tam, K. W., and Chen, K. C., "Turbulence Mixing Noise from Supersonic Jets," *AIAA Journal*, Vol. 32, No. 9, 1994, pp. 1774–1780.
doi:10.2514/3.12173

[32] Seiner, J. M., Bhat, T. R. S., and Ponton, M. K., "Mach Wave Emission from a High-Temperature Supersonic Jet," *AIAA Journal*, Vol. 32, No. 12, 1994, pp. 2345–2350.
doi:10.2514/3.12298

[33] Du, Y., and Morris, P. J., "The Separation of Radiating and Non-Radiating Near-Field Pressure Fluctuations in Supersonic Jets," *Journal of Sound and Vibration*, Vol. 355, Oct. 2015, pp. 172–187.
doi:10.1016/j.jsv.2015.06.020

[34] Kuo, C. W., Buisson, Q., McLaughlin, D. K., and Morris, P. J., "Experimental Investigation of Near-Field Pressure Fluctuations Generated by Supersonic Jets," *19th AIAA/CEAS Aeroacoustics Conference*, AIAA Paper 2013-2033, 2013.
doi:10.2514/6.2013-2033

P. Givi
Associate Editor

Downloaded by VIRGINIA TECH on September 27, 2019 | http://arc.aiaa.org | DOI: 10.2514/1.J058531

Chapter 4

The Density Near-Field of a Non-Uniformly Heated Jet

This draft was prepared using the LaTeX style file belonging to the Journal of Fluid Mechanics

The Density Near-Field of a Non-Uniformly Heated Jet

Kyle A. Daniel[1]†, David E. Mayo Jr.[2] and K. Todd Lowe[1] and Wing F. Ng[2]

[1]Department of Aerospace and Ocean Engineering, Virginia Polytechnic Institute and State University, Blacksburg, VA 24060, USA

[2]Department of Mechanical Engineering, Virginia Polytechnic Institute and State University, Blacksburg, VA 24060, USA

(Received xx; revised xx; accepted xx)

We present a quantitative analysis of time-resolved schlieren images that describes the spatio-temporal structure of the density near-field of a heated supersonic jet and the changes induced in it by altering the thermal boundary condition by way of a centered total temperature non-uniformity. The thermal non-uniformity consists of a concentrated region of locally lower total temperature flow surrounded by a higher temperature primary flow in an ideally expanded jet, and is shown to reduce jet noise by up to 2 ± 0.5 dB in peak narrowband spectral sound pressure levels as compared to a thermally uniform baseline. Space-time correlations are performed using a frequency filtered time series of the near-field density gradient. The low frequency content of the density near-field is dominated by convecting Mach waves which, in the case of the thermally non-uniform jet, are found to be decorrelated at locations in the near-nozzle region and far downstream. Space-time coherence measurements of the fluctuating density gradient support this finding and indicate a reduction in the axial coherence of large scale instabilities. Correlations of the high frequency content capture the convection of integral length scale turbulent structures and the birth of a curved acoustic wave. Results indicate the perturbations induced by the thermal non-uniformity can persist far into the developing flow field and can disorganize the coherent structures in regions far from the nozzle exhaust. This suggests centerline base flow changes can be optimized to reduce the acoustic efficiency of sources present near strong noise-producing areas such as the potential core collapse region.

Key words: (jet noise, thermal non-uniformity, near-field, schlieren)

1. Introduction

A more complete understanding of the physics linking the energetic turbulent sources in supersonic free jets to the significantly weaker radiated sound field is of value to the aircraft industry and a necessary step towards optimizing noise reduction techniques. Jet noise reduction efforts are driven by several factors, which include renewed interest in supersonic transport over land (Huff *et al.* 2016) and reducing the hearing loss experienced by aircraft carrier personnel who work near tactical aircraft (Aubert & McKinley 2011).

† Email address for correspondence: Kyled1@VT.edu

Fundamentally, jet noise reduction techniques function be either shaping the base flow by purposefully changing nozzle boundary conditions or by introducing unsteady perturbations in order to alter the acoustically important characteristics of the turbulent source. Several noise reduction methods are highlighted below, each of which use distinct means to manipulate the nozzle boundary condition and impact different features of the large-scale turbulence development (wavelength, amplitude, convection velocity). Fluidic injection in the expansion contour of a supersonic nozzle simulates hard walled corrugations and shapes the mean flow by inducing streamwise vorticity, providing noise benefits up to 5 dB in the over-all sound pressure level (OASPL) (Powers *et al.* 2013). Offset mulit-stream nozzles create a locally thinner and thicker shear layer, reduces the convection speed of correlated structures on the thick side and in the vicinity potential core collapse (Stuber *et al.* 2019; Papamoschou & Phong 2017), and can achieve reductions up to 8 dB in the narrowband spectra at azimuthal locations aligned with the "thicker" shear layer (Henderson & Leib 2015) while an increase is observed on the "thinner" side (Henderson & Huff 2016). Inverted velocity profile jets (IVP) are multi-stream jets where the inner plume operates at a slower velocity then the bypass flow and have demonstrated noise benefits up to 4 dB OASPL compared to jets with equivalent thrust, mass flow rate, and area (Tanna 1980). Noise reductions in IVP jets occur primary at low frequencies and are attributed to slower convection velocities and increased axial turbulence levels (Tanna 1980).

Heated jets with thermal non-uniformities, the topic of the current study, are characterized by distorted total temperature exhaust profiles that create a locally "cooler" stream of slower velocity flow. Mayo Jr *et al.* (2019) showed strong similarities in the axial turbulence development between heated jets with a radially offset cooler stream and offset multi-stream jets. Previous studies of centered thermal non-uniformities found amplitude reductions in the tail of the inferred near-field wavenumber spectra (Daniel *et al.* 2019*b*) and a decorrelation of Mach wave structures, which resulted in noise reductions of up to 2.5 dB OASPL (Daniel *et al.* 2019*a*).

We emphasize there are important differences between thermally non-uniform jets and IVP jets. Thermally non-uniform jets consist of a single stream with a non-uniform thermal profile while IVP jets are multi-stream co-axial jets. Multi-stream jets have multiple shear layers and contain an inner potential core surrounded by a potential annulus (Dahl & Morris 1997). As shown by the axial turbulence development reported in (Daniel *et al.* 2019*b*), jets with centered thermal non-uniformities do not have separate, clearly defined potential flow regions. The mean axial turbulence profile of thermally non-uniform jets will not have the same number of inflection points as multi-stream IVP jets and therefore will have fundamentally different instability wave characteristics. This difference is significant when considering how thermal non-uniformities could potentially be achieved by selectively activating flameholders in the afterburning section of tactical aircraft engines (Brès *et al.* 2019).

While the above noise reduction methods show promise, a more complete theoretical description linking the nozzle boundary condition to characteristics of the acoustically important turbulence is necessary to optimize noise reduction. Efforts towards developing this description have taken the form of experimental measurements in the periphery of the shear layer, which have identified the relevant acoustic features of the large-scale turbulence structures and their associated pressure fields.

The irrotational near-field directly outside of the shear layer contains both the beginnings of an acoustic field and rapidly decaying hydrodynamic pressure fluctuations. The origin of hydrodynamic pressure fluctuations can be traced directly to large scale structures in the shear layer (Zaman 1986) as they represent the convective signature

of fluctuations which have experienced the 'wavenumber filtering' effect of the scalar pressure field (George *et al.* 1984). However, the perturbations in the linear hydrodynamic region decay rapidly as $ky^{-6.67}$ (Arndt *et al.* 1997); so, to fully capture the nature of the underlying turbulence, measurements must be taken as close as possible to the shear layer (Papamoschou & Phong 2017).

A detailed study of the hydrodynamic and acoustic components of the near-field was performed by Tinney & Jordan (2008), who used a linear microphone array to measure the pressure near-field of co-axial subsonic jets with and without serrations over a range of velocity and temperature ratios. The authors performed a wavenumber-frequency analysis to separate the hydrodynamic and propagating acoustic pressure fluctuations and found the latter to be to be comprised of two distinct signatures. These signatures consisted of low frequency component with extensive axial coherence that radiated at shallow angles to the jet axis and a disorganized high frequency component which radiated in the sideline direction. Nozzle serrations were found to increase the energy of the high frequency component and decrease the energy of the low frequency component without changing its organized structure.

The literature review above demonstrates that a characterization of the near-field space-time structure is integral to understanding how changes in the nozzle boundary condition, i.e., the temperature, pressure, and density distribution at the exhaust impact the turbulence development and the radiated acoustic field. A detailed description of the near-field structure can be achieved with time-resolved schlieren imaging, which offers a unique way to quantitatively characterize spatio-temporal structures via visualization of the density gradient. Despite its apparent utility, few studies have used schlieren to extract quantitative information from jet flows. These studies are summarized as follows.

Murray & Lyons (2016) measured shock propagation angles from shadowgraph images of a supersonic jet to determine the convection speed and axial location of turbulent structures. Recently, Tinney & Schram (2019) applied proper orthogonal decomposition (POD) to a single horizontal row of pixels from high speed schlieren images of a Mach 3 jet. The authors extracted the most energetic spatial POD eigenvectors to predict the far-field sound using the one-dimensional wave equation. Berry *et al.* (2017) applied POD to time-resolved schlieren measurements of a supersonic multi-stream rectangular jet equipped with an aft deck and described distinct flow structures related to the vortices downstream of the aft deck. Here an aft deck is defined as a flat plate that captures the effects of an embedded engine exhausting over an aircraft surface.

The current study utilizes time-resolved schlieren to describe the two dimensional temporal evolution of structures present in the density near-field of supersonic jets and to identify changes induced by a non-uniform thermal boundary condition. We aim to demonstrate that the noise benefit observed in thermally non-uniform jets is due to a decorrelation of Mach wave radiation resulting from a decoherence of large scale instabilities in both the near-nozzle region and far downstream.

This study investigates the structure of the density near-field using space-time correlations of frequency filtered density gradient fluctuations. These correlations describe the temporal evolution of Mach waves and curved acoustic waves produced by integral length scale turbulence and the decorrelation that occurs with the introduction of the thermal non-uniformity. These results are supported by a space-frequency coherence analyses of the density near-field which demonstrates a reduction in the axial coherence of low frequency fluctuations representative of large scale instabilities.

The remainder of this paper is organized as follows. §2 provides a description of the Virginia Tech heated supersonic jet rig, the experimental apparatus used to generate the centered thermal non-uniformity, and a characterization of the far-field acoustic

Uniform		Heated Plume		Unheated Plume		Ratios	
TTR_j	NPR_j	TTR_p	NPR_p	TTR_s	NPR_s	$\frac{\dot{m}_s+\dot{m}_p}{\dot{m}_j}$	$\frac{F_s+F_p}{F_j}$
2	3.67	2	3.67	1.0	4.6	1.01	0.99

TABLE 1. Experimental Conditions

benefit. Section §3 presents key results describing the spatio-temporal behavior of the density near-field using space-time correlation and space-frequency coherence analyses. A summary the results and their impact follows in section §4.

2. Thermal Non-uniformity Methodology

2.1. *Experiment Apparatus*

Experiments were conducted using the Virginia Tech heated supersonic jet rig. A perfectly expanded, heated Mach 1.5 flow with a nozzle pressure ratio, NPR=3.67, and Reynolds number, $Re_D = 8.5 \times 10^5$, was generated using a converging-diverging nozzle with exit diameter $D = 0.0381$ m. The nozzle expansion contour was designed using the method of characteristics to produce a nearly shock-free flow and is a scaled version of the one used in experiments performed at the Pennsylvania State University (Kuo *et al.* 2014).

A total temperature non-uniformity was generated by introducing a secondary stream of unheated air into the centerline of the heated jet plenum via a secondary converging nozzle, which terminates 2.23D upstream of the primary nozzle exhaust plane figure 1. Once introduced, the unheated air stream accelerates through the supersonic nozzle and generates a concentrated volume of locally lower total temperature fluid along the jet centerline. The jet with temperature non-uniformity will be referred to as the NUC jet (non-uniform centered). Flow variables of the unheated and heated streams on the NUC jet and the uniform jet are defined by subscripts s, p, and j respectively. See Daniel *et al.* (2019*b*) for an in-depth description of the centered non-uniformity hardware and the Virginia Tech facility.

Flow conditions of the heated and unheated streams were continuously monitored and recorded. Total temperature and total pressure measurements were made using a National Instruments 9213 thermocouple module in a NI cDAQ-9184 chassis and a Scanivalve Corp. ZOC17IP/8Px-APC pressure transducer, respectively. The mass flowrate of the unheated flow ($\dot{m}_s$) was measured using a Lambda-Square orifice meter. The total temperature profiles of the NUC and uniform jets were characterized near the nozzle exhaust plane (0.04 x/D) using total temperature probe measurements taken over a period of 5 seconds at 676 points spread over a grid of 1.1D $\times$ 1.1D. The total temperature ratios (TTR), nozzle pressure ratio (NPR), and ratios of the massflow ($\dot{m}$) and thrust (F), are calculated from these measurements using standard isentropic relations and are reported in table 1.

2.2. *Plume Characteristics*

Here we describe the change in the nozzle boundary condition and examine the average total temperature profile at the nozzle exhaust plane. Total temperature probe surveys of the uniform and NUC jet are presented in figure 1(b) and 1(c). The temperature distribution of the uniform and heated portion of the NUC jet are nearly constant, with

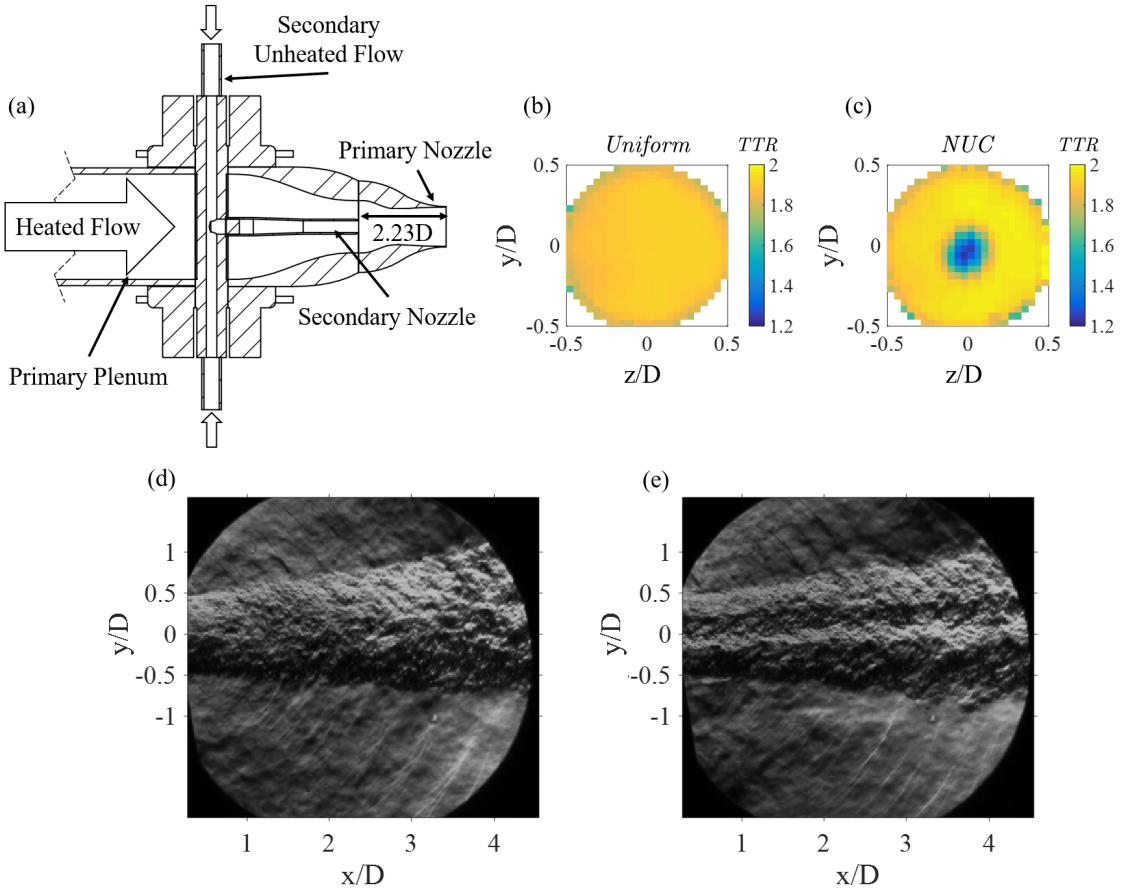

FIGURE 1. Diagram of the (a) thermal non-uniformity geometry. TTR contours for the (b) uniform and (c) NUC jets. Example schlieren images of the (d) uniform and (e) NUC jets.

a 2.4% root-mean square variation. The thermal non-uniformity is clearly observed in the NUC jet, where a concentrated spot of fluid with an average temperature of TTR=1.2 is generated by the unheated air plume introduced upstream along the heated jet plenum centerline.

The difference in temperature between the cooler secondary plume (T_s) and surrounding annulus of heated fluid from the primary jet (T_p) drives a velocity difference between the two streams whose ratio scales roughly as the square-root of the temperature ratio, i.e., $U_s/U_p \propto \sqrt{T_s/T_p}$. This creates small, local flow field changes that influence the global jet flow development (Daniel *et al.* 2019*b*), suggesting that source mechanisms may be altered over a range of axial locations. This hypothesis motivates the rest of the study, which aims to quantify the impact of the thermal non-uniformity on the acoustic far-field and evaluate changes to the organized structure of acoustically efficient turbulence via spatially-and temporally-resolved measurements of the density near-field.

2.3. *Far-Field Narrowband Spectra*

Next we present a subset of the acoustic far-field data reported by Daniel *et al.* (2019*b*) to demonstrate the frequency range and directivity of the acoustic benefit of the centered thermal non-uniformity. The acoustic far-field was measured using a ground array consisting of eight PCB 378C10 microphones located on a 100D radius polar arc at observer angles, θ_0 from 125° to 160° in 5° increments as shown by the narrowband spectra in figure 2(a). Signals were amplified and low-pass filtered at 100 kHz using a PCB model 482C series signal conditioner. All channels were simultaneously digitally sampled

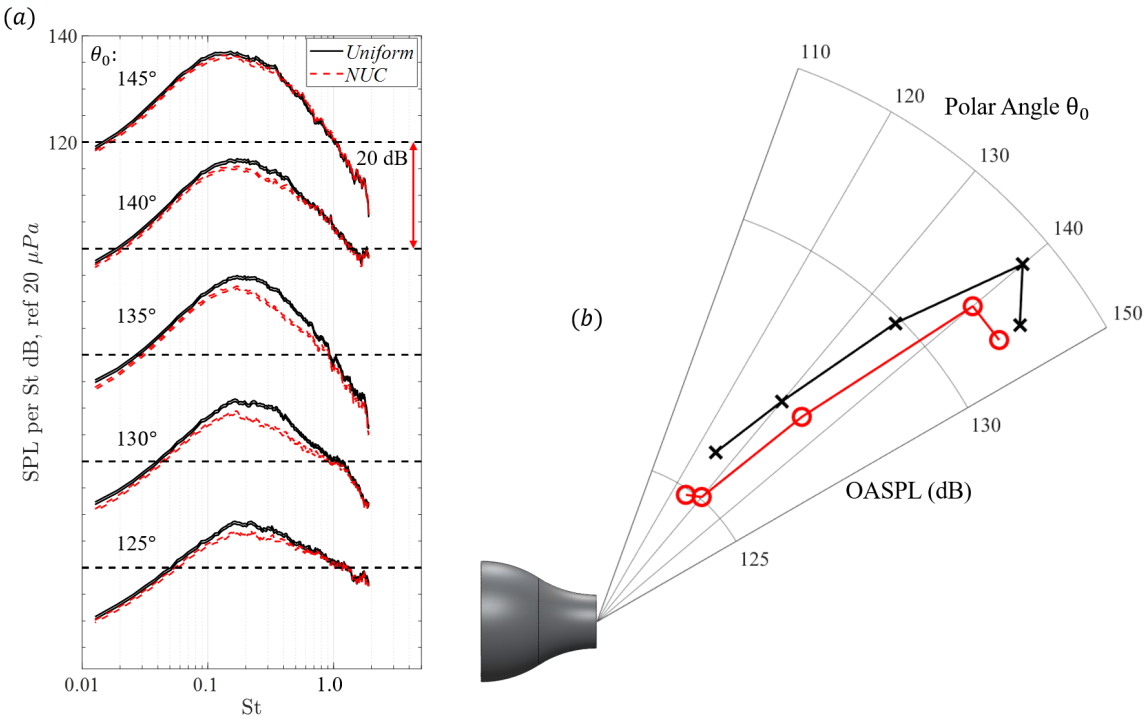

FIGURE 2. Far-field narrowband spectra (a) and OASPL (b).

using a 16-bit NI PIXe-6358 module a rate of 200 kHz for 7 s over a ± 10V bipolar range, yielding 1.4×10^6 data points per microphone. Measurements were performed outside of the facility with the ground microphone array located on the concrete pad surrounding the test cell. This ground microphone array technique follows SAE standard AIR 1672B. See Quinn *et al.* (2019) for details of the ground array and comparisons of measurements made at the Virginia Tech facility to others in the literature. Single-sided spectral densities were calculated using Welch's method with a 50% overlap and a Hanning window, resulting in 1499 records. Corrections for atmospheric absorption due to humidity effects and a conversion to Strouhal number scaling were applied to the uncorrected sound pressure levels in the same manner as in Daniel *et al.* (2019*b*). The resulting spectra shown in figure 2(a) are offset by 20 dB for clarity and the thickness of each line represents the 95% confidence interval of the measurement.

The narrowband spectra in figure 2(a) demonstrate that the NUC jet has reduced noise levels compared to the uniform jet, with reductions of 2 ±0.5 dB over a polar range of 130° to 135° over Strouhal numbers ranging from 0.1 to 0.7. Smaller, but still statistically significant reductions occur at angles just downstream (140°) and upstream (125°) of this area. The OASPL results in figure 2(b) show a similar trend, with a maximum reduction of 2.5 dB OASPL at 135°.

The observed far-field reduction, albeit small, may scale with the temperature-driven velocity deficit. Evidence of this scaling comes from Brès *et al.* (2019), who performed LES simulations of over-expanded jets with non-uniform temperature profiles. The non-uniform jets studied had large temperature differences, with the hot and cool streams of the thermally non-uniform jet operating at TTR's of 7 and 3 respectively. The authors found the non-uniform jet had a maximum reduction of 4dB in the overall sound pressure as compared to the uniform case. This, as well as evidence from the current work, suggests that larger noise reductions could be achieved by increasing the difference in TTR, which could be attained in full-scale engines operating at afterburning conditions.

3. Spatio-temporal Behavior of the Density Near-field

3.1. *Space-time Correlations*

In the following analysis we visualize the two-dimensional time evolution of coherent structures in the acoustic near-field using space-time correlations of time-resolved schlieren images. Schlieren images are created by the refraction of light rays as they pass through a flow volume due to variations in the refractive index, leading to locally darker and lighter areas in the resulting image. Because the refractive index of a fluid is proportional to the density gradient, the pixel intensities of schlieren images provide a path integrated measure of the fluctuating density gradient, which in turn can be used to visualize the evolution of pressure disturbances in the near-field. This is effect is captured in figure 1(d) and 1(e), where a Mach wave is visualized by the lighter intensity pixels that represent the sudden change in the radial density gradient across the wave front. The schlieren images presented are recorded using a Z-type schlieren system that measures the fluctuating radial density gradient, $\partial\rho'/\partial y$. A set of 40,000 time-resolved images were recorded using a Phantom v2512 high-speed camera to record at 110 kHz with an exposure time of 1 μs. Images were spatially calibrated using a rectangular object of known height and length that was located a measured distance away from a datum at the nozzle exhaust.

We use these time-resolved schlieren images to indirectly examine the structure of the near pressure field, and the hydrodynamic pressure fluctuations it contains, by performing cross correlations of the fluctuating pixel intensity of the schlieren images, $A'(x, y, t)$. This analysis provides a visualization of the two-dimensional time evolution of statistical structures that represent acoustically important features in the near-field. The temporal development of these structures reveals information about their sources, i.e., the coherent turbulent fluctuations in the shear layer, and provides insight into the changes the thermal non-uniformity induces in the near-field space-time structure and the coherent structures in the shear layer. The large scale structures contained within the shear layer can be examined via their convective hydrodynamic 'footprint' in the near-field (Arndt *et al.* 1997) and has in the past been measured by extensive near-field microphone arrays (Suzuki & Colonius 2006; Tinney & Jordan 2008). In the current analysis we examine the statistical relationship between the full convective signature of the turbulence and the rest of the near-field by calculating the cross correlation between the fluctuating pixel intensity at a point located directly outside of the shear layer $A'(x, y, t)$ and every other point in the field of view $A'(x + \xi, y + \zeta, t + \tau)$. Correlations are calculated with probe points at axial stations in the near- and far-nozzle regions (x/D=3 and x/D=7) to visualize the space-time structure of the near-field produced by coherent structures at distinctly different points in their evolution. Here cross correlations are calculated as

$$R_{AA}(x, y; \xi, \zeta, \tau) =< A'(x, y, t)A'(x + \xi, y + \zeta, t + \tau) > \tag{3.1}$$

where the normalized coefficient, ρ_{AA}, is defined as,

$$\rho_{AA}(x, y; \xi, \zeta, \tau) = R_{AA}(x, y; \xi, \zeta, \tau)/R_{AA}(x, y; 0, 0, 0). \tag{3.2}$$

While the visualization of the acoustically important near-field structures is a powerful analysis tool, the uncertainties inherent in the schlieren measurement and the space-time correlations must be taken into consideration when analyzing the results. The first uncertainty in the present measurement is the averaging uncertainty introduced by the space-time correlations. The averaging uncertainty in the correlation coefficient is a function of the number of samples, N, and is calculated according to

$$\delta[\rho_{AA}(x,y;\xi,\zeta,\tau)] = \frac{2}{\sqrt{N}}(1-(\rho_{AA}(x,y;\xi,\zeta,\tau))^2). \tag{3.3}$$

In the current analysis, where 40,000 images were used, the averaging uncertainties are very small and are on the order of 10^{-2}. This uncertainty is much smaller than the difference in the contour levels in the figures of the space-time correlations.

The largest uncertainty in the current analysis is related to the integration of the density gradient that occurs over the entire path of the light beam. Due to how the schlieren images provide path integrated values, the space-time correlations of these images do not represent the evolution of structures within a single stream-wise plane, but rather describe correlated structures integrated over a line perpendicular to the imaging plane.

The impact of the circumferential integration on the interpretation of the current results are likely minimal due to the type of flow being imaged and the density gradient that the images are sensitive to. The fluctuating images intensities in the current measurement are proportional to the fluctuating radial density gradient, $\partial\rho'/\partial y$, and therefore are most sensitive to the large radial gradients present at the top edge of the shear layer and at the wave front of radially propagating density disturbances. The largest factor that will introduce errors in the current measurement therefore are the azimuthal modes of the density field that have large radial gradients at locations offset from the centerline stream-wise plane.

The dominate mode in moderately heated axisymmetric jets is the axisymmetric mode ($m = 0$), which takes the form of axially spaced rings (Jordan & Colonius 2013; Kuo *et al.* 2013). The largest density gradient in the axisymmetric mode occurs at the 'top' and 'bottom' of the axisymmetric rings at locations that coincide with the stream-wise plane located on the jet centerline. At stream-wise planes offset from the centerline, the radial density gradient decreases due to the cross-stream curvature of the mode shape. Therefore the dominate portion of the path integration only occurs over a cross stream distance related to the curvature of the leading order modes. This alternatively can be thought of as integration over the chord of a circle that represents the axisymmetric mode, where the length of the chord is defined by the arc length over which the radial density gradient is strong enough to be sensed by the schlieren. Because the density field of the jet is dominated by the axisymmetric mode, the features that experience the highest level of path integration are those radiating at small azimuthal angles offset from the vertical axis. The integration of these out of plane features will result in an artificial extension of the correlated structures towards the jet centerline. Therefore while integration effects will be present in the space-time correlations, the distance over which features are integrated is likely small and the effect the integration has on the interpretation of the results is minimal.

Next, we analyze the space-time structure of acoustically important features in the near-field by calculating the space-time correlation of the uniformly heated jet. The resulting correlated structures at different non-dimensional time lags, $\tau^* = \tau U_j/D$, as shown in figure 3 take the form of a wave packet structure comprised of two substructures with distinct time evolutions. The first distinct substructure is characterized by the shape of the outermost correlations contours and represents a traveling Mach wave that is qualitatively similar to the structures observed in the conditional POD analysis of Schmidt & Schmid (2019). The shape of the Mach wave structure stays relatively constant, particularly at negative time lags. This lack of evolution implies a majority of the large wavelength Mach wave structures in figure 3 are likely produced by sources

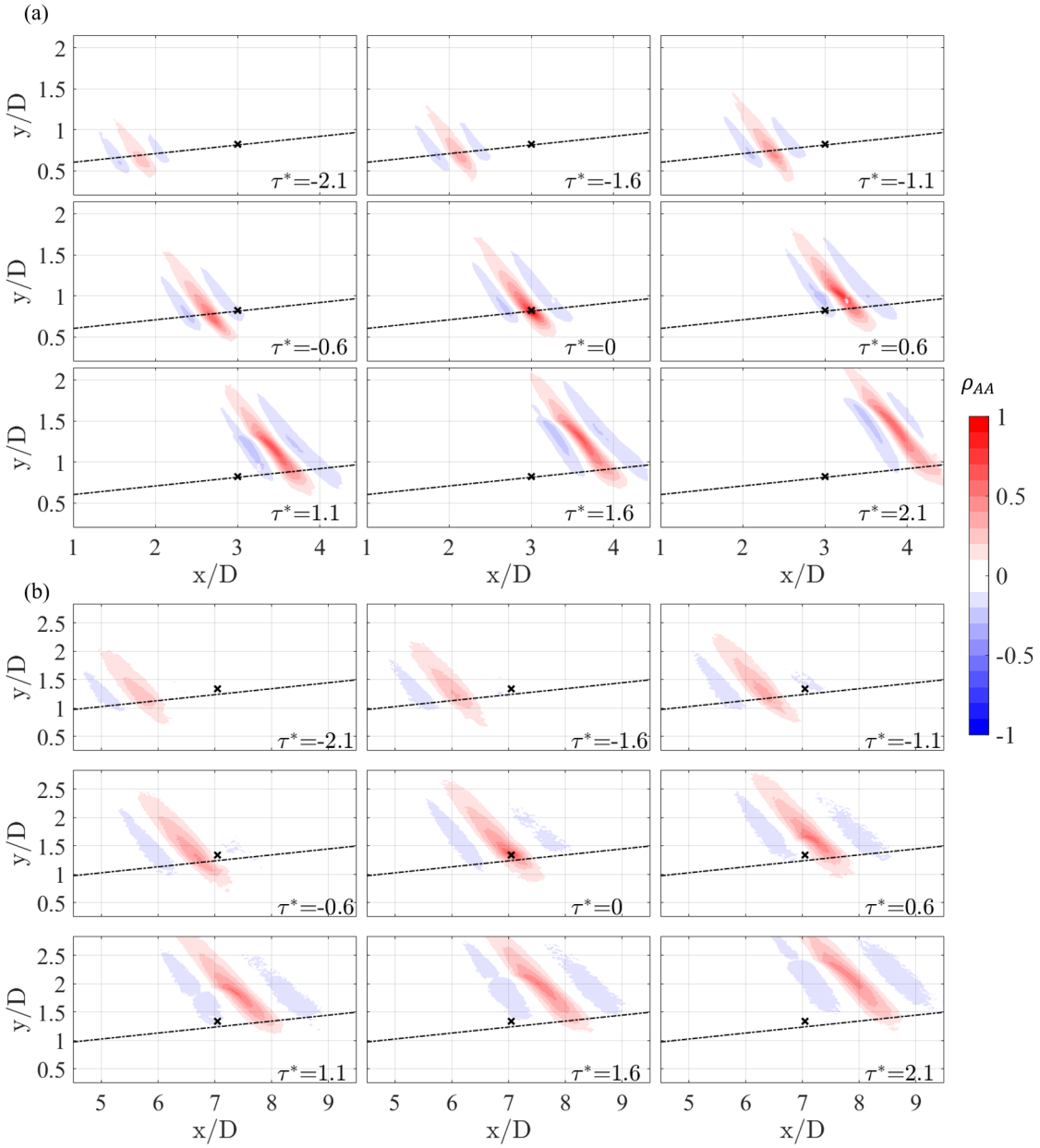

FIGURE 3. Space time correlations of the density near-field of the uniform jet in the (a) near-nozzle (x/D=3) and (b) far-nozzle (x/D=7) region. The dash dot line represents the approximate location of the shear layer edge and the correlation probe point is indicated by the x. Animations of the space-time correlations can be found in the supplementary material available at XxxxX.

upstream of the probe point. The second substructure is the small wavelength feature contained within the center lobe that appears at $\tau^* = 0$ and, in contrast to the Mach waves, evolves rapidly with time. This rapid development implies the acoustic feature this wave represents is produced at the probe point.

The space-time correlations shown in figure 3 demonstrate the highly organized structure of the near-field and identify two substructures with distinctly different time evolutions. The first of these substructures are clearly Mach waves produced by the supersonic convection of large scale instabilities. The source of the small wavelength structure, however, is not as obvious. In the space-time correlations the small wavelength structure

appears to have a very high level of correlation because its signature is summed with fluctuations that describe the Mach waves, i.e., $A'(x,y,t) = A'_1(x,y,t) + A'_2(x,y,t)$. Thus if the signature of the small wavelength structure can be separated from the Mach wave signature, the correlation of each signature may be found and the evolution of the different features can be viewed separately. A proof detailing how the space-time correlations can be separated if the time series of each signal is assumed to be linearly summed is located in Appendix A.

3.2. *Frequency Filtered Space-time Correlations*

The evolution of the distinct substructures in figure 3 are separated based on their dominate wavelength using a frequency filter. First, we isolate a signal $A'_2(x,y,t)$ that contains high frequency fluctuations by using a high-pass filter to remove the large wavelength, low frequency Mach waves from the original signal $A'(x,y,t)$. The cutoff frequency, f_{cut}, of the high-pass filter is defined by the ambient speed of sound, c_∞, and the wavenumber magnitude, $|\boldsymbol{k}|$, of the largest wavelength Mach wave structures present in the correlations shown in figures 3(a) and 3(b), i.e.,

$$c_\infty = 2\pi f_{cut}/|\boldsymbol{k}|. \tag{3.4}$$

The high-pass filter consists of a centered moving average of length n_{ave} that is subtracted from the fluctuating image intensity, $A'(x,y,t)$, and is defined formally as,

$$A'_2(x,y,t) = A'(x,y,t) - \frac{1}{n_{ave}} \sum_{i=-n_b}^{n_b} A'(x,y,t+i/f_s) \tag{3.5}$$

where n_{ave} is a odd integer and n_b is a positive integer such that the averaging occurs over the interval $2n_b + 1$. Note near the end points, the moving average window size is shrunk to only include only existing points.

This filter yields the high frequency signal, $A'_2(x,y,t)$, by averaging out fluctuations that have wave periods similar to the wave period associated with f_{cut}. The moving average was found to be most effective at filtering out the low frequency Mach waves for a n_{ave} corresponding to a fraction of the wave period associated with the cutoff frequency. In this case we round n_{ave} to the nearest odd integer value and define it as,

$$n_{ave} = \frac{1}{3}\frac{f_s}{f_{cut}}. \tag{3.6}$$

The signal representing the large wavelength, low frequency Mach waves, $A'_1(x,y,t)$, is obtained by subtracting the high-pass filtered signal from the original signal.

$$A'_1(x,y,t) = A'(x,y,t) - A'_2(x,y,t). \tag{3.7}$$

In the following section the signal representing the large wavelength Mach waves, $A'_1(x,y,t)$, will be referred to as the low-pass signal while the signal representing the high frequency, small wavelength structures, $A'_2(x,y,t)$, will be referred to as the high-pass signal.

First, we examine the space-time correlations of the low-pass filtered signal shown in figure 4. These correlations capture the time evolution of Mach waves without the contribution of the small wavelength structure, indicating that Mach waves dominate the low frequency content of the near-field. Correlations of the low-pass signal again have a wave packet like structure and exhibit minimal temporal evolution at negative time lags. At time lags $\tau^* > 0$ the shape of the correlation does change, with the correlation amplitude increasing and the size of the wave packet lobes growing slightly

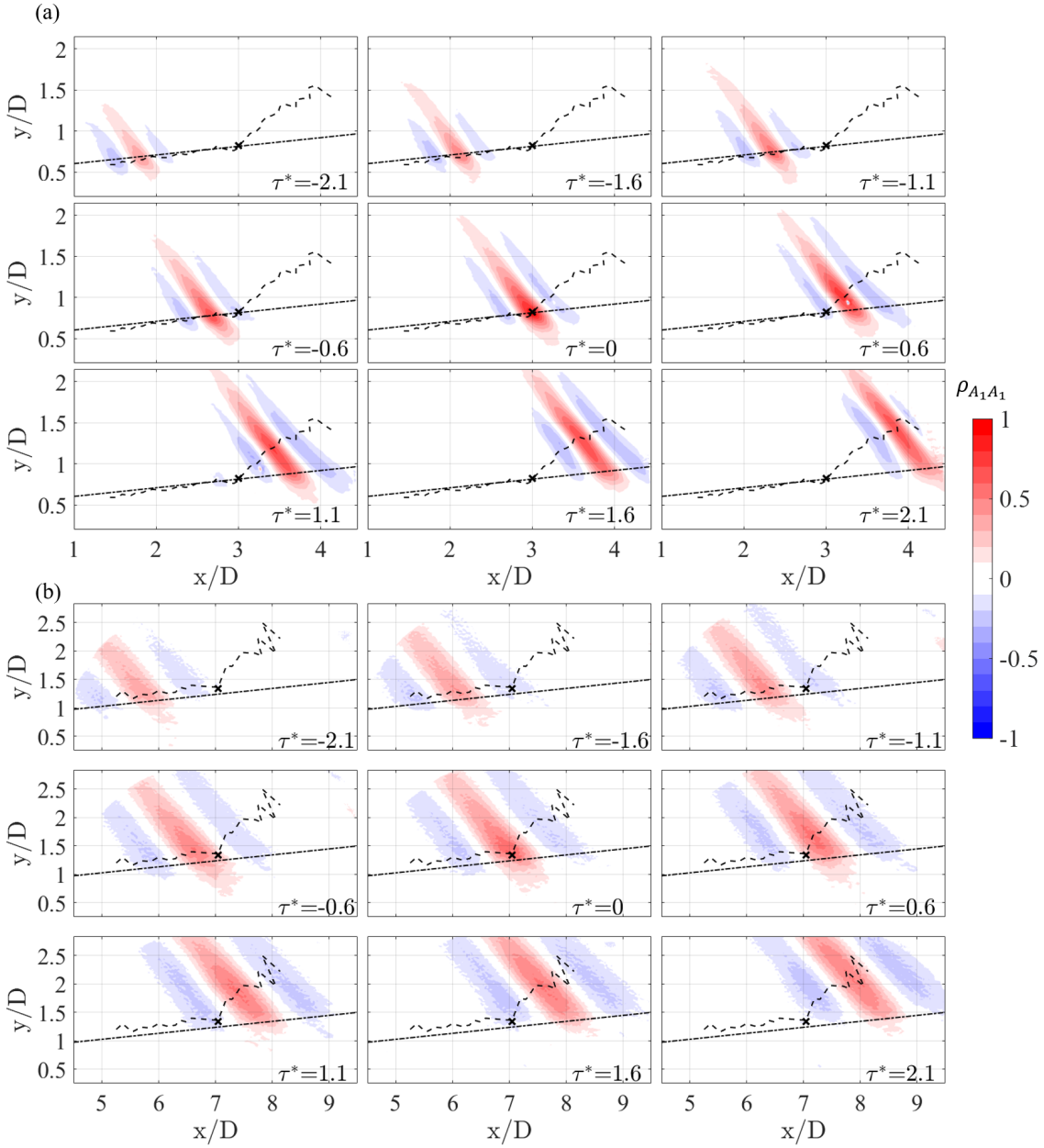

FIGURE 4. Space time correlations of the low-pass filtered density near-field of the uniform jet in the (a) near-nozzle (x/D=3) and (b) far-nozzle (x/D=7) region. The dash dot line represents the approximate location of the shear layer edge, the dotted line shows the locus of the correlation maxima, and the correlation probe point is indicated by the x. Animations of the space-time correlations can be found in the supplementary material available at XxxxX.

while maintaining a similar shape. The evolution at positive time lags represents a Mach wave produced at the probe point that propagates with a well-defined ejection angle as shown by the locus of the peak correlation indicated by the dotted lines in figure 4. The ejection angle of the local Mach wave is $\theta_0 = 145^\circ$ and $\theta_0 = 135^\circ$ for the x/D=3 and x/D=7 correlations, respectively. These angles are very close to the peak noise directivity angle indicated by the OASPL polar plot shown in figure 2 and demonstrate that these large wavelength structures are indeed intense Mach waves that dominate the far-field at shallow angles to the jet axis.

Space-time correlations of the high-pass filtered signal shown in figure 5 take the form

of a curved structure that is distinct from Mach wave radiation, suggesting a majority of the high frequency content in the near-field is produced by an underlying mechanism different from the supersonic convection of instability waves. At negative time lags the correlation captures a wave packet structure inside the shear layer that has an axial length scale less than a diameter. Note the shear layer edge is approximated by a spreading angle determined from the PIV measurements of Mayo Jr *et al.* (2019) and is shown by the dash dot line. As time moves forward, the wave packet structure convects parallel to the shear layer with the locus of the correlation maxima located along the lip line for the x/D=3 case (figure 5(a)) and at a radial location further away from the centerline, but still within the shear layer, for the x/D=7 case (figure 5(b)).

At negative time lags just before zero the correlation structure abruptly changes its propagation direction and undergoes rapid evolution. The lobes of the wave packet structure begin to rotate at $\tau^* = -1$ and then rapidly stretch as the locus of the correlation maxima travels radially outward from the shear layer. At positive time lags the correlation structure continues to evolve as it forms the arc of a curved wave which is confirmed to be acoustic by calculating its phase speed using the distance between maxima points and the corresponding time lag. The curved acoustic wave displays a level of super directivity with the locus of the correlation maxima traveling at $\theta_0 = 135^\circ$ and $\theta_0 = 115^\circ$ for the x/D=3 and x/D=7 cases, respectively.

The peak correlation value of the wave packet features observed in the shear layer occur near locations that coincide with the peak Reynolds shear stress and therefore likely represent compact turbulent structures. In the x/D=3 case the locus of the maxima lies along the nozzle lip line, which is consistent with the location of the peak Reynolds stress in supersonic jets at similar conditions e.g., Mayo Jr *et al.* (2019). While the locus of the correlation maxima in the x/D=7 case does not directly align with the peak shear stress, which remains along the lip line at downstream locations, the feature in the space-time correlations still likely represents a coherent turbulent structure. At far downstream locations the correlations of the path integrated schlieren likely cannot capture the peak due to the increased thickness of the shear layer and instead correlates the coherent portions of the structure at larger radii where the integration effects through the shear layer are not as great.

The time history of the high-pass filtered correlations describe the birth of an acoustic wave that is likely produced by the energetic disintegration of integral length scale turbulence or, statistically, is caused by compactly correlated turbulence. At time lags just before $\tau^* = 0$ the coherent turbulent structure in the shear layer undergoes rapid evolution as it rotates and begins to form a curved acoustic wave. At positive time lags just past $\tau^* = 0$ the coherent turbulent feature in the shear layer completely disappears and the only correlations left inside the shear layer are features representing propagating acoustic waves.

This finding bears a striking resemblance to the results of Hileman *et al.* (2005) who conditionally sampled flow images of a cold Mach 1.28 jet at periods of noise generation and relative quiet. The authors found that the flow was characterized by integral length turbulent structures during periods before an intense noise event. Directly before the moment of noise emission the coherent structures were observed to disintegrate. This led the authors to hypothesize the abrupt disappearance of these features is related to a dynamic interaction of coherent structures which in turn produces an intense acoustic event. Note the noise event observed by Hileman *et al.* (2005) is not related to Mach wave radiation, as the convection velocity of the most energetic structures in the jet the authors studied are subsonic.

The noise emission by integral length scale structures observed in the current study

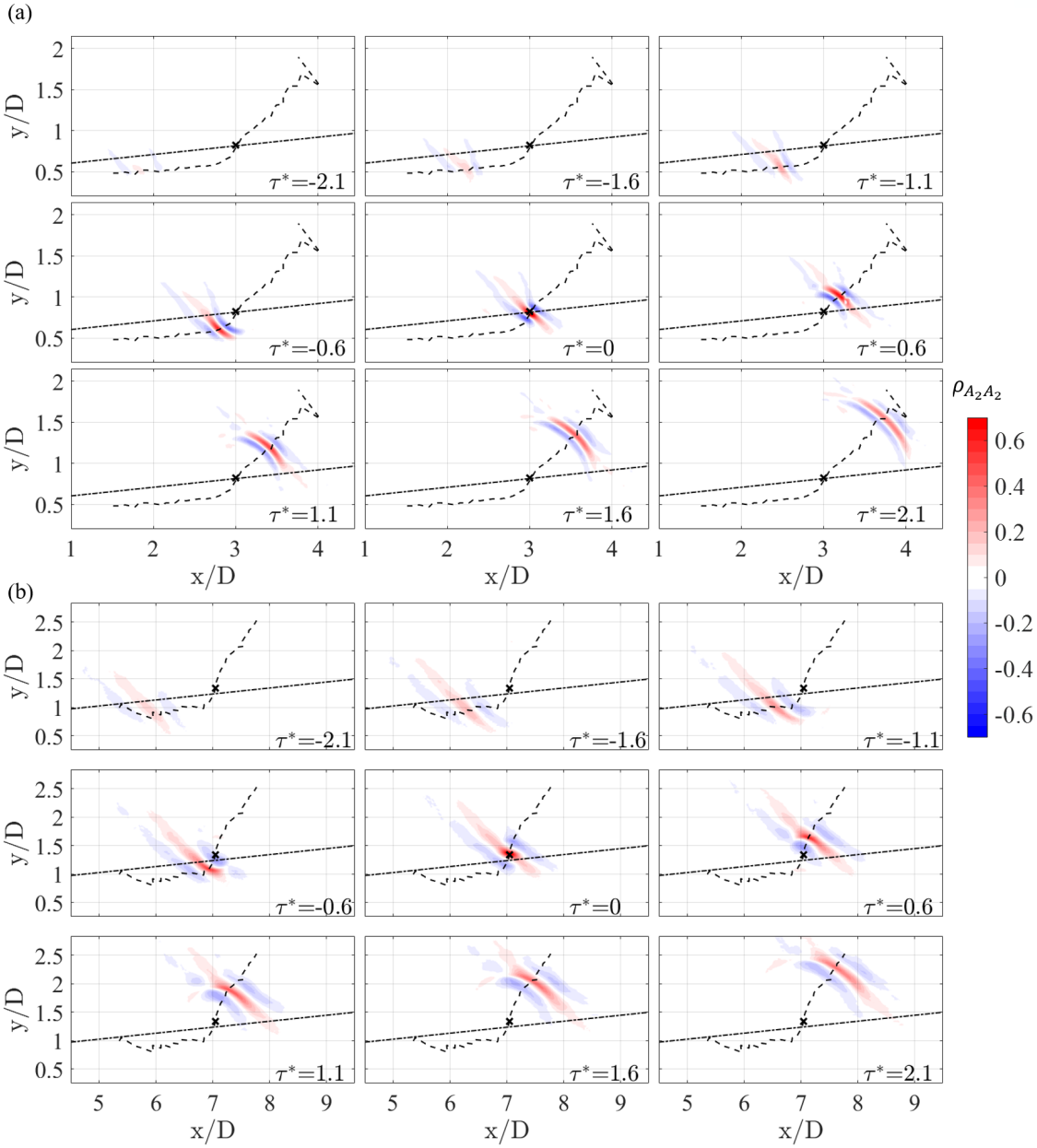

FIGURE 5. Space time correlations of the high-pass filtered density near-field of the uniform jet in the (a) near-nozzle (x/D=3) and (b) far-nozzle (x/D=7) region. The dash dot line represents the approximate location of the shear layer edge and the dotted line shows the locus of the correlation maxima. Animations of the space-time correlations can be found in the supplementary material available at XxxxX.

and in Hileman *et al.* (2005) may be related to the process described by Morrison & McLaughlin (1979). The authors hypothesized the intense noise events observed near the collapse of the potential core in a low Reynolds number jet was related to a sudden decay of instability waves. This 'relatively violent fluid dynamic action' is likely the result of a vortex interaction event and may be related to the 'tilt-stretch-tear-pair' observed by Thurow *et al.* (2002) or the tearing or roll up of structures observed by Hileman & Samimy (2001) and Hileman *et al.* (2002). The actual mechanism leading to the sudden disintegration of these integral length structures, however, is likely a combination of these interactions.

These observations indicate the high frequency content in the near-field is dominated by features that are inconsistent with the representation of wave packets as linear, time periodic instability waves. Wave packets in the shear layer are known to be correlated over distances much larger than the integral turbulent length scale as demonstrated by Fuchs (1972), who measured significant correlation magnitudes for axial separations larger then x/D=4. In contrast, the compactly coherent structures in figure 5 are correlated over much smaller distances that are approximately equal to the integral turbulent length scale. While the small axial length scale of the compactly coherent structures in figure 5 does not prohibit them from being described as linear instability waves, their characteristics depart from the typical description of wave packets as large scale features. This suggests the observed structures may represent characteristics of wave packets that are not yet fully understood.

Further, the rapid disintegration of the coherent structures in figure 5 is also inconsistent with the representation of wave packets as time-periodic linear instability waves. The sudden dissipation of the observed structures cannot be described by time-periodic linear models (Cavalieri & Agarwal 2014), and again suggests the compactly coherent structure may represent a feature of wavepackets not yet fully described by current models. While time-periodic linear instability models are capable of accurately predicting peak noise directives, they under predict the far-field noise at angles $\theta_0 > 130^\circ$, particularly at high frequencies (Cavalieri *et al.* 2012). The inability of linear instability wave models to accurately predict off peak directivities have led researchers to incorporate non-periodic time evolutions into linear wave packet models in the form of 'jitter' (Cavalieri *et al.* 2011) or coherence decay (Cavalieri & Agarwal 2014). In both cases the incorporation of non-periodic time evolution leads to an increase in the acoustic efficiency of the wave packets, particularly for directives above $\theta_0 = 130^\circ$. The angles that these non-time-periodic wave packet models predict increased noise radiation, as compared to time-periodic models, are similar to the directivies of the acoustic structures in figure 5, which propagate at $\theta_0 = 135^\circ, 115^\circ$. Thus is it likely the non-time-periodic feature that these models attempt to describe through the inclusion of 'jitter' or coherence decay may be the integral length scale feature observed in the high-pass correlations.

It is likely that the curved acoustic waves observed in figure 5 play an important role in the sound radiated by supersonic jets and should be accounted for in order to accurately predict the far-field sound, particularly at angles upstream of the peak directivity. In the current supersonic jet, the peak directivity is dominated by Mach waves which radiate at $\theta_0 = 140^\circ$ as shown by the far-field OASPL in figure 2(b) while the curved acoustic waves propagate at polar angles upstream of the peak directivity angle. Further, because the curved acoustic waves are likely produced by energetic vortex interaction events, they represent relatively intense pressure waves (Hileman *et al.* 2005; Thurow *et al.* 2002; Hileman & Samimy 2001; Hileman *et al.* 2002). The combination of the relative intensity of the curved acoustic waves along with the fact that they propagate at angles not dominated by Mach waves implies that these high frequency features must be accounted for in order to accurately predict the far-field at off peak directivities.

The results also highlight the importance of the radial wavenumber component and how its measurement is necessary to accurately capture the evolution of coherent structures in the near-field. A large component of the wavenumber magnitude of the curved acoustic waves in figures 5(a) and 5(b) are in the radial direction as these features travel at a large angles to the downstream axis, indicating the axial wavenumber alone will not provide an accurate estimation of the wavenumber magnitude of these features.

Lastly we note that the features visualized in the correlations of the high- and low-pass filtered signals demonstrate a high level of statistical independence. The relationship

between the high and low-pass filtered signals is evaluated by taking the correlation between a probe point in the high-pass filtered signal and every other point in the low-pass filtered field, i.e.,

$$R_{AA_{1,2}} = A_2'(x,y,t)A_1'(x+\xi, y+\zeta, t+\tau)] > \tag{3.8}$$

The resulting correlations shown in figure 6 have very low correlation values, around $\rho_{AA_{12}} = 0.5$. While the level of correlation of these structures is above the averaging uncertainty of the measurement, it very small compared to high correlation levels of the high- and low-pass filtered signals in figures 4 and 5. These results demonstrate that the curved acoustic wave, the Mach waves, and their sources are generally statically independent. Note this also indicates the unfiltered near-field density gradient is composed two linearly added, statistically independent, signals as is shown in the proof located in Appendix A.

3.3. *Comparison of NUC and Uniform Correlations*

The above section identifies two distinct near-field features that dominate high and low frequency ranges and provides physical insight regarding the differences in their relative origins. In the following section we directly compare the structure of these features in the NUC and uniform jets. This comparison provides insight into the slight changes the thermal non-uniformity induces in the structure of the near-field and how it relates to turbulent source mechanisms in the shear layer. Note in this section the schlieren images of the NUC and uniform cases were taken back to back without changing the setup. This was done to ensure the schlieren images of the compared cases have the same calibration, the same field of view, and to improve the confidence in the conclusions drawn from their direction comparison.

Correlations of the low- and high-pass filtered fields of the NUC and uniform jets are compared in figure 7 and 8 using constant contour levels of -0.1 and 0.2. In the NUC case the low-pass filtered correlations representing Mach waves (figure 7) exhibit an appreciable level of decorrelation as compared to the uniform case. This occurs for correlations in the far downstream region and less so for the upstream. The high-pass correlations in the NUC case (figure 8) also exhibit a visible level of decorrelation, with a reduction in the spatial extent of the correlations that represent the compactly coherent turbulent features and the curved acoustic waves they produce. However the decorrelation is only observed in the far-nozzle region, with no observed difference in the correlation shape of the high-pass filtered signal at the upstream location.

These observations imply that the perturbations induced by the thermal non-uniformity decorrelate the large scale instabilities that radiate Mach waves and the integral length turbulent structures that produce the curved acoustic waves at locations far from the nozzle exhaust. This is a significant result as it implies that the perturbations induced by the thermal non-uniformity are able to persist within the potential core and decrease the correlation length scales of both noise-producing instabilities and coherent turbulent structures at locations far downstream. The radiation efficiency of turbulent structures, as shown by Papamoschou *et al.* (2014), can be diminished by reducing four fundamental factors: the turbulent kinetic energy (TKE), the convection velocity, and the correlation time and length scales. The noise reduction benefit observed in the current case is unlikely to be driven by reduction in TKE, as a 50% reduction is needed to reduce the radiated noise be 3 dB (Papamoschou *et al.* 2014). It is highly unlikely the thermal non-uniformity studied in the current case produces the 2.5 dB reductions in the OASPL through a reduction in the TKE. A change in convection velocity is also

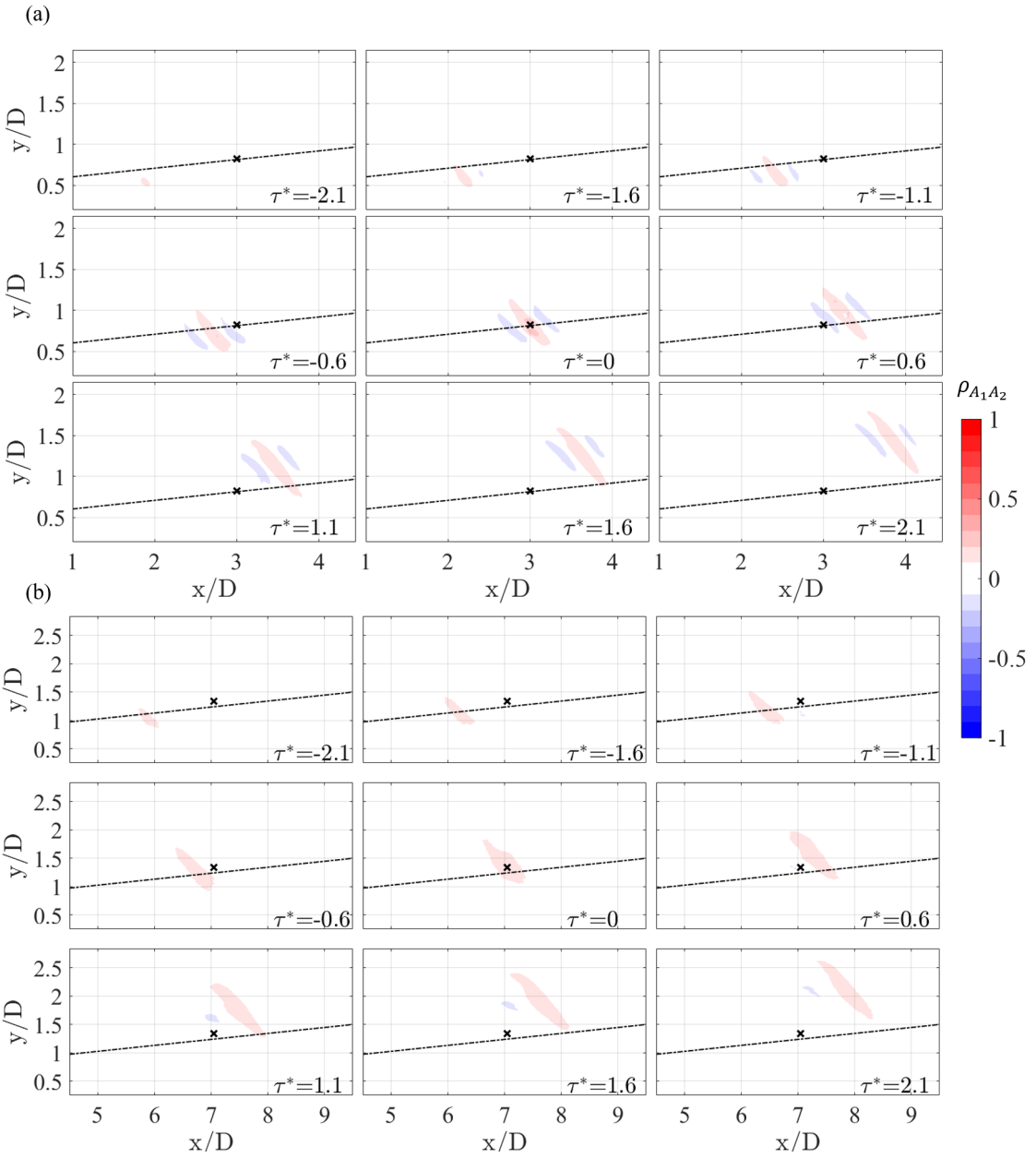

FIGURE 6. Space time correlations between the high-pass and low-pass filtered density near-field of the uniform jet in the (a) near-nozzle (x/D=3) and (b) far-nozzle (x/D=7) region. The dash dot line represents the approximate location of the shear layer edge and the correlation probe point is indicated by the x. Animations of the space-time correlations can be found in the supplementary material available at XxxxX.

unlikely as the locus of the peak correlations across all cases are similar, indicating the directivity, and by extension the convection velocity, has not changed significantly. Therefore, the acoustic efficiency of the turbulence is likely reduced by a decrease in the correlation length scale of turbulent features which, as demonstrated by the current analysis, occurs in both the near- and far-nozzle regions. The observed reduction in the correlation length scale is a major finding given, as Papamoschou (2018) states, "While it is possible to disorganize the turbulence in the vicinity of the nozzle, the extent to which structures at large distances from the nozzle can be affected is not clear, given the natural tendency of the shear layer to self-organize into large vortical

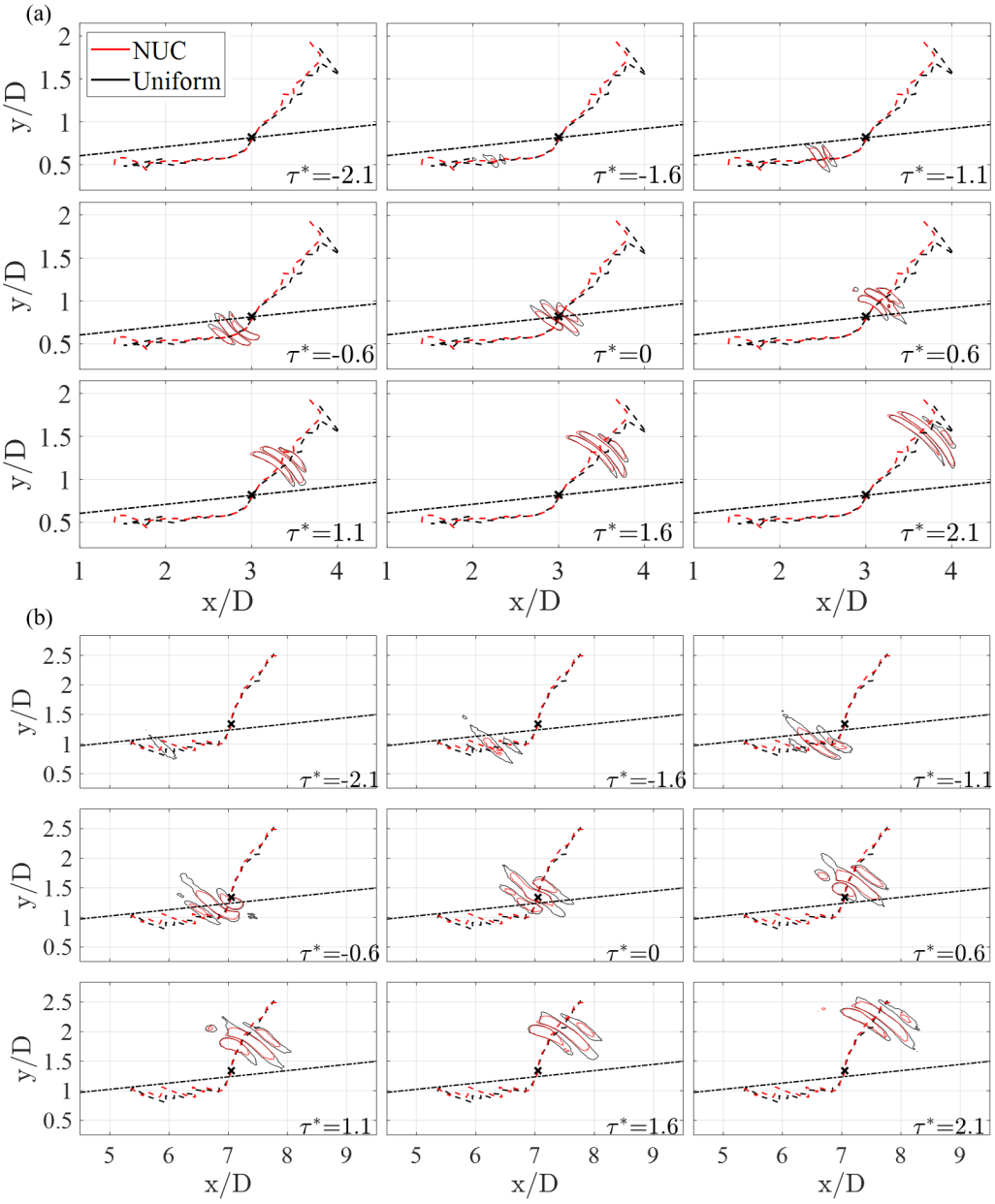

FIGURE 7. Comparison of constant contours (-0.1, 0.2) of the space time correlations of the low-pass filtered density near-field of the Uniform and NUC jet in the (a) near-nozzle (x/D=3) and (b) far-nozzle (x/D=7) region. The dash dot line represents the approximate location of the shear layer edge and the correlation probe point is indicated by the x. Animations of the space-time correlations can be found in the supplementary material available at XxxxX.

motions (Fiedler 1988)." The essence of previous statement is consistent with the results of Tinney & Jordan (2008), who compared the near pressure fields of multi stream high subsonic jets with nozzle serrations to a non-serrated baseline case. Using a linear array of microphones located in the near-field the authors found a significant reduction in the acoustic and hydrodynamic components of the axial coherence at locations in the near nozzle region. However, no structural difference in the axial coherence of the acoustic and hydrodynamic components were observed at locations beyond x/D=3.

The current results suggest a more effective way to reduce the axial coherence of turbulent structures in the far nozzle region is to introduce perturbations along the jet

centerline rather than into the shear layer directly at the nozzle exhaust. Centerline perturbations are likely shielded from the outer shear layer by the irrotational fluid of the jet potential core, and may be able to convect over long distances and interact directly with the shear layer at locations far downstream.

In terms of thrust loss, centerline perturbations may also be a much more cost effective method to reduce noise as a centerline boundary condition change can likely be further optimized to target the intense noise sources near the potential core collapse region. The area near the potential core collapse region of the jet is a strong producer of noise due to the large correlation length scale of the turbulence and the presence of the strong intermittent noise events that occur near the core collapse region (Fisher *et al.* 1977; Morrison & McLaughlin 1979; Juvé *et al.* 1980). Therefore, for a given amount of energy with which to induce flow perturbations, the most cost effective distribution may likely involve a form that targets the jet centerline.

3.4. *Space-Frequency Coherence*

In this section the space-frequency coherence of the fluctuating density gradient is examined in order to more precisely view the frequency content of the density near-field, with specific emphasis on the low frequency hydrodynamic waves that capture the signature of the large scale instabilities directly beneath. The frequency information the coherence provides can be used to roughly separate the acoustic and hydrodynamic content of the near-field. As described by Arndt *et al.* (1997), rapidly decaying hydrodynamic fluctuations dominate low frequencies at very small distances from the shear layer and represent the convective 'footprint' of the large scale instabilities. Thus, the coherence measured between points near the shear layer edge provides an indirect measure of the coherence length scale of the large scale instabilities.

In the current analysis the coherence, γ_{12}^2, calculated according to

$$\gamma_{12}^2(x, y; \xi, \zeta, f) = \frac{|G_{12}(x, y; \xi, \zeta, \tau)|^2}{G_{11}(x, y, f)G_{22}(x + \xi, y + \zeta, f)}. \tag{3.9}$$

Here the autos-pectrum, G_{11}, is calculated at a probe directly outside of the shear layer, G_{22} is calculated at second point located on a line parallel to the shear layer (as shown in figure 9(g), and G_{12} is the cross-spectrum between these two points. Note the probe point used in the space-frequency coherence are the same points used in the space-time correlations. The auto- and cross-spectrum are calculated using a window length of 100 with 50% overlap, resulting in 799 records for spectral averaging.

The resulting space-frequency coherence plots shown in figure 9 show qualitative agreement with the microphone based measurements of Tinney & Jordan (2008) and exhibit extensive axial coherence at low frequencies followed by a rapid decrease in the coherence length with increasing frequency. This marked contraction of the coherence length with increased frequency represents the frequency dependent boundary of the hydrodynamic dominated near-field. This observation was first described by Arndt et al. (1997), who showed a sharp change in the decay rate of pressure fluctuations occurred at non-dimensional wavenumbers in the range $1 < ky_s < 2$, where y_s is the distance to the center of the shear layer. This same demarcation is observed in figure 9 where the edge of the near-field occurs at approximately St = 1.25, which given the corresponding acoustic wavenumber results in $ky_s = 1.6$. Lastly we note the sharp vertical edges on the right side of the contours represents the end of the measurement field of view.

A direct comparison of the space-frequency coherence of the NUC and uniform jets indicates a large reduction in the axial coherence, providing further evidence that the thermal non-uniformity reduces the correlation length scales of large scale instabilities in

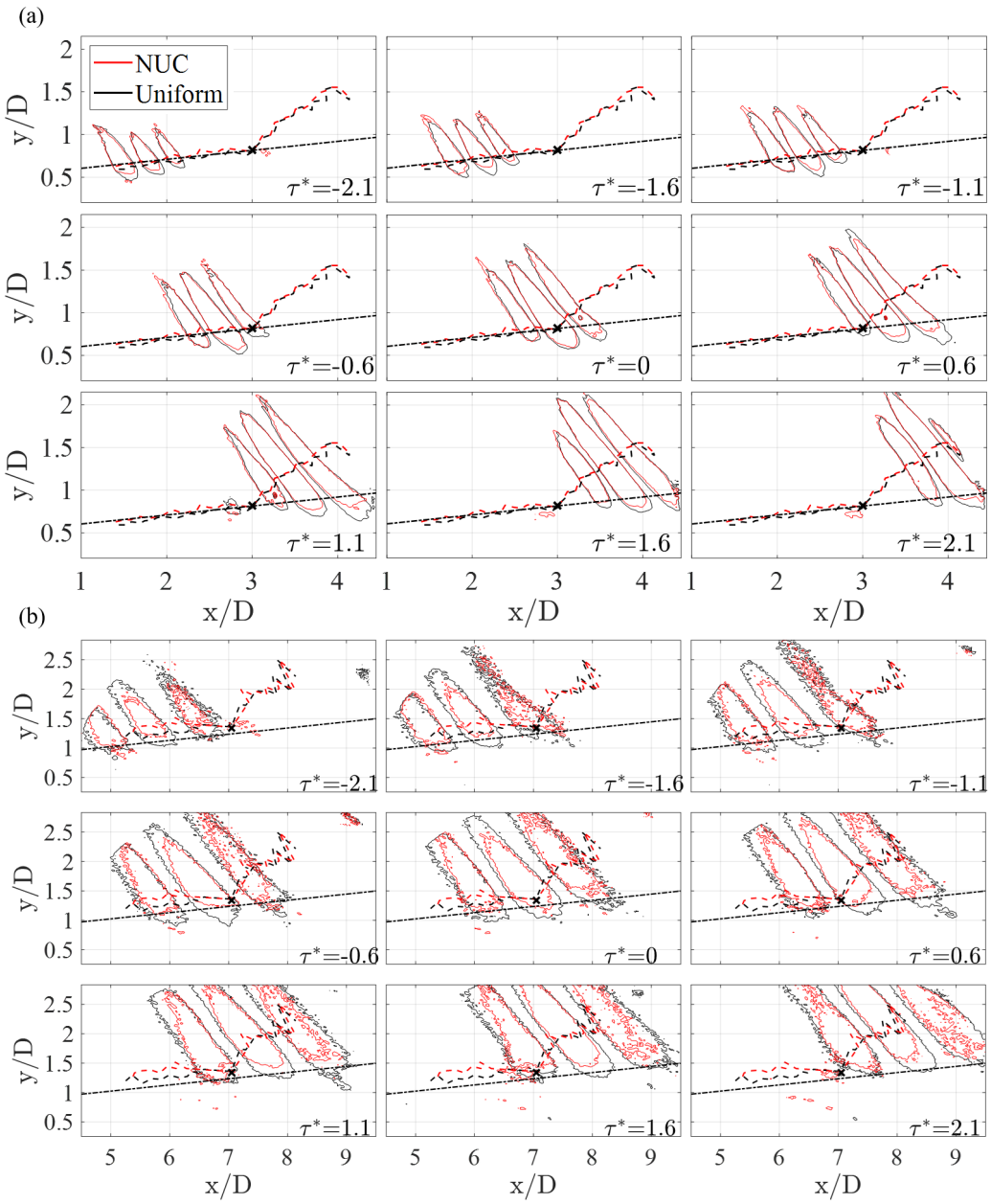

FIGURE 8. Comparison of constant contours (-0.1, 2) of the space time correlations of the high-pass filtered density near-field of the Uniform and NUC jet in the (a) near-nozzle (x/D=3) and (b) far-nozzle (x/D=7) region. The dash dot line represents the approximate location of the shear layer edge and the correlation probe point is indicated by the x. Animations of the space-time correlations can be found in the supplementary material available at XxxxX.

regions near the nozzle and far downstream. The decrease in the coherence length is shown explicitly in figure 9(e) and 9(f), which shows the difference between coherence contours uniform and NUC jets, i.e., $\Delta\gamma^2_{1,2} = \gamma^2_{NUC} - \gamma^2_U$. A large decrease in the coherence occurs in the frequency range $0.2 < St < 0.3$ which is the same frequency range where the largest reductions are observed it the far-field narrowband spectra. These results indicate a decrease in the coherence length of the instability waves that produce Mach wave radiation and serve to bolster the conclusions from the previous section, namely the thermal non-uniformity reduces the correlation length scale of large scale instabilities in both the near- and far- nozzle regions.

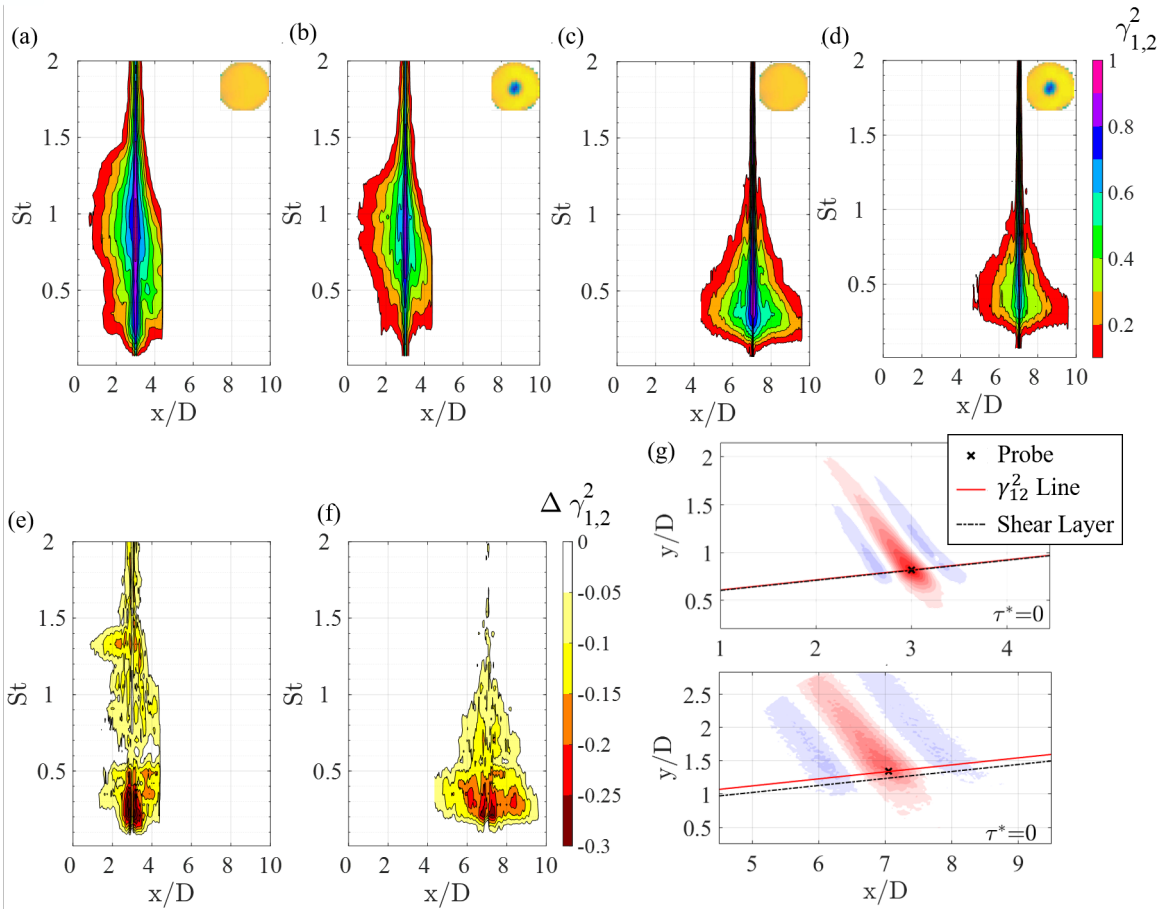

FIGURE 9. Space-frequency coherence the fluctuating radial density gradient of the Uniform (a,c) and NUC jets (b,d). Reduction in the coherence for the (e) x/D=3 and (f) x/D=7 probe points where $\Delta\gamma^2_{1,2} = \gamma^2_{NUC} - \gamma^2_U$

4. Summary and Conclusion

The ability of jet noise reduction techniques to reach out into the flow field and interrupt the formation of large scale coherent structures at locations far downstream from the nozzle have thus far been unclear. In the current work we examine the signature of these coherent structures through a space-time analysis of the density near-field and demonstrate that the perturbations induced by a centered thermal non-uniformity reduce the coherence length of these structures at far downstream regions.

A space-time analysis of the frequency filtered near-field captures the two-dimensional time evolution of two coexisting structures that are both decorrelated by the thermal non-uniformity at downstream locations. Mach wave structures were found to dominate low frequency ranges while high frequency ranges were characterized by a curved acoustic wave. The spatial extent of the large Mach wave structures captured by the space-time correlations of the low frequency density near-field fluctuations were reduced in the case of the thermal non-uniformity, indicating a decorrelation in the Mach wave strength. These decorrelations were appreciable in the downstream correlations (x/D=7) and less so for the upstream (x/D=3). The signature of the large scale instability waves that produce Mach waves were examined indirectly using the coherence between points along a line directly outside of the shear layer. The coherence analysis indicated a reduction in the axial coherence of low frequency fluctuations in the case of the thermally non-uniform

jet. This decoherence was found to be extensive for probe locations centered at x/D=7 and smaller, but still present, at x/D=3.

In contrast to the quasi-one-dimensional Mach waves, curved acoustic waves were observed in correlations of the high frequency near-field fluctuations. These features displayed a level of superdirectivity and have a peak that travels at large angles to the downstream direction, $\theta_0 = 135^\circ$, $\theta_0 = 115^\circ$ for the x/D=3, x/D=7 correlations respectively. The source of the curved acoustic wave is related to the small wavelength wave packet structure inside the jet shear layer observed in negative time lags. The integral length structure likely represents a compactly coherent turbulent structure as it convects in the shear layer at radial locations at or very close the peak Reynolds shear stress. At time lags approaching $\tau^* = 0$ the integral length feature rotates and rapidly begins to distort and form the arc of a curved acoustic wave that abruptly ejects from the shear layer at a large angle from the downstream direction. As the curved wave begins to propagate, the correlations in the shear layer representing the coherent turbulence structure suddenly dissipate. The abrupt disintegration of the compactly coherent structure and the subsequent emission of an acoustic bears significant similarities to the observations of Hileman *et al.* (2005) and suggests a causal relationship between these two features that is likely is related to an energetic vortex interaction that produces an intense acoustic signature. Both the compactly coherent structures in the shear layer and the spherically spreading waves they produce are decorrelated in the far nozzle region in the case of the thermal non-uniformity.

These results indicate that base flow changes induced by the introduction of a centered thermal non-uniformity have a direct impact on the correlation length scale of compactly coherent turbulence and large scale instabilites at locations far from the nozzle exit. These changes reduce the strength of radiated Mach waves and result in noise reductions up to 2 ± 0.5 dB in the peak narrowband spectral sound pressure levels. These findings are significant as they suggest that centerline boundary condition changes may be an efficient way to reduce jet noise. The centerline perturbations induced by the thermal non-uniformity aare able to persist within the potential core and decrease the correlation length scales of both noise-producing instabilities and coherent turbulent structures at locations far downstream. This suggests nozzle boundary condition changes along the jet centerline may be the most efficient method to reduce noise while minimizing thrust loss.

Appendix A. Separation of Correlations from Linearly Added Signals

In the results of §3 the fluctuating intensity gradient of schlieren images, A', was separated into two sub-signals representing high, A'_2, and low frequency, A'_1, fluctuations whose sum is equal the original signal.

$$A'(x,y,t) = A'_1(x,y,t) + A'_2(x,y,t) \tag{A 1}$$

In this appendix section we provide a proof that demonstrates that the cross correlation the original signal, R_{AA}, is equal to the sum of the correlations of the low and high frequencies signals, $R_{AA_1} + R_{AA_2}$, if the high and low frequency signals are themselves uncorrelated.

We begin by calculating the cross correlation between the fluctuating schlieren intensity at a probe point $A'(x,y,t)$ and every other point in the field of view $A'(x+\xi, y+\zeta, t+\tau)$. The resulting cross correlation is the expected value, $<>$, of the product of the probe point time series and another point in the image separated in the axial and radial

directions by ξ and ζ respectively, and separated in time by τ. The cross correlation is formally defined as

$$R_{AA}(x,y;\xi,\zeta,\tau) =< A'(x,y,t)A'(x+\xi,y+\zeta,t+\tau) > . \tag{A 2}$$

Next, we replace the original signal with the linearly summed signals. Note we drop the argument of the correlation function for brevity.

$$\begin{aligned} R_{AA} =< [A'_1(x,y,t) + A'_2(x,y,t)] \\ [A'_1(x+\xi,y+\zeta,t+\tau) + A'_2(x+\xi,y+\zeta,t+\tau] > \end{aligned} \tag{A 3}$$

Distributing the components inside of the expected value yields,

$$\begin{aligned} R_{AA} = R_{AA_1} + R_{AA_2} + < [A'_1(x,y,t)A'_2(x+\xi,y+\zeta,t+\tau)] > \\ + < [A'_1(x+\xi,y+\zeta,t+\tau)A'_2(x,y,t] > . \end{aligned} \tag{A 4}$$

This equations demonstrates if the cross correlation between the high and low frequency signals are uncorrelated, i.e,

$$\begin{aligned} < [A'_1(x,y,t)A'_2(x+\xi,y+\zeta,t+\tau)] >= \\ < [A'_1(x+\xi,y+\zeta,t+\tau)A'_2(x,y,t] >= 0 \end{aligned} \tag{A 5}$$

then the cross correlation of the original fluctuating schlieren intensity is equal to the sum of the cross correlations of the individual sub-signal signals

$$R_{AA} = R_{AA_1} + R_{AA_2}. \tag{A 6}$$

REFERENCES

Arndt, Roger EA, Long, DF & Glauser, Mark N 1997 The proper orthogonal decomposition of pressure fluctuations surrounding a turbulent jet. *Journal of Fluid Mechanics* **340**, 1–33.

Aubert, Allan & McKinley, Richard 2011 Measurements of jet noise aboard us navy aircraft carriers. In *AIAA Centennial of Naval Aviation Forum" 100 Years of Achievement and Progress"*, p. 6947.

Berry, MG, Magstadt, AS & Glauser, Mark N 2017 Application of pod on time-resolved schlieren in supersonic multi-stream rectangular jets. *Physics of Fluids* **29** (2), 020706.

Brès, Guillaume A, Towne, Aaron & Lele, Sanjiva K 2019 Investigating the effects of temperature non-uniformity on supersonic jet noise with large-eddy simulation. In *25th AIAA/CEAS Aeroacoustics Conference*, p. 2730.

Cavalieri, André VG & Agarwal, Anurag 2014 Coherence decay and its impact on sound radiation by wavepackets. *Journal of Fluid Mechanics* **748**, 399–415.

Cavalieri, André VG, Jordan, Peter, Agarwal, Anurag & Gervais, Yves 2011 Jittering wave-packet models for subsonic jet noise. *Journal of Sound and Vibration* **330** (18-19), 4474–4492.

Cavalieri, André VG, Jordan, Peter, Colonius, Tim & Gervais, Yves 2012 Axisymmetric superdirectivity in subsonic jets. *Journal of Fluid Mechanics* **704**, 388–420.

Dahl, Milo D & Morris, Philip John 1997 Noise from supersonic coaxial jets, part 3: Inverted velocity profile. *Journal of Sound and Vibration* **200** (5), 701–719.

Daniel, Kyle, Mayo Jr, David E, Lowe, K Todd & Ng, Wing F 2019*a* Space-time

description of the density near-field in a non-uniformly heated jet. In *25th AIAA/CEAS Aeroacoustics Conference*, p. 2474.

Daniel, Kyle A, Mayo Jr, David E, Lowe, K Todd & Ng, Wing F 2019*b* Use of thermal non-uniformity to reduce supersonic jet noise. *AIAA Journal* .

Fiedler, HE 1988 Coherent structures in turbulent flows. *Progress in Aerospace Sciences* **25** (3), 231–269.

Fisher, MJ, Harper-Bourne, M & Glegg, SAL 1977 Jet engine noise source location: The polar correlation technique. *Journal of Sound and Vibration* **51** (1), 23–54.

Fuchs, Helmut V 1972 Space correlations of the fluctuating pressure in subsonic turbulent jets. *Journal of Sound and Vibration* **23** (1), 77–99.

George, William K, Beuther, Paul D & Arndt, Roger EA 1984 Pressure spectra in turbulent free shear flows. *Journal of Fluid Mechanics* **148**, 155–191.

Henderson, Brenda S & Huff, Dennis L 2016 The aeroacoustics of offset three-stream jets for future commercial supersonic aircraft. In *22nd AIAA/CEAS Aeroacoustics Conference*, p. 2992.

Henderson, Brenda S & Leib, Stewart J 2015 Measurements and predictions of the noise from three-stream jets. In *21st AIAA/CEAS Aeroacoustics Conference*, p. 3120.

Hileman, James & Samimy, Mo 2001 Turbulence structures and the acoustic far field of a mach 1.3 jet. *AIAA Journal* **39** (9), 1716–1727.

Hileman, James, Thurow, Brian & Samimy, Mo 2002 Exploring noise sources using simultaneous acoustic measurements and real-time flow visualizations in jets. *AIAA Journal* **40** (12), 2382–2392.

Hileman, James I, Thurow, Brian S, Caraballo, Edgar J & Samimy, Mo 2005 Large-scale structure evolution and sound emission in high-speed jets: real-time visualization with simultaneous acoustic measurements. *Journal of Fluid Mechanics* **544**, 277–307.

Huff, Dennis L, Henderson, Brenda S, Berton, Jeff J & Seidel, Jonathan A 2016 Perceived noise analysis for offset jets applied to commercial supersonic aircraft. In *54th AIAA Aerospace Sciences Meeting*, p. 1635.

Jordan, Peter & Colonius, Tim 2013 Wave packets and turbulent jet noise. *Annual Review of Fluid Mechanics* **45**, 173–195.

Juvé, D, Sunyach, M & Comte-Bellot, G 1980 Intermittency of the noise emission in subsonic cold jets. *Journal of Sound and Vibration* **71** (3), 319–332.

Kuo, Ching-Wen, Buisson, Quentin, McLaughlin, Dennis K & Morris, Philip J 2013 Experimental investigation of near-field pressure fluctuations generated by supersonic jets. In *19th AIAA/CEAS aeroacoustics conference*, p. 2033.

Kuo, Ching-Wen, McLaughlin, Dennis K, Morris, Philip J & Viswanathan, K 2014 Effects of jet temperature on broadband shock-associated noise. *AIAA Journal* **53** (6), 1515–1530.

Mayo Jr, David E, Daniel, Kyle A, Lowe, K Todd & Ng, Wing F 2019 Mean flow and turbulence of a heated supersonic jet with temperature nonuniformity. *AIAA Journal* pp. 1–8.

Morrison, GL & McLaughlin, DK 1979 Noise generation by instabilities in low reynolds number supersonic jets. *Journal of Sound and Vibration* **65** (2), 177–191.

Murray, Nathan E & Lyons, Gregory W 2016 On the convection velocity of source events related to supersonic jet crackle. *Journal of Fluid Mechanics* **793**, 477–503.

Papamoschou, Dimitri 2018 Modelling of noise reduction in complex multistream jets. *Journal of Fluid Mechanics* **834**, 555–599.

Papamoschou, Dimitri & Phong, Vincent C 2017 The very near pressure field of single-and multi-stream jets. In *55th AIAA Aerospace Sciences Meeting*, p. 0230.

Papamoschou, Dimitri, Xiong, Juntao & Liu, Feng 2014 Reduction of radiation efficiency in high-speed jets. In *20th AIAA/CEAS Aeroacoustics Conference*, p. 2619.

Powers, Russell W, Kuo, Ching-Wen & McLaughlin, Dennis K 2013 Experimental comparison of supersonic jets exhausting from military style nozzles with interior corrugations and fluidic inserts. In *19th AIAA/CEAS Aeroacoustics Conference*, p. 2186.

Quinn, Allison M, Daniel, Kyle, Lowe, K Todd Lowe & Ng, Wing F 2019 Outdoor acoustic measurements of the virginia tech heated supersonic jet rig using ground microphones. In *AIAA Scitech 2019 Forum*, p. 1581.

Schmidt, Oliver T & Schmid, Peter J 2019 A conditional space–time pod formalism for intermittent and rare events: example of acoustic bursts in turbulent jets. *Journal of Fluid Mechanics* **867**.

Stuber, Marcie, Lowe, K Todd & Ng, Wing F 2019 Synthesis of convection velocity and turbulence measurements in three-stream jets. *Experiments in Fluids* **60** (5), 83.

Suzuki, Takao & Colonius, Tim 2006 Instability waves in a subsonic round jet detected using a near-field phased microphone array. *Journal of Fluid Mechanics* **565**, 197–226.

Tanna, HK 1980 Coannular jets — are they really quiet and why? *Journal of Sound and Vibration* **72** (1), 97–118.

Thurow, Brian, Hileman, James, Lempert, Walter & Samimy, Mo 2002 A technique for real-time visualization of flow structure in high-speed flows. *Physics of Fluids* **14** (10), 3449–3452.

Tinney, CE & Jordan, P 2008 The near pressure field of co-axial subsonic jets. *Journal of Fluid Mechanics* **611**, 175–204.

Tinney, Charles E & Schram, Christophe F 2019 Acoustic modes from a mach 3 jet. In *25th AIAA/CEAS Aeroacoustics Conference*, p. 2598.

Zaman, KBMQ 1986 Flow field and near and far sound field of a subsonic jet. *Journal of Sound and Vibration* **106** (1), 1–16.

Appendices

Appendix A

The Heated Supersonic Jet Rig

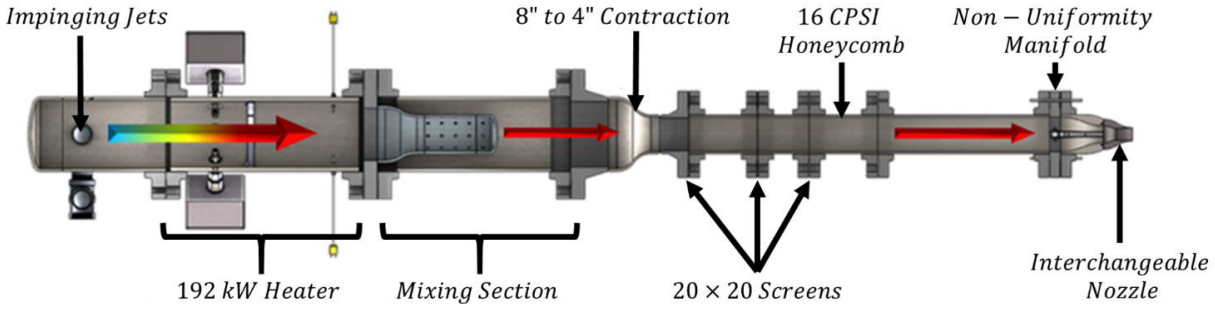

Figure A.1: Virginia Tech Heated Supersonic Jet Rig

The experimental measurements described within this dissertation were taken using the Virginia Tech Heated Jet Rig located at the Advanced Power and Propulsion Laboratory (APPL). A schematic of the rig shown in Figure B.1 identifies some of the major features of the rig. These include a 192 kW heater that can be used to achieve temperature ratios up to TTR=3, a mixing section that ensures the flow is evenly heated, and a series of screens and honey combs that condition the flow. The Heated Jet Rig also has a downstream section that allows new flange sections and nozzle geometries to be quickly interchanged.

The set of experiments described in this dissertation used a round nozzle with an exit diameter of 1.5 in (38.1 mm) and an expansion section designed using the axisymmetric method of characteristics to produce a shock free Mach 1.5 flow at design conditions. Note this nozzle is a scaled version of the one used in experiments by Kuo et al. [1].

A centered thermal non-uniformity was generated by feeding unheated air into a secondary nozzle located far upstream along the primary jet centerline using a custom flange manifold system described in Figure B.2. Two separate air streams were fed into both sides of the manifold system where they impinged and accelerated through the converging nozzle located inside the primary heated plume. Note the secondary nozzle terminated in the subsonic portion of the flow at a distance of 2.23D from the primary nozzle exhaust plane.

Total temperature and total pressure measurements of both the primary heated and secondary unheated streams were recorded using a National Instruments (NI) 9213 thermocouple module in a NI cDAQ-9184 chassis and a Scanivalve Corp. ZOC17IP/8Px-APC pressure scanner respectively. In order to more accurately monitor the mass flow changes between the

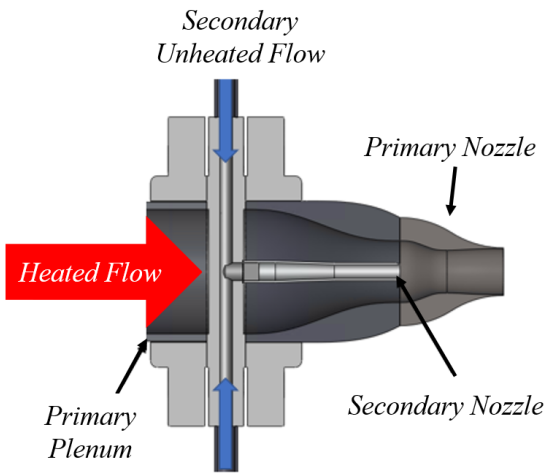

Figure A.2: Centered Thermal Non-uniformity Hardware

uniform and non-uniform conditions, the mass flow rate of unheated stream was measured directly using the static pressure difference across a Lambda-Square venturi meter.

References

[1] Kuo, C. W., McLaughlin, D. K., Morris, P. J., and Viswanathan, K., "Effects of Jet Temperature on Broadband Shock-Associated Noise," AIAA Journal, Vol. 53, No. 6, 2015, pp. 1515–1530.

Appendix B

Far-field Ground Array

The acoustic far-field presented in the current dissertation was characterized using a ground array consisting of 378C10 PCB microphones located on a 100D radius polar arc. Measurements were performed outside the facility with the ground microphone array located on the concrete pad surrounding the test cell. The ground microphone array technique follows SAE standard AIR 1672B, which primarily guides outdoor acoustic tests of full-scale engines. The working principal of the standard is the flat concrete pad acts as an almost perfect acoustic reflector, whose effect is simply a doubling of the power spectra over a frequency range dependent on the distance between the microphone and the ground.

The ground array consisted of a tripod that holds a microphone inverted above the ground at a specific distance. An example of the ground array used in this dissertation is shown in Figure C.1. The microphone was held in place by a tripod like device consisting of a cylindrical sleeve with thin metal tubes attached to the outside surface. The sleeve was 3D printed and included small triangular wedges spaced evenly around the outside surface. These wedges provide an area for 1/16" brass tubes to be glued to the outside of the sleeve. The tripod feature is also glued to an 8" x 8" piece of aluminum flashing to ensure the surface below the microphone is as smooth as possible. A rough surface below the microphone will cause reflections and degrade accuracy of the 'free field' measurement. Lastly the height of the microphone above the ground is set to 0.25" using a gauge block. Once the microphone is set to the calibrated height, an O-ring around the end of the microphone is used to hold it in place at the correct distance above the ground. Far-field measurements were taken by deploying the ground array to the appropriate locations on the 100D arc and by rolling

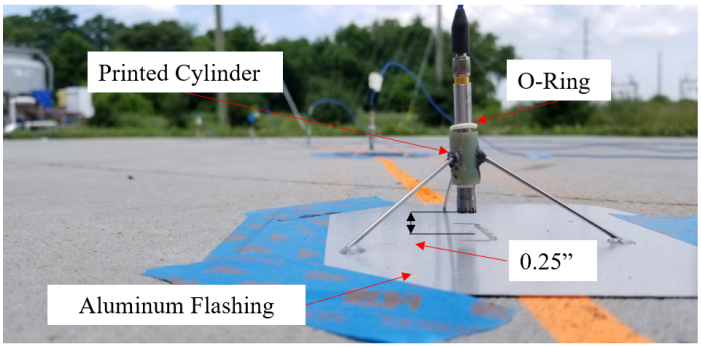

Figure B.1: Ground Array Tripod

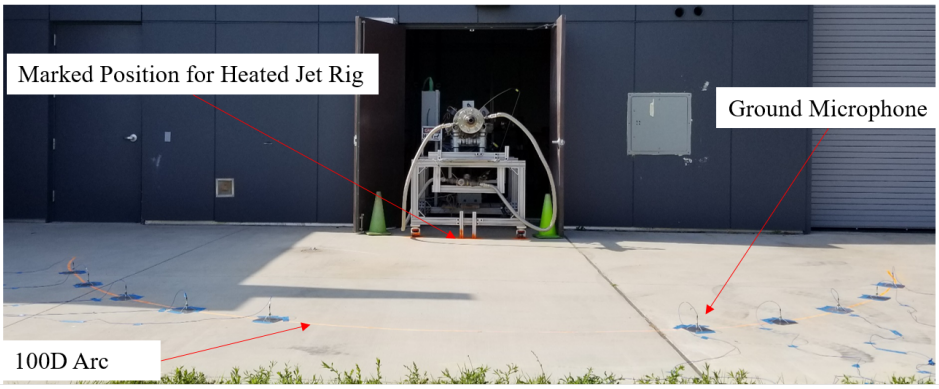

Figure B.2: Ground Array Setup

Heated Jet Rig outside onto the concrete pad as shown in Figure C.2. To ensure the distance between the nozzle exhaust and the microphones remains consistent between tests, an area on the concrete pad was spray-painted to mark the correct position. The Heated Jet Rig is aligned when the casters on the front of the cart and the pieces of extruded aluminum framing are aligned with the spray-painted mark.

Appendix C

Schlieren Imaging

Schlieren imaging is a technique that provides a path integrated quantity representing the density gradient in a flow field. Traditional schlieren imaging systems utilize a beam of collimated light that passes through a flow area. Variations in the refractive index of the flow caused by the density gradients bend the light in the collimated beam and cause areas of the resulting image to be lighter or darker. The use of just a collimated beam is called a shadowgraph, which provides the second derivative of the density. A schlieren image is generated by focusing the collimated light beam after it passes through the flow using a lens or curved mirror and placing a knife edge at the focal point to block half of the light. This has the effect of creating light and dark areas corresponding to the first derivative of the density gradient, where the direction of the gradient is normal to the knife edge. Both schlieren and shadowgraph provide integrated quantities, meaning that the variations in density at any point along the light path are summed.

The schlieren system used in the current dissertation was a traditional Z-type system shown in Figure D.1. Here a ABET 150 Watt Xenon Arc Lamp was used with an iris diagram to create a point light source. The light was collimated using two parabolic mirrors and a horizontal knife edge provided the radial density gradient. Time-resolved images were captured using a Phantom v2512 high-speed camera set to record at 110 kFrames/s with an exposure time of $1\mu s$.

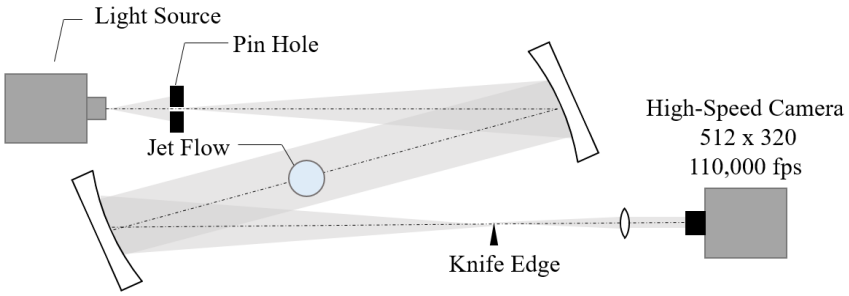

Figure C.1: Z-Type Schlieren System